ANALYSIS OF NORMAL AND STRONG - LINED K - TYPE DWARF AND GIANT STARS

Thesis by

Valdar Oinas

In Partial Fulfillment of the Requirements

for the Degree of

Doctor of Philosophy

California Institute of Technology

Pasadena, California

1971

(Submitted December 16, 1971)

To
HD 112127

There's not the smallest orb which thou behold'st
But in his motion like an angel sings,

(Shakespeare)

ACKNOWLEDGEMENTS

There are many people to whom I am grateful for assistance and advice in this work.

Special thanks go to my advisor, Dr. Jesse Greenstein, who not only obtained the bulk of the plate material that was used, but was always ready with helpful suggestions for new approaches to the problems that cropped up.

Thanks are due also to Deane Peterson for providing me with the model atmosphere programs developed by himself and the Harvard - Smithsonian group and to Robert O'Connell, who instructed me in the use of the Cassegrain scanner and its attendant reduction program.

I am indebted to Drs. Hyron Spinrad and Olin Wilson for helpful discussions and encouragement and to Drs. Roger Bell, Roger Ulrich, and George Wallerstein for their assistance and interest.

I also wish to acknowledge the many stimulating conversations ranging from astronomy to dental floss technology that I have had with my fellow graduate students - Seth Shostak, Pat Osmer, Saul Adelman, and many others.

A special note of thanks to Helen Holloway, who gave unselfishly of her time to make the first draft of the thesis legible, and to Della Harris, who helped type the final copy.

Thanks also to the staff at Mt. Wilson, in particular the night assistants, who often helped the cold nights to pass more quickly with their jovial banter.

Last of all, I would be remiss if I were to forget the U.S. taxpayers, who provided me with an NDEA fellowship for three years of my stay at Caltech.

PREFACE

The extensive list of spectral line measurements obtained during the course of this work is not reproduced here, but has been placed in a separate volume on file at Caltech. It is available to anyone who wishes to use it.

A small portion of the thesis has appeared in The Astrophysical Journal and is reproduced here in its original form.

ABSTRACT

In this work a detailed analysis is carried out for twenty-six normal and super-metal-rich (SMR) K dwarfs and giants in the solar neighborhood. The observational material consists of line measurements on tracings of high dispersion spectra along with photoelectric scans covering a wide range of wavelengths. The program Atlas was employed to construct the model atmospheres; the temperature fit was provided by a matching of the predicted continua to the de-blanketed scans. H_α wing profiles were also used to obtain information on the temperatures. The major conclusions that were reached are the following:

1) A gravity defect sets in at about spectral type K2 in both dwarfs and giants; its nature is such that progressively lower gravities are required in order to obtain equal ion and neutral abundances as one goes to cooler stars. In the coolest stars the spectroscopic gravities imply masses lower than $0.1M_\odot$. It is suggested that the effect may be caused by a new opacity source that is acting to steepen the spectral gradient in the visual and near-infrared, thereby falsifying the temperatures. The dependence of the unknown absorber on the temperature and gravity are discussed and a

rough formula describing this dependence is given. It is shown that the new opacity also explains various discrepancies noted by other observers.

2) The SMR stars are generally overabundant by about 0.2 - 0.3 dex relative to the normal-abundance comparison stars of the same temperature. An overabundance of sodium by about 0.5 dex is found for all the SMR stars, with the exception of the dwarf 54 Psc, which is found to have essentially normal metal abundances. θUMi, the coolest giant in the program, is also the most super-metal-rich, with a general overabundance of about 0.4 dex and a sodium enhancement of 0.8 dex. The iron overabundance is rather marginal in most of the giants (ΔFe ~ 0.1).

3) No correlation is found between metal abundance and turbulence. In particular, the SMR stars in this program are not found to possess high microturbulent velocities. The U-B deficiencies can be explained by the effects of a slight metal enhancement on the colors (Strom et al. 1971) and the line blocking due to the CN violet system.

4) The SMR dwarfs all lie high on the main sequence, in keeping with their derived metal abundances. It is not necessary to invoke substantial variations in helium content to account for their positions.

Table of Contents

Table of Contents (continued)

I. INTRODUCTION

Recent studies by Spinrad and Taylor (1969; hereafter referred to as ST) and Taylor (1970) on metal abundances in late type stars have pointed to the possible existence of a class of "super-metal-rich" (SMR) stars (i.e., possessing greater than Hyades abundances) among field stars and cluster members. Their technique has consisted of narrow-band photoelectric photometry of strong spectral features and selected continuum points in conjunction with a simple theoretical treatment relating line strengths to abundances. The major conclusions are the following: (1) approximately 5% of the field dwarfs and 15% of the field giants are SMR; (2) there exists a tight correlation between nitrogen, sodium and iron abundances; (3) a cutoff in the production of SMR stars took place around the time of formation of the old galactic cluster M67 (age $\sim 3 \times 10^9$ years). Published broad-band colors also support the interpretation of SMR stars as being metal rich in that these stars exhibit a marked ultraviolet deficiency when compared to normal stars with the same infrared colors.

When the abundances derived by the scanner technique are compared with those based on model-atmosphere or curve of growth methods, however, a discrepancy is seen to arise. In the case of the giants the scanner abundances are system-

atically too high for spectral types later than about K1, a situation that holds also for the G7 giant λHya. ST interpret this as evidence for a systematic error in the conventional abundance determination procedures for late type giants (in the case of the dwarfs there are too few abundance analyses available in the literature for a meaningful comparison). Since their method involves the comparison of program stars with a set of standards having the same temperature, while nearly all other published abundance of cool stars have involved comparison with a hotter star (the sun, Hyades or εVir) ST propose that an unknown temperature dependent opacity source is operating to increase the continuous absorption. This would decrease the line strengths in the cooler stars and would therefore result in speciously low abundances when comparison is made with a hotter star in which the opacity is presumably known.

A model-atmosphere analysis of four SMR giants has recently been published by Strom, Strom and Carbon (1971) in which it is concluded that the ultraviolet deficiency and the apparent strengthening of the lines in these stars is caused by one or a combination of the following effects: (1) increased turbulence which results in considerable line blocking in the blue and ultraviolet regions of the spectrum, thereby affecting the broad-band colors in such a way as to mimic metal enhancement; (2) a small increase in metal abun-

dance which, due to the overlapping of line wings in cool stars, has the same effect on broad-band colors as an increase in the turbulence; (3) a lowering of the boundary temperature resulting from the enhanced molecular bands (CN and CO) observed in these stars in addition to effects (1) and (2), the result of which would be a strengthening of the lines formed in the outer layers of the atmosphere.

The question of supermetallicity is important in our understanding of the past history of the Galaxy - if the phenomenon is real, serious doubt is cast on the theory of a uniform enrichment of the disk. Moreover, evidence for supermetallicity has been found in other galaxies - in the cores of giant ellipticals and in the nuclei of spirals (Spinrad 1966, 1967; McClure and van den Bergh 1968). A source of some puzzlement is the large difference in the percentages of SMR dwarfs and giants found by ST in the solar neighborhood (5% vs. 15%) and the fact that the SMR giants attain much higher metallicities than do the dwarfs.

In view of the importance of the SMR phenomenon it was decided to undertake a detailed analysis of a selection of SMR giants and dwarfs along with a group of apparently normal or previously analyzed stars included for purposes of comparison. It was also decided to place particular emphasis on the dwarfs since they would be expected to be free of complications resulting from possible evolutionary effects

(e.g., surface phenomena such as mixing with enriched material from the interior). Hopefully an explanation could be found for the discrepancies between the scanner and model-atmosphere abundance results as well as the difference in the range of abundance in the SMR giants and dwarfs.

II. PROGRAM STARS

The stars included in the program are listed in Table 1 along with the MK classification, the apparent visual magnitude, and the broad-band color indices. Nearly all the stars have been analyzed by ST and Taylor (1970), and those found by them to be SMR (or suggested as being SMR from incomplete data) are marked by an asterisk. The MK classifications as well as the apparent visual magnitudes are from the Bright Star Catalogue in nearly all cases (the dwarfs are all luminosity Class V and the giants, except for 18 Lib A, are Class III). The sources of the color indices are also listed.

In the following, the results of previous work, as well as features of interest are described for each star in the program. All scanner results refer to Taylor (1970) or ST.

ξ Boo A, a well known Yerkes G8 V standard, possesses strong H and K reversals as well as a high lithium abundance (Herbig 1965). Taylor's scans indicate a moderate metal deficiency ([Fe/H] = -0.4), a result that is supported by the small U-B index. Herbig's (1965) value of [Fe/H] = 0.0 is too high due to an incorrect choice of temperature ($\Delta\theta$ = .02 rel. to the sun).

70 Oph A is also a Yerkes standard with strong H and K reversals. A rough analysis by Dijke (1946), based on esti-

TABLE 1

PROGRAM STARS

HD	Name	Sp.	m_v	U-B	B-V	R-I	Source
		Dwarfs					
131156	ξ Boo A	G8V	4.72	.23	.72	.43	2,5
165341	70 Oph A	K0V	4.25	.57	.78	.38	5
75732*	ρ^1 Cnc	K0V	5.94	.63	.86	.40	2,4
145675*	14 Her	K0V	6.64	.66	.87	.40	2,4
185144	σ Dra	K0V	4.68	.37	.80	.41	1
3651*	54 Psc	K0V	5.84	.57	.85	.39	1
22049	ε Eri	K2V	3.73	.58	.88	.47	1
166620	HR 6806	K2V	6.30	.59	.87	.49	1
219134	HR 8832	K3V	5.57	.89	1.00	.53	1
32147*	HR 1614	K5V	6.21	1.00	1.06	.49	1
201092	61 Cyg B	K7V	6.02	1.23	1.37	.83	1
		Giants					
28307	θ^1 Tau	K0III	3.85	.72	.95	.47	1
27371	γ Tau	K0III	3.66	.79	.99	.47	1
28305	ε Tau	K0III	3.54	.87	1.01	.50	1
22148*	HR 8924	K3III	6.25	1.14	1.08		1
206952	11 Cep	K0III	4.71	1.09	1.10	.54	1
140573*	α Ser	K2III	2.65	1.25	1.17	.56	1
39003	ν Aur	K0III	4.06	1.09	1.14	.56	1
85503*	μ Leo	K2III	3.94	1.40	1.22	.58	1
12929	α Ari	K2III	2.00	1.13	1.15	.62	1
112127*		K2III	6.87	1.43	1.26	.58	6
132345*	18 Lib A	K3III-IVp	6.02	1.49	1.32	.60	3,4
34334	16 Aur	K3III	4.65	1.27	1.27	.71	1
98262	ν UMa	K3III	3.48	1.55	1.40	.70	1
50778	θ CMa	K4III	4.06	1.69	1.43	.78	1
139669*	θ UMi	K5III	5.14	1.89	1.58	.87	3,4

Sources:

1. Johnson et al. (1966)
2. Gliese (1969)
3. Hansen and Kjaergaard (1971)
4. Dickow et al. (1970)
5. Lutz (1971)
6. Helfer and Sturch (1970)

Table 1 (continued)

Remarks:

ξ Boo A: R-I is for ξ Boo AB.
18 Lib A, θ UMi: The R-I colors are based on a calibration of narrow-band photometric indices (Hansen and Kjaergaard 1971).
*SMR or suspected SMR.

mates of line strengths on high dispersion spectra, indicates approximately solar abundances.

ρ^1 Cnc is a good example of a SMR dwarf. A visual inspection of the spectrum reveals that the lines, particularly those due to CN, are considerably stronger than in 70 Oph A. The scanner data, in fact, indicates that this star has the strongest bands of CN found among the dwarfs in Taylor's program.

14 Her is very similar to ρ^1 Cnc - in fact, high dispersion spectra of the two stars are nearly indistinguishable.

σ Dra is another Yerkes standard and was added to the program at a later time in order to check a rather surprising gravity effect that will be described in subsequent chapters. Taylor's scans indicate that the star may be slightly underabundant in CN and Fe.

54 Psc is another example of a SMR dwarf, but not as extreme as ρ^1 Cnc or 14 Her. According to the scans the CH absorption at λ4300 is very strong and the CN bands are reasonably pronounced. This star is also a Yerkes standard.

ε Eri, a Yerkes K2 V standard, has been analyzed by Krishna Swamy (1966), who finds essentially solar abundances from a study of strong damping lines in the spectrum. In Taylor's diagrams of line strength vs. temperature, it falls roughly on a mean line for all the dwarfs in the

program, somewhat below the Hyades.

HR 6806, a dwarf rather similar to ε Eri, appears to possess Hyades abundances of Na, Mg and Ca and noticeably lower abundances of Fe and CN, according to the scanner data.

HR 8832, a Yerkes K3 V standard, falls near the Hyades in all except Fe in Taylor's abundance diagrams. G. Cayrel (1966) concludes that the star has solar abundances on the basis of a model-atmosphere analysis. Wilson (1962) has noted that the CN bands appear stronger than normal.

HR 1614, classified as K5 V on the basis of its line strengths, has a smaller R-I than HR 8832. It is a good example of a SMR star, lying well above the Hyades in the scanner abundance diagrams.

61 Cyg B was added to the program in order to check the aforementioned gravity effect, just as σ Dra. It is the fainter component of a well-known high velocity double and possesses strong H and K reversals. Kandel (1968) was unable to fit the measured profiles of Ca λ4227 and Na D to calculated profiles without employing a rather high effective temperature. (This result will be discussed in more detail in subsequent chapters.)

θ^1 Tau, γ Tau and ε Tau have been analyzed by many authors (e.g., Helfer and Wallerstein 1964, Griffin 1969, Strom et al. 1971), with the general conclusion that they, as well as the other members of the Hyades, are slightly overabundant in metals in comparison with the sun (between

0.1 and 0.2 dex). In fact, Alexander (1967) obtains $\left|Fe/H\right|$ = 0.2 to 0.3 for the Hyades G dwarfs, a value that is a bit higher than obtained by Helfer et al. (1959). The Hyades giants, with the exception of θ^1 Tau, are known to possess exceptionally strong CN absorption for their spectral class (Griffin and Redman 1960); conversely, θ^1 Tau exhibits stronger H and K reversals than do the other giants (Wilson 1959).

HR 8924 is one of the most extreme SMR giants observed by ST. Its MK spectral type, K3 III, assigned on the basis of the line strengths, is much too late for its infrared energy distribution - in fact, the ST temperature index suggests a spectral type closer to K1 III. Eggen (1962), using an absolute magnitude of M_V = 2.25, places it among the high-velocity stars with Q = 91 km/sec ($Q = \sqrt{U^2+V^2+W^2}$). Wilson (1971), however, obtains M_V = 3.2 from the H and K reversal strengths on three plates, a result which lowers the total space velocity to Q = 61 km/sec. The absolute magnitude indicates that the star may actually be Type IV or III-IV.

11 Cep is a normal giant, with slightly enhanced CN and Na D. It and ν Aur were included as comparison stars.

ν Aur is a normal star with slightly weaker lines than 11 Cep. Its CN lies a bit above the mean for the ST survey stars.

α Ser exhibits SMR features such as strong CN and Na D,

but not to the same extent as HR 8924 or μ Leo. A study of the molecular bands by Greene (1969) shows that the C/O ratio as well as the N abundance are greater than in the sun, thus explaining the CN strength. A curve of growth analysis by Griffin (1969) yields metal abundances greater than solar by 0.2 to 0.3 dex.

μ Leo may be regarded as the SMR giant prototype, lying well above the mean in all the scanner line strength vs. temperature curves except in the case of CH λ4300 (this band is quite saturated, with the result that the CH index is more sensitive to blanketing in the comparison bands than to changes in CH abundance). From their scanner data ST derive a mean metallicity of 0.6 dex compared to the sun. Peat and Pemberton (1968), however, derive a solar abundance and Strom et al. (1971) obtain an abundance only slightly higher than solar.

α Ari is a normal field giant, departing by more than one error bar from the mean line in the ST line strength diagrams only in the case of Na.

HD 112127 is listed by ST as a possible SMR giant on the basis of its extremely strong CN bands (Keenan 1963). Helfer and Sturch (1970) derive $\left[\mathrm{Fe/H}\right] = 0.29$ from the broad-band colors, the highest value in their sample of 132 K giants near the North Galactic Pole.

18 Lib A is a SMR star with very strong CN and Na D.

16 Aur falls near the mean line in all the ST line strength diagrams except for CN, in which it appears to be somewhat deficient.

ν UMa was not analyzed by ST and was included in the present program at a later date in order to check the gravity effect. Although assigned the same spectral type as 16 Aur its U-B and B-V indices are both larger and the CN absorption appears more pronounced (Deeming [1960], however, assigns a CN deficiency to both stars).

θ CMa also is not included in the ST program. An indication that the star has normal composition is the fact that it falls on the mean giant curve in the color-color plot of Johnson (1966). It is a high-velocity star, with a radial velocity of 97 km/sec and a total space velocity of 103 km/sec (Eggen 1962).

θ UMi has very strong Na D and Ca λ4227, but both the Mg λ5175 and the CN absorption depart rather little from the mean lines in the ST diagrams. Griffin (1960), on the basis of photoelectric measurements, noted that the star is extremely strong lined.

III. PHOTOGRAPHIC PHOTOMETRY

a) Observations and Calibration

The spectrograms used in this work were all obtained with the 100" telescope at Mt. Wilson or with the 200" at Palomar by various observers. The relevant data for the plates are listed in Table 2 (the P and C prefixes denote Palomar and Mt. Wilson spectra respectively). The plates were all traced with the direct intensity microphotometer of the California Institute of Technology, with a projected slit width of approximately 10μ. The intensity calibration was in most cases provided by a wedge-slit spectrogram taken with an auxiliary spectrograph and, in some cases, by means of intensity-strip calibrations recorded next to the stellar spectrum itself. A comparison of the calibrations provided by the two methods showed good agreement. Great care was taken to adjust the microphotometer to changing clear plate levels, since on some baked plates this quantity varied by as much as 10% from one end of the spectrum to the other.

b) Line Measurements

The clear plate level and continuum were drawn on all the tracings by hand. The proper placement of the continuum posed a rather serious problem, particularly toward the shorter wavelengths. It is felt, however, that for wavelengths greater than about λ5300 a reasonably accurate level has been drawn even in the case of the cooler giants.

TABLE 2

PLATE MATERIAL

HD	Name	Plate No.	Emulsion	Dispersion	Observer
131156	ξ Boo A	Pb 4367[2]	IIa-O	4.5	JBO
		Pb 4546	IIa-D	6.7	JBO
		Pb 5941	103a-F	6.7	JLG
165341	70 Oph A	Ce 11422[1]	IIa-D	6.7	WKB
		Pb 10093[b]	103a-F	6.7	JLG
		Pb 10098[b]	IIa-O	4.5	JLG
		Pb 10099[a]	IIa-D	6.7	JLG
		Pb 10099[b]	103a-F	6.7	JLG
75732	ρ[1] Cnc	Pb 9802[b]	IIa-F	6.7	JLG
		Pb 9819[b]	IIa-O	4.5	JLG
		Pb 9996[a]	IIa-D	6.7	JLG
		Pb 9996[b]	103a-E	6.7	JLG
		Pb 10000[a]	IIa-O	6.7	JLG
		Pb 10000[b]	103a-E	6.7	JLG
145675	14 Her	Pb 10096[a]	IIa-D	6.7	JLG
		Pb 10096[b]	103a-F	6.7	JLG
		Pb 10097[b]	IIa-O	4.5	JLG
		Pb 10220[a]	IIa-D	6.7	JLG
		Pb 10220[b]	103a-F	6.7	JLG
185144	σ Dra	Pb 7552	IIa-F	6.7	RPK
3651	54 Psc	Ce 19404	IIa-D	16.3	VO
		Ce 19405	103A-F	16.3	VO
		Ce 19406	IIa-D	16.3	VO
		Ce 19959	103a-F	16.3	SJA
22049	ε Eri	Ce 11755[1]	103a-D	6.7	WKB
		Ce 11755[2]	103a-F	6.7	WKB
166620	HR 6806	Pb 10094	103a-F	6.7	JLG
		Pb 10100[a]	IIa-D	6.7	JLG
		Pb 10100[b]	103a-F	6.7	JLG
		Pb 10101[b]	IIa-O	4.5	JLG
		Pb 10105[a]	IIa-D	6.7	JLG
		Pb 10105[b]	103a-F	6.7	JLG

Table 2 (continued)

PLATE MATERIAL

HD	Name	Plate No.	Emulsion	Dispersion	Observer
219134	HR 8832	Pc 6239	IIa-O	9.0	OCW
		Pb 10117[a]	IIa-D	6.7	JLG
		Pb 10117[b]	103a-F	6.7	JLG
32147	HR 1614	Ce 14303	IIa-O	9.0	OCW
		Ce 19404	IIa-D	16.3	VO
		Pb 9999[a]	IIa-D	6.7	JLG
		Pb 9999[b]	IIa-E	6.7	JLG
201092	61 Cyg B	Pb 9625[b]	IIa-O	4.5	JLG
		Pb 9633[a]	IIa-D	6.7	JLG
		Pb 9633[b]	IIa-F	6.7	JLG
28307	θ^1 Tau	Ce 11661[1]	103a-D	6.4	GW
		Ce 14280	103a-D	6.4	GW
		Ce 15028[b]	103a-D	6.4	GW
		Ce 16536[b]	103a-F	6.4	GW
27371	γ Tau	Ce 13171	103a-D	6.4	GW
		Ce 13173	IIa-F	6.4	GW
28305	ε Tau	Ce 11581[1]	IIa-D	6.7	WKB
		Ce 11660[1]	103a-D	6.7	WKB
		Ce 11660[2]	103a-F	6.7	WKB
		Ce 16536[a]	103a-F	6.4	GW
221148	HR 8924	Pb 9810[a]	IIa-D	6.7	JLG
		Pb 9810[b]	IIa-F	6.7	JLG
206952	11 Cep	Pb 9799[a]	IIa-D	6.7	JLG
		Pb 9799[b]	IIa-F	6.7	JLG
		Pb 9811[a]	IIa-D	6.7	JLG
		Pb 9811[b]	IIa-F	6.7	JLG
140573	α Ser	Pb 9597[b]	IIa-F	6.7	JLG
		Ce 19733[a]	IIa-D	6.4	VO
		Ce 19733[b]	IIa-D	6.4	VO
		Ce 19734[b]	IIa-F	6.4	VO

Table 2 (continued)

PLATE MATERIAL

HD	Name	Plate No.	Emulsion	Dispersion	Observer
39003	ν Aur	Pb 9804^{a}	IIa-D	6.7	JLG
		Pb 9804^{b}	IIa-F	6.7	JLG
85503	μ Leo	Pb 9806^{a}	IIa-D	6.7	JLG
		Pb 9806^{b}	IIa-F	6.7	JLG
		Pb 9821	IIa-D	6.7	JLG
		Pb 9997^{a}	IIa-D	6.7	JLG
		Pb 9997^{b}	103a-E	6.7	JLG
12929	α Ari	Ce 11427^{1}	IIa-D	6.7	WKB
		Ce 11427^{2}	IIa-F	6.7	WKB
112127		Ce 19732^{a}	IIa-D	16.3	VO
		Ce 19732^{b}	IIa-D	16.3	VO
		Ce 19740	103a-F	16.3	VO
132345	18 Lib A	Pb 9601^{a}	IIa-D	6.7	JLG
		Pb 9601^{b}	IIa-F	6.7	JLG
		Pb 9995^{1}	IIa-D	6.7	JLG
		Pb 9995^{2}	IIa-F	6.7	JLG
		Pb 10103^{a}	IIa-D	6.7	JLG
34334	16 Aur	Ce 19735^{a}	IIa-D	6.4	VO
		Pb 9803^{a}	IIa-D	6.7	JLG
		Pb 9803^{b}	IIa-F	6.7	JLG
98262	ν UMa	Ce 19739^{b}	103a-D	6.4	VO
50778	θ CMa	Ce 19735^{b}	IIa-D	6.4	VO
		Pb 9805^{a}	IIa-D	6.7	JLG
		Pb 9806^{b}	IIa-F	6.7	JLG
139669	θ UMi	Pb 7336^{2}	IIa-F	6.7	JLG
		Pb 8125$^{A}_{I}$	IIa-D	6.7	JLG
		Pb 8125$^{A}_{II}$	IIa-D	6.7	JLG
		Pb 8125$^{B}_{I}$	IIa-F	6.7	JLG
		Pb 8125$^{B}_{II}$	IIa-F	6.7	JLG
		Pb 8268^{1}	IIa-D	6.7	JLG

Table 2 (continued)

PLATE MATERIAL

Observers:

JLG - Greenstein, J. L.
WKB - Bonsack, W. K.
OCW - Wilson, O. C.
JBO - Oke, J. B.
SJA - Adelman, S. J.
VO - Oinas, V.
RPK - Kraft, R. P.

The line list was compiled with the aid of the second revision of Rowland's Atlas (Moore, Minnaert, and Houtgast 1966) and the Utrecht Atlas (Minnaert, Mulders, and Houtgast 1940). Only lines relatively free from blending were chosen, in the belief that a small amount of good data is far superior to a large collection of doubtful measurements.

Except for the strongest lines, all the measurements were done using the triangle approximation - if the line was weak its area was approximated as nearly as possible by drawing a triangle directly on the tracing. In the case of stronger lines a triangle was also drawn to measure the wing area, and a planimeter was used for very strong damping lines.

Since spectrograms taken at two different telescopes as well as with somewhat varying dispersions were employed, it was important to determine whether this resulted in any systematic differences between the measured line strengths. In particular, Helfer and Wallerstein (1968) obtain slightly greater equivalent widths from Mt. Wilson spectra than they do from Palomar material. In order to check this effect, equivalent widths from Mt. Wilson and Palomar plates were plotted against each other for 70 Oph A and 16 Aur. In the case of 70 Oph A there was no systematic difference, while for 16 Aur lines weaker than log $w/\lambda = -4.8$ tended to be stronger by about .05 dex in the Mt. Wilson measurements.

This difference could be entirely due to a slight difference in the placement of the continuum (the continuum is much easier to locate in the hotter dwarf 70 Oph A), and is not considered significant. In order to check the effects of varying dispersion, equivalent widths measured on 6.7 Å/mm and 16.3 Å/mm plates (for HR 1614) were plotted against each other, and a definite trend in the direction of larger equivalent widths for the lower dispersion was apparent. Beginning at about log $w/\lambda = -4.5$ the discrepancy reaches a maximum of approximately .10 dex at log $w/\lambda = -5.0$. Since there is good agreement for log $w/\lambda > -4.5$, the discrepancy is probably due to differences in the placement of the continuum, since lines that were possible unresolved blends in the 16.3Å/mm spectrum were eliminated by comparison with the tracing of the higher resolution plate. Measurements made at the lower dispersion were given 1/3 weight when calculating the mean in the case of HR 1614. The only stars for which there are only 16.3 Å/mm plates available are 54 Psc and HD 112127. In the case of the former the line spectrum is considerably weaker than in HR 1614; therefore, errors in the placement of the continuum and the inclusion of possible blends should be diminished. In the case of the SMR candidate HD 112127, however, some error is to be expected in the strengths of the weaker lines, and the results for this star are necessarily of lower weight than for the others.

Comparison of the equivalent widths with those derived by other observers is obviously in order. In particular, very good agreement is achieved with the results of Strom et al. (1971) for μ Leo and with Griffin (1969) for θ^1 Tau. The values obtained by Helfer and Wallerstein (1964), however, are all systematically too high by about .07 to .10 dex, even though the very same plates measured by them were used in the present work. Griffin (1969) notes similar differences between his measurements and those of Helfer and Wallerstein (1964). Some discrepancies are also apparent in a comparison with Mrs. Cayrel's (1966) measurements of HR 8832 on 12.5 Å/mm spectra, in that her values tend to be about .06 dex too high. These results point to the necessity of having all spectra reduced and measured by the same individual if uniformity is to be achieved.

It should be noted that the instrumental profile of a spectrograph is of the dispersion type (van de Hulst and Reesinck 1947), which will result in substantial wing structure even in weak spectral lines. The usual effect will be a placement of the continuum that is too low, particularly in fairly crowded regions of the spectrum. For this reason the measured equivalent widths may all be slightly too small, but since all the conclusions in this work depend on relative line strengths and abundances, a constant correction factor will not have much effect.

IV. PHOTOELECTRIC OBSERVATIONS

a) 60" Observations

The second major observational basis on which this work rests is a series of narrow-band photoelectric measurements obtained for the program stars with the Cassegrain scanner at the 60" telescope on Mt. Wilson. The instrument has been described previously by Oke (1964). It features Ebert-Fastie optics and a plane grating which provides a dispersion of 10 Å/mm in the second order; the wavelength is changed by rotating the grating, with a setting accuracy of about 1 Å. An RCA 7102 tube cooled to dry ice temperature was used for all the measurements, which extended from 5000 Å to 10800 Å.

The main purpose of the scans was to obtain accurate temperatures for the stars by a comparison with predicted fluxes from model atmospheres. Several wavelengths were also included between 7000 Å and 9000 Å in order to provide information about the CN red system. The band width employed was generally 40 Å, although a 20 Å width was also used for many of the brighter stars. The instrument was not actually used to "scan" the spectra; rather measurements were made at discrete wavelengths with integration times chosen to provide good photon counting statistics (at least 2000 total counts per setting). A series of measurements was always repeated in the opposite direction in wavelength, and if agreement was not good to a few percent the data was discarded. The

wavelengths (Table 3) were chosen to fall in regions of uniform line absorption and near the Oke (1970) standard points. Several wavelengths were added during the latter part of the observing program, so that some of the stars have more complete data than others.

Calibration of the instrumental intensities was provided by observations of standard stars (Oke 1964), of which a minimum of three were included during each night's run. The absolute calibration rests ultimately on the energy distribution of Vega, which has undergone rather large revisions during the past few years. The two most recent calibrations, those of Hayes (1970) and Oke and Schild (1970), show excellent agreement except for wavelengths longward of 1μ and shortward of the Balmer jump, where the Oke values are brighter by about .05 mag. The Oke and Hayes calibrations agree at 9950 Å, but the use of Hayes' calibration for wavelengths beyond this point results in a pronounced dip with respect to 9950 Å in the case of the hotter dwarfs, which are quite free of blanketing in this region (except at 10800Å). Oke's calibration was therefore used in all the reductions (a difference of .05 mag produces a change of less than 100° in the derived temperatures). The atmospheric extinction coefficients employed are listed by Oke (1965), who also describes the general reduction procedure. The computer program that was used to do the calculations was originally written by

TABLE 3

SCANNER WAVELENGTH LIST

λ(Å)	Oke's λ's
5000	5000
5100	
5263	5263
5350	
5460	
5546	5556
5584	
5638	
5730	
5750	
5832	5840
5892	
6055	6050
6370	6370
6440	
6720	
6800	6800
6820	
7100	7100
7400	
7530	7550
7850	7850
8080	8080
8400	8400
8804	8804
9950	9950
10250	10250
10400	10400
10520	
10800	10800

J. B. Oke and later modified by Robert O'Connell, whom I thank for instruction in its use.

b) The Taylor and ST Scans

The spectral scans of ST and Taylor (1970) are based on an instrumental intensity system defined by observations of a set of standard stars with the Wampler scanner at Lick Observatory. These include three of the Oke standard stars (29 Psc, 109 Vir and 58 Aql), a circumstance which allows a transformation to the absolute intensity system. Unfortunately, one of the stars (58 Aql) has an absolute calibration that extends only to 6055 Å, while of the two remaining stars one (29 Psc) is stated by ST as having somewhat lower accuracy with respect to the instrumental system. Transformation coefficients were calculated for each of the stars, and the values for 29 Psc were given 1/3 wt. in computing the mean. For wavelengths greater than about 5000 Å the internal agreement for the three stars is quite good (within a few percent) but for wavelengths closer to 4000 Å the discrepancies become rather large (10% in some cases). ST and Oke (1964) both claim internal accuracy to within a few percent for their measurements so it is difficult to decide where the error lies. In any case, the transformation to the absolute system is accurate to a few percent in the main region of interest ($\lambda > 5000$ Å), while for shorter wavelengths the standard deviation is on the order of five percent. All the stars in

the program that were also studied by ST and Taylor (1970) were converted to the absolute system for comparison with the results obtained with the 60" telescope and in order to extend the wavelength range below 5000 Å. Figure 1 illustrates the comparison in the case of ρ^1 Cnc - as can be seen the agreement is quite good.

c) Blanketing Corrections

In order to compare the measured energy distributions with fluxes from model atmospheres it is necessary to correct for the effects of line absorption in the various passbands. This was done by measuring the energy subtracted from the continuum by planimetry of the tracings. The usual blanketing coefficients η are defined by

$$\eta = 1 - \frac{\int F_\lambda d\lambda}{\int F_c d\lambda}$$

where F_λ and F_c refer to the observed flux and the estimated continuum respectively and the integrals are taken over the width of the band. The η's were converted to differences in magnitude Δm and these quantities are tabulated in Table 4 ($\Delta m \sim \eta$ for small η). The 15 Å and 30 Å measurements refer to passbands employed by ST or Taylor (1970), who used a 30 Å band width for wavelengths greater than 5360 Å and 15 Å for shorter wavelengths. Both widths were used for the normalization band at 5360 Å, at which point the grating order was

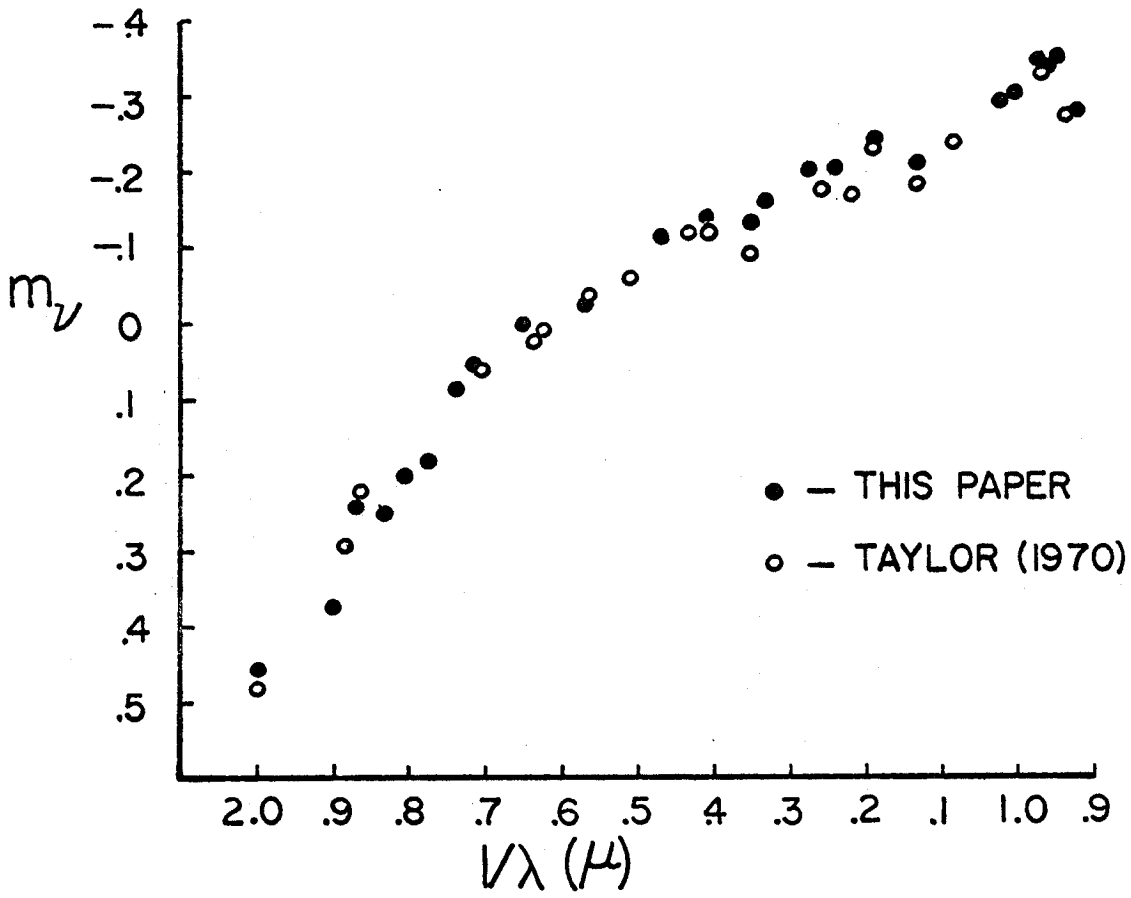

Fig. 1.--Comparison of the energy distribution of ρ^1 Cnc obtained in this work with Taylor's (1970) data.

TABLE 4

BLANKETING CORRECTIONS Δm

λ(Å)	$\Delta\lambda$	ξ Boo A	70 Oph A	ρ^1 Cnc	14 Her	σ Dra	54 Psc
5000	15			.28	.28		.26
	20		.18	.26	.25		.23
	40		.20	.27	.27		.23
5100	40						.20
5264	40	.16		.27	.27		.25
5300	15	.10		.18	.16		.13
5350	20	.08	.10	.12	.13		.11
	40		.10	.12	.12		.11
5360	15	.06		.09	.09		.09
	30	.10		.14	.14		.14
5460	40	.08		.14	.14		.13
5546	20		.05	.08	.08		.07
	40	.06	.07	.10	.10		.09
5584	20			.16	.16		.15
5638	20	.04	.06	.09	.08		.06
	40		.07	.09	.10		.08
5731	20		.03	.03	.04		.03
5750	40	.03	.05	.04	.05		.04
5832	20		.02	.03	.02		.02
	40	.01	.02	.03	.02		.02
5864	30	.03		.06	.06		.05
5892	20			.27	.30		
	30	.08					.17
6044	20		.02	.02	.02		.02
6055	40	.02	.02	.02	.02	.04	.02
6110	30	.05		.07	.07		.07
6180	30	.06		.07			.07
6370	40	.02		.04	.04	.02	.03
6382	20			.02	.02		.01
6386	30	.03		.05	.05		.04
6440	40					.03	.07
6620	30	.02			.05		.02
6720	40						.05
6800	40	.01			.03		.07
6820	20				.03		.07

Table 4 (continued)

BLANKETING CORRECTIONS Δm

λ(Å)	Δλ	ε Eri	HR 6806	HR 8832	HR 1614	61 Cyg B	θ^1 Tau
5000	15	.23	.22	.26	.33	.30	.30
	20		.18	.23	.31	.31	
	40	.24	.20	.26	.34	.33	.31
5100	40	.20	.20	.34		.47	
5264	40	.27	.20	.28	.33	.30	.25
5300	15	.15	.12	.17	.22	.17	.19
5350	20		.09	.12	.18	.18	
	40	.14	.09	.13	.18	.17	.14
5360	15	.08	.06	.11	.13	.13	.11
	30	.14	.12	.17	.20	.19	.15
5460	40	.13	.10	.15	.18	.20	.15
5546	20		.04	.08	.10	.10	
	40	.09	.06	.10	.13	.12	.12
5584	20		.11		.20	.18	
5638	20		.05	.08	.10	.08	
	40	.08	.06	.09	.11	.09	.14
5731	20		.03	.05	.08	.07	
5750	40	.06	.03	.06	.08	.06	.09
5832	20		.02	.02	.04	.04	
	40	.02	.02	.02	.04	.04	.07
5864	30	.07	.04	.05	.08	.07	.11
5892	20		.21			.60	
	30	.19		.23	.36	.40	.19
6044	20		.01	.01	.03		
6055	40	.03	.02	.02	.05		.06
6110	30	.08	.07	.08	.12	.15	.10
6180	30	.07	.07	.09	.12	.15	.12
6370	40	.03	.03	.04	.05	.12	.09
6382	20		.01	.02	.03	.15	
6386	30	.05	.03	.06	.07	.18	.08
6440	40	.06	.04	.07		.09	.09
6620	30	.03	.03			.04	.07
6720	40	.04	.03	.05		.06	
6800	40	.03	.02	.04		.14	
6820	20			.04		.16	

Table 4 (continued)

BLANKETING CORRECTIONS Δm

λ(Å)	Δλ	γ Tau	ε Tau	HR 8924	11 Cep.	α Ser	ν Aur
5000	15		.30	.39	.30	.36	.26
	20				.27	.33	.23
	40		.31	.38	.31		.26
5100	40	.18	.19				
5264	40	.27	.28		.34		.30
5300	15		.20	.24	.23	.27	.20
5350	20	.14			.17	.21	.16
	40		.16	.20	.18		
5360	15		.09	.14	.13	.15	.13
	30		.14	.20	.18	.22	.16
5460	40	.15	.15		.18		
5546	20				.13	.15	.11
	40	.12	.13	.15	.14		.13
5584	20				.19	.21	.15
5638	20				.12	.17	
	40	.14	.13	.18	.14		.14
5731	20					.14	
5750	40	.09	.09	.12			.09
5832	20				.06	.08	
	40	.07	.07	.08	.07		.04
5864	30		.09	.11	.09	.13	.07
5892	20				.25	.32	
	30		.17	.33	.20	.25	.14
6044	20				.04	.06	
6055	40	.06	.06	.07	.06		
6110	30		.09	.10	.12	.12	
6180	30		.12	.13	.14	.14	
6370	40	.08	.12	.12	.09		
6382	20				.07	.09	
6386	30		.10	.12	.08	.12	
6440	40	.08	.09		.09		
6620	30		.08		.10	.12	
6720	40	.09	.08		.09		
6800	40	.06	.06	.12	.08		.06
6820	20			.12	.07	.06	.05

Table 4 (continued)

BLANKETING CORRECTIONS Δm

λ(Å)	Δλ	μ Leo	α Ari	HD 112127	18 Lib A	16 Aur	ν UMa
5000	15	.39	.30	.36	.39	.25	
	20	.36		.33	.35	.23	
	40	.39		.36	.39	.26	
5100	40						
5264	40	.37		.36	.42	.30	
5300	15	.27	.21	.25	.30	.21	
5350	20	.19		.22	.21	.15	.24
	40	.19		.22		.15	
5360	15	.13	.14	.16	.15	.13	
	30	.20	.19	.23	.21	.16	
5460	40	.20		.25	.24	.15	
5546	20	.12		.20	.17	.11	.16
	40	.15		.23	.19	.13	
5584	20	.20		.31	.24	.15	.20
5638	20	.15		.22	.18	.12	.17
	40	.17		.24	.19	.13	
5731	20	.13		.14	.16		.16
5750	40	.14		.16	.17	.09	
5832	20	.08		.10	.10	.05	.09
	40	.08		.11	.11	.07	
5864	30	.10	.09	.15	.12	.09	
5892	20	.39		.40	.37		.36
	30	.28	.18	.32	.29	.18	
6044	20	.07		.08			.08
6055	40	.08		.10		.07	
6110	30	.14	.10	.16		.10	
6180	30	.14	.12	.16	.18	.11	
6370	40	.14		.16	.16	.10	
6382	20	.12		.11	.12		
6386	30	.14	.08	.13	.16	.09	
6440	40						
6620	30	.13	.09	.14		.07	
6720	40						
6800	40	.12				.06	
6820	20	.09					

Table 4 (continued)

BLANKETING CORRECTIONS Δm

λ(Å)	$\Delta\lambda$	θ CMa	θ UMi
5000	15		
	20	.30	
	40		
5100	40		
5264	40		
5300	15		.37
5350	20	.20	.29
	40		
5360	15		.18
	30		.27
5460	40		
5546	20	.16	.18
	40		
5584	20	.21	.24
5638	20	.15	.20
	40		
5731	20	.14	.18
5750	40		
5832	20	.08	.12
	40		
5864	30		.16
5892	20	.28	.53
	30		.42
6044	20	.05	.08
6055	40		
6110	30		.14
6180	30		.19
6370	40		
6382	20	.07	.19
6386	30		.17
6440	40		
6620	30		
6720	40		.15
6800	40	.08	
6820	20		

changed. The choice of 5360 Å as the fitting point for the 30 Å and 15 Å scans is rather unfortunate, however, in that there are large differences in the mean blanketing under the two bands at this wavelength; i.e., while the 15 Å band contains few strong lines, a somewhat wider band covers several very strong ones. This difference had to be taken into account when the scans were converted to the absolute system, with the direction of the change being such that the points below 5360 Å must be raised by an amount equal to the difference in the blanketing under the 30 Å and 15 Å bands. This circumstance necessarily introduces some additional error into the energy distribution for shorter wavelengths.

The scanner intensities obtained with the 60" telescope are listed in Table 5 with the results expressed in magnitudes and normalized to m_v=.00 at 6055 Å. Although most stars had measurements taken with 20 Å and 40 Å passbands, only the 40 Å data are listed unless exclusively 20 Å measurements were made. Aside from a few exceptions, all the intensities are a mean from two or more scans - in the few cases where there is only one scan available there is good agreement with the intensities obtained at 20 Å. Two of the program stars, 70 Oph A and α Ari, do not appear in Table 5. In the former, the secondary is too close to permit separation from the primary star image in the scanner entrance aperture, and in the case of the latter no scans were taken since the star

TABLE 5

SCANNER ENERGY DISTRIBUTIONS m_ν

λ(Å)	1/λ	ξ Boo A	ρ^1 Cnc	14 Her	σ Dra	54 Psc	ε Eri
5000	2.000	.36	.46	.47	.41	.51	.50
5100	1.960				.39	.47	.48
5264	1.900	.29	.37	.36	.32	.39	.38
5350	1.869	.24	.24	.28	.23	.25	.28
5460	1.832	.19	.25	.24	.20	.25	.24
5546	1.803	.14	.20	.21	.15	.20	.17
5584	1.791						
5638	1.774	.15	.18	.18	.14	.18	.15
5731	1.745						
5750	1.739	.07	.09	.07	.09	.10	.08
5832	1.715	.06	.06	.05	.05	.07	.04
5892	1.697						
6044	1.655						
6055	1.651	.00	.00	.00	.00	.00	.00
6370	1.570	-.01	-.03	-.01	-.05	-.02	-.06
6382	1.567						
6440	1.553				-.05	-.02	-.06
6720	1.488				-.08	-.09	-.13
6800	1.471	-.08	-.11	-.12	-.09	-.10	-.15
6820	1.466						
7100	1.408	-.15	-.14	-.12		-.12	
7400	1.351		-.13				
7530	1.328	-.16	-.16	-.16		-.17	
7850	1.274	-.17	-.21	-.21		-.18	
8080	1.238	-.18	-.21	-.20		-.19	
8400	1.190	-.23	-.24	-.27	-.30	-.25	-.34
8804	1.136	-.17	-.21	-.17	-.24	-.20	-.28
9700	1.031	-.28	-.29	-.28			
9950	1.005	-.28	-.31	-.32	-.36	-.33	-.42
10250	.976	-.26	-.34	-.34	-.37	-.34	-.44
10400	.962	-.28	-.34	-.35	-.37	-.35	-.44
10520	.951	-.28	-.35	-.34	-.37	-.37	-.46
10800	.926	-.27	-.28	-.30		-.28	

Table 5 (continued)

SCANNER ENERGY DISTRIBUTIONS m_ν

λ(Å)	1/λ	HR 6806	HR 8832	HR 1614	61 Cyg B	θ^1 Tau	γ Tau
5000	2.000	.50	.65	.71	1.08	.56	.56
5100	1.960	.46	.67		1.20	.44	.47
5264	1.900	.34	.51	.55	.72	.40	.42
5350	1.869	.27	.37	.42	.59	.28	.30
5460	1.832	.24	.32	.33	.53	.24	.26
5546	1.803	.21	.26	.26	.38	.20	.20
5584	1.791						
5638	1.774	.16	.21	.24	.30	.18	.18
5731	1.745						
5750	1.739	.09	.13	.18	.18	.10	.12
5832	1.715	.05	.08	.08	.13	.06	.06
5892	1.697						
6044	1.655						
6055	1.651	.00	.00	.00	.00	.00	.00
6370	1.570	-.07	-.05	-.01	-.07	-.04	-.02
6382	1.567						
6440	1.553	-.11	-.06		-.14	-.05	-.05
6720	1.488	-.15	-.14		-.23	-.11	-.13
6800	1.471	-.16	-.15	-.14	-.21	-.14	-.15
6820	1.466						
7100	1.408	-.20	-.20	-.19	-.40		
7400	1.351			-.26			
7530	1.328	-.28	-.28	-.26	-.59		
7850	1.274	-.30	-.32	-.32	-.66		
8080	1.238	-.31	-.33	-.32	-.73		
8400	1.190	-.35	-.40	-.37	-.79	-.33	-.32
8804	1.136	-.28	-.34	-.35	-.77	-.30	-.30
9700	1.031			-.49			
9950	1.005	-.43	-.51	-.51	-1.01	-.44	-.43
10250	.976	-.48	-.53	-.54	-1.04	-.47	-.47
10400	.962	-.45	-.54	-.55	-1.05	-.46	-.47
10520	.951	-.48	-.55	-.55	-1.06	-.47	-.48
10800	.926	-.48	-.47	-.53	-1.04		

Table 5 (continued)

SCANNER ENERGY DISTRIBUTIONS m_ν

λ(Å)	1/λ	ε Tau	HR 8924	11 Cep	α Ser	ν Aur	μ Leo
5000	2.000	.56	.64	.64	.64	.57	.73
5100	1.960	.47		.60			
5264	1.900	.46		.47			.57
5350	1.869	.31	.33	.33	.35	.33	.41
5460	1.832	.26		.30			.36
5546	1.803	.23	.25	.25	.25	.22	.30
5584	1.791						
5638	1.774	.20	.27	.24	.26	.22	.29
5731	1.745				.16		
5750	1.739	.12	.17	.15		.15	.17
5832	1.715	.07	.07	.08	.08	.08	.09
5892	1.697				.30		
6044	1.655				.00		
6055	1.651	.00	.00	.00		.00	.00
6370	1.570	-.03	-.01	-.03	-.05	-.06	-.01
6382	1.567						
6640	1.553	-.06		-.06			
6720	1.488	-.12		-.15			
6800	1.471	-.15	-.15	-.17		-.19	-.17
6820	1.466				-.18		
7100	1.408		-.16	-.17	-.18	-.23	-.17
7400	1.351						-.24
7530	1.328		-.26	-.28	-.30	-.30	-.29
7850	1.274		-.34	-.35	-.36	-.37	-.39
8080	1.238		-.31	-.29		-.36	-.33
8400	1.190	-.31	-.38	-.39	-.39	-.41	-.41
8804	1.136	-.30	-.38	-.39	-.41	-.41	-.43
9700	1.031						-.54
9950	1.005	-.43	-.52	-.55		-.57	-.60
10250	.976	-.48	-.57	-.60	-.63	-.62	-.67
10400	.962	-.49	-.57	-.58	-.63	-.62	-.67
10520	.951	-.51	-.58	-.61	-.64	-.62	-.71
10800	.926		-.53	-.55	-.64	-.61	-.66

Table 5 (continued)

SCANNER ENERGY DISTRIBUTIONS m_ν

λ(Å)	1/λ	HD 112127	18 Lib A	16 Aur	ν UMa	θ CMa	θ UMi
5000	2.000	.72	.71	.74	.85	.91	1.03
5100	1.960						
5264	1.900	.56	.57	.58			
5350	1.869	.41	.39	.44	.44	.53	.51
5460	1.832	.36	.34	.39			
5546	1.803	.31	.30	.30	.30	.34	.35
5584	1.791				.34	.37	.42
5638	1.774	.29	.26	.26	.30	.32	.41
5731	1.745				.23	.25	.25
5750	1.739	.15	.16	.18			
5832	1.715	.08	.08	.11	.11	.13	.14
5892	1.697				.32	.33	.54
6044	1.655				.00	.00	.00
6055	1.651	.00	.00	.00			
6370	1.570	-.01	-.01	-.08			
6382	1.567				-.08	-.10	-.10
6440	1.553						
6720	1.488						
6800	1.471	-.18	-.20	-.22			
6820	1.466				-.25	-.25	-.29
7100	1.408	-.19	-.23	-.30	-.30	-.32	-.31
7400	1.351	-.28	-.26	-.38			
7530	1.328	-.34	-.36	-.42	-.46	-.53	-.66
7850	1.274	-.42	-.45	-.49	-.44	-.59	-.71
8080	1.238	-.36	-.36	-.50			
8400	1.190	-.44	-.45	-.57	-.63	-.68	-.83
8804	1.136	-.49	-.53	-.60	-.63	-.71	-.85
9700	1.031	-.59	-.60	-.75			
9950	1.005	-.68	-.69	-.80			
10250	.976	-.71	-.76	-.84	-.91	-1.02	-1.17
10400	.962	-.73	-.77	-.86	-.92	-1.00	-1.18
10520	.951	-.73	-.81	-.87	-.93	-1.03	-1.22
10800	.926	-.72	-.75	-.85	-.94	-1.04	-1.22

was added too late in the program. ST scans, transformed to the absolute system are, however, available for α Ari. The ST and Taylor (1970) scans are not listed here but the transformation coefficients R(λ) from their instrumental system to the absolute system are given in Table 6. R(λ) is defined as

$$R(\lambda) = \frac{10^{-.4m_v}}{I(\lambda)}$$

where I(λ) is the instrumental intensity normalized to 1000 at 5360 Å.

For purposes of illustration deblanketed scans of ρ^1 Cnc, HR 8832, HR 8924 and HD 112127 are shown in Figures 2-5, with the continuum from the appropriate models drawn in. No blanketing measurements could be made in the 1μ region, so the continuum fit is a bit uncertain at this point. However, Griffin (1964) has published equivalent widths of all measureable lines in the 1μ region of Arcturus (K2IIIp) from tracings of I-Z plates obtained at Mt. Wilson. These measurements were used to calculate the blanketing in the relevant passbands, with the result that all the corrections are on the order of .01 mag. A comparison of Arcturus and Betelgeuse (K5III) in this region by Griffin (1964) reveals that the spectra are remarkably similar, even though great differences are apparent at shorter wavelengths. Furthermore, an

TABLE 6

COEFFICIENTS R(λ)* FOR TRANSFORMATION OF ST INSTRUMENTAL SCANS TO OKE (1970) ABSOLUTE SYSTEM

λ(A)	R(λ)x10^8
4040	.78
4200	.79
4227	.81
4300	.88
4340	.93
4364†	.96
4384†	.96
4474†	1.08
4500	1.06
4715	1.39
4788†	1.58
4900	2.11
5000	1.91
5175	1.90
5300	2.37
5360	2.68
5864	3.37
5892	3.43
6110	3.51
6180	3.65
6386	4.40
6564	5.25
6620	5.91
7000	12.6
7100	15.9
7400	42.4
7980	58.4
8190	65.1
8400	76.1
8662	79.0
8800	81.6
9200	108.
10300	221.
10700	394.

*R(λ) is defined on page 37

†From Taylor's (1970) scans

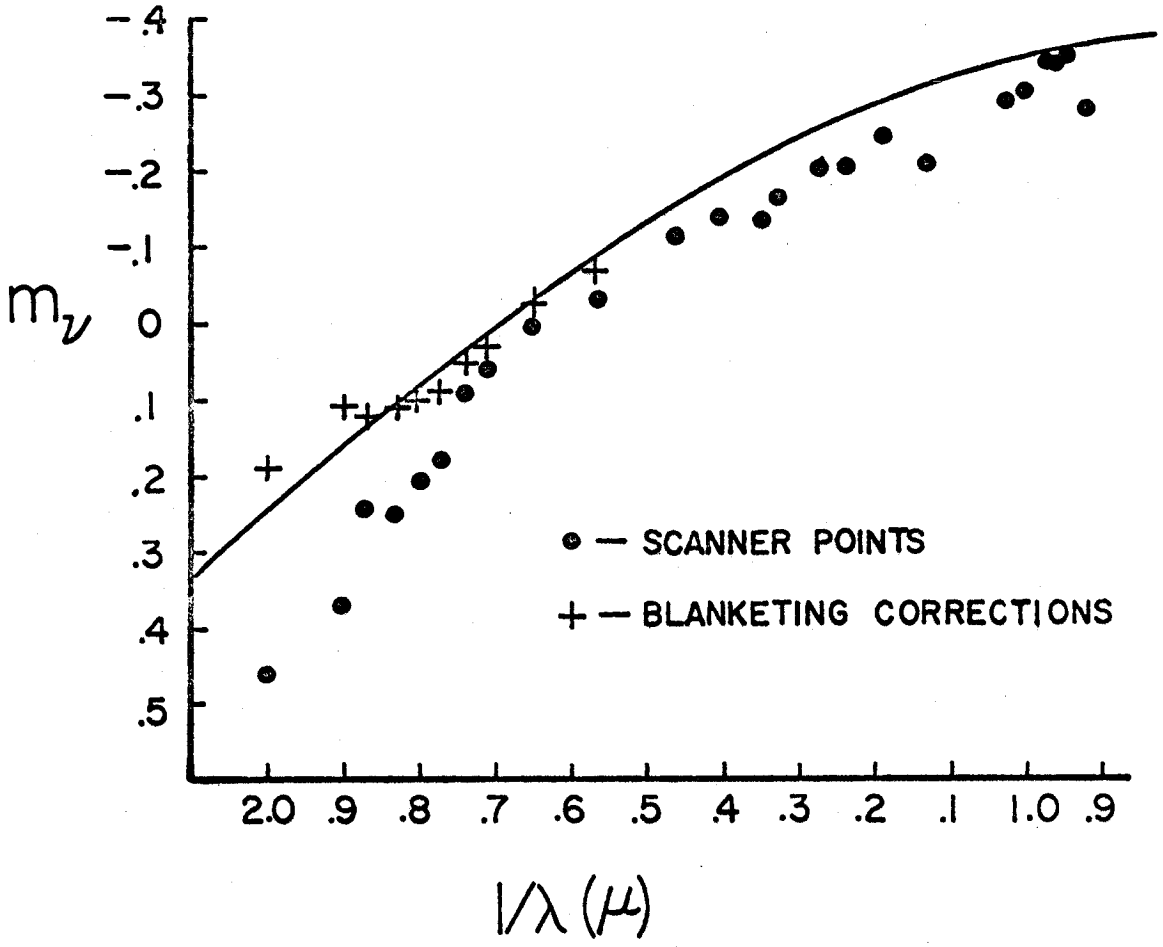

Fig. 2.--ρ^1 Cnc: deblanketed scan with the energy distribution from the adopted model (T_{eff} = 5400 K) drawn in.

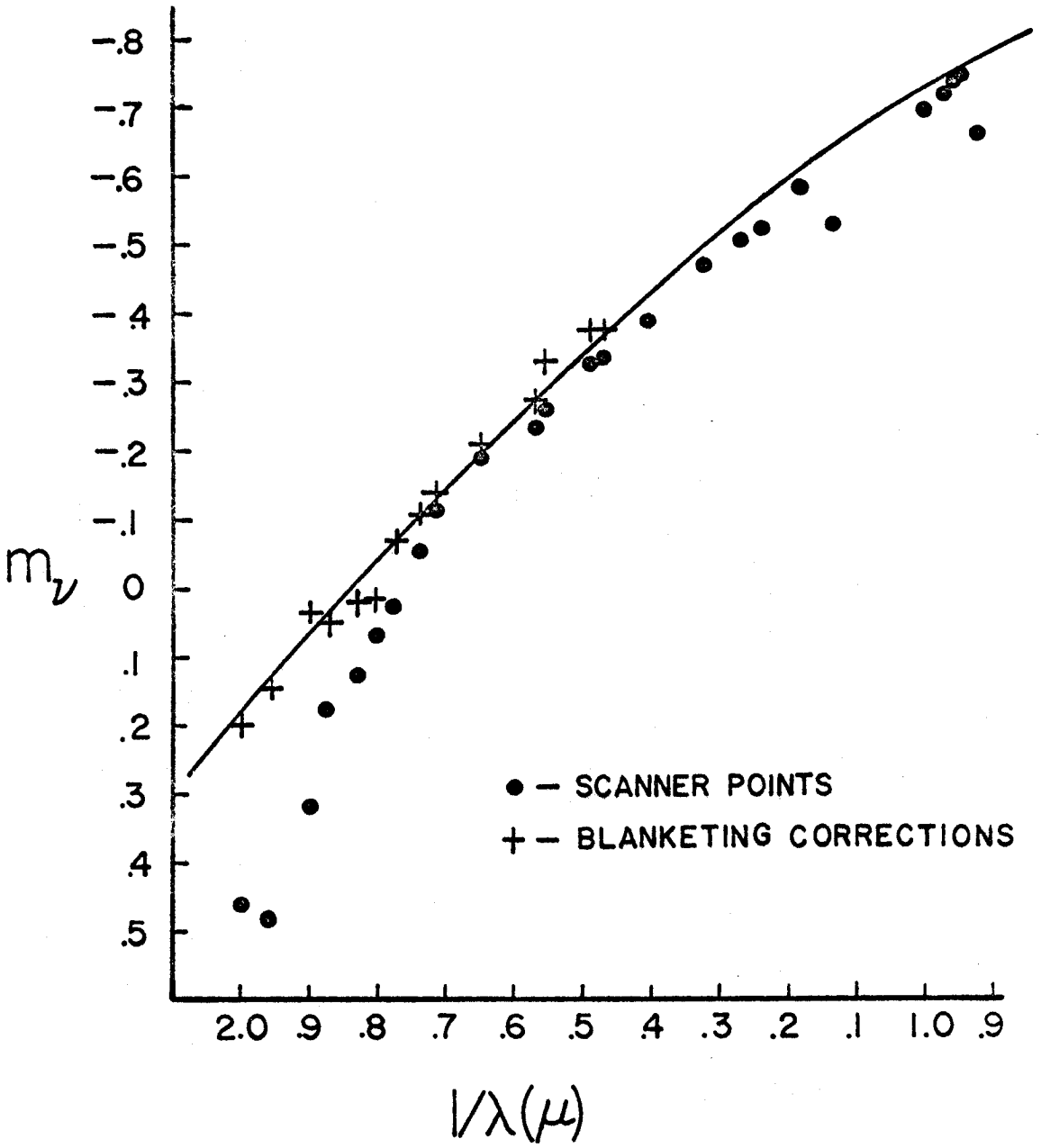

Fig. 3.--HR 8832: deblanketed scan with the energy distribution from the adopted model (T_{eff} = 4800 K) drawn in.

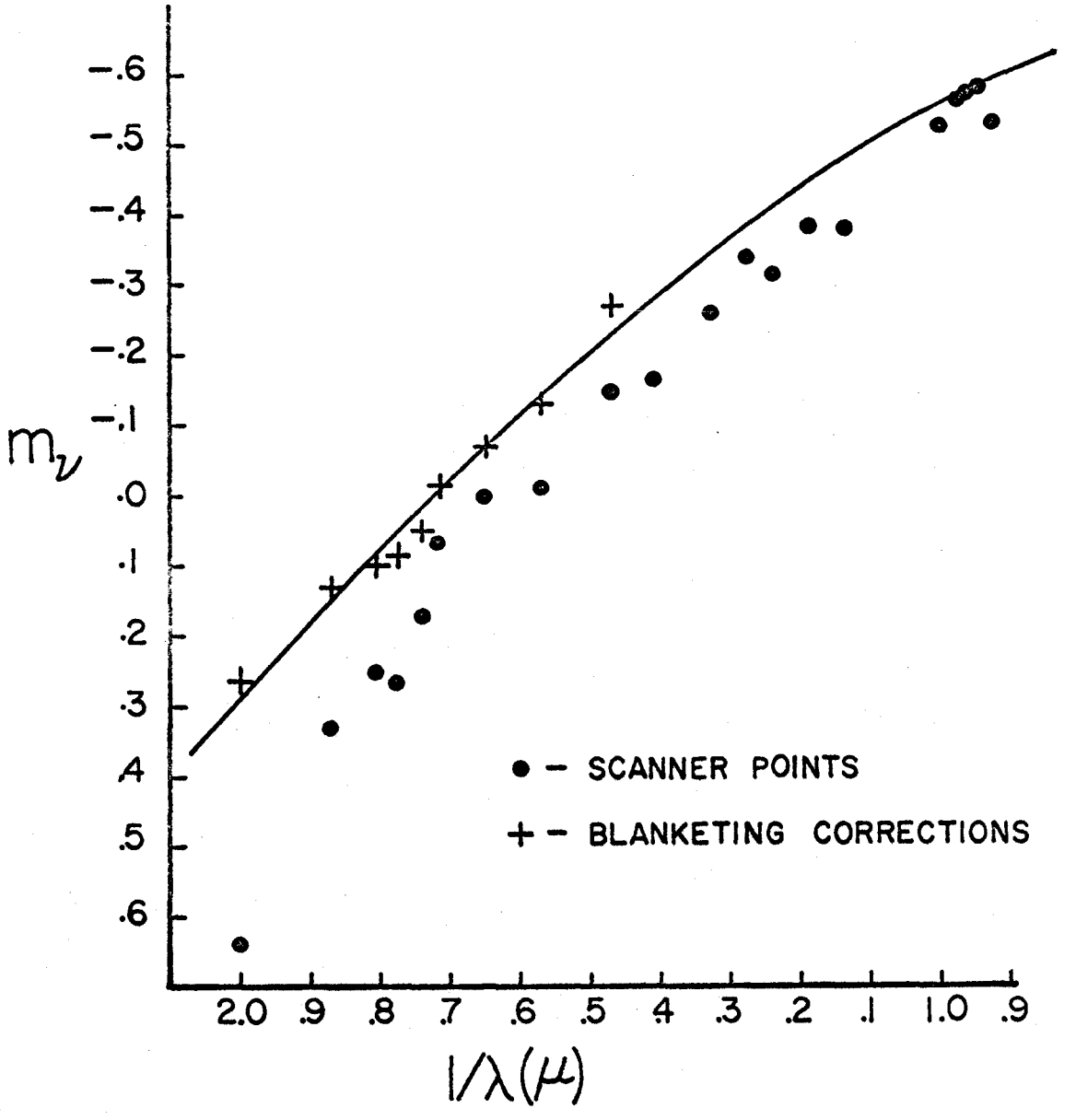

Fig. 4.--HR 8924: deblanketed scan with the energy distribution from the adopted model (T_{eff} = 4900 K) drawn in.

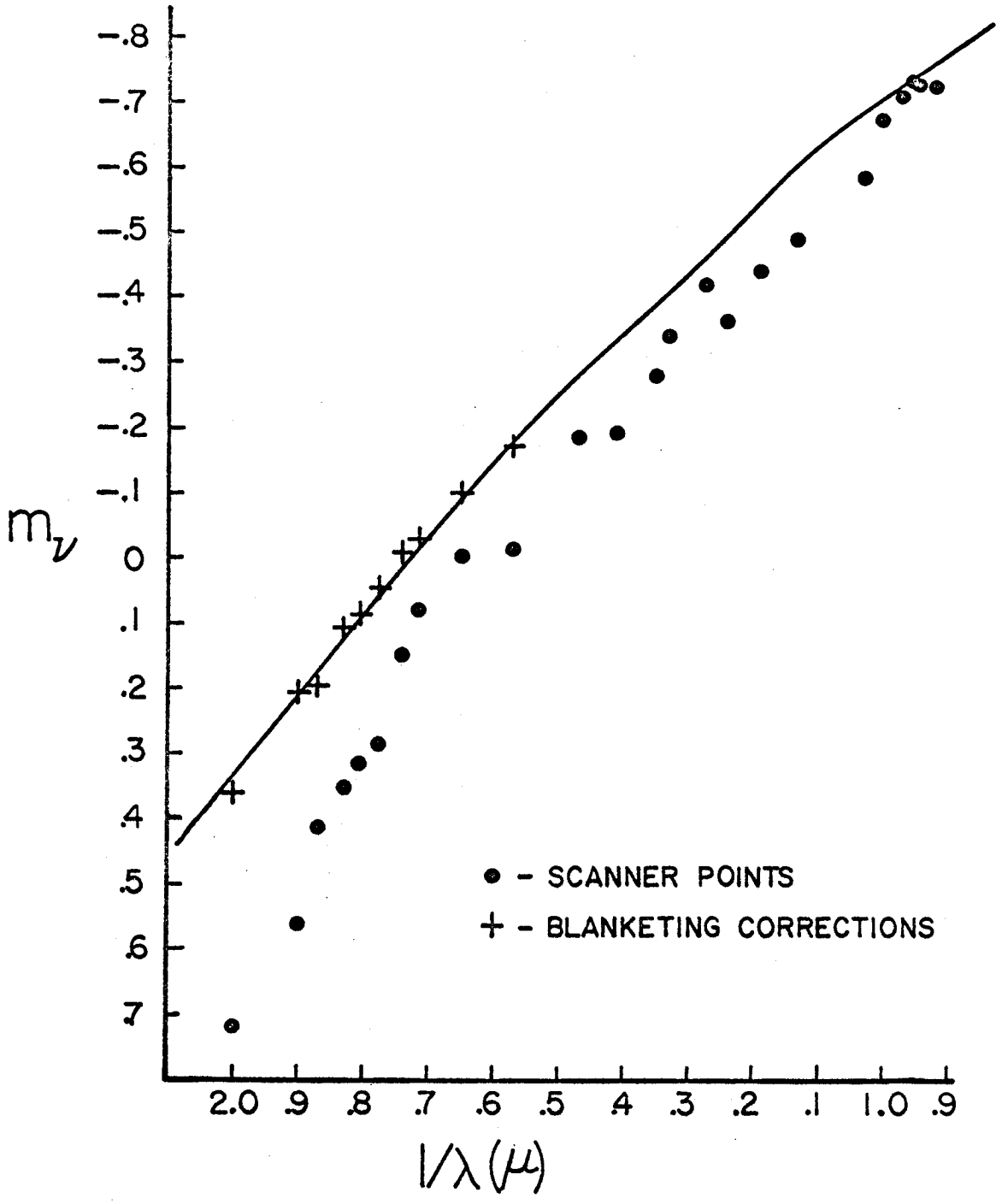

Fig. 5.--HD 112127: deblanketed scan with the energy distribution from the adopted model (T_{eff} = 4600 K) drawn in.

inspection of the 1μ region in the solar spectrum (Mohler et al. 1950) reveals entirely negligible blanketing. It therefore seems safe to assume that blanketing will be quite small even for the coolest stars in the program, particularly since there is no contamination of the passbands by the CN red system (Davis and Phillips 1963).

Two rather surprising features are revealed by an inspection of the scans. The most striking is the persistence of a large dip at 8804 Å that is present in all the program stars and often amounts to more than .1 mag. That the dip cannot be due to a sharp spectral feature is shown by the fact that the same discontinuity is observed with passbands of varying widths. An inspection of the Photometric Atlas of Arcturus (Griffin 1969) reveals the absence of significant blanketing in this region (except for one moderately strong Mg line); the same conclusion is reached in the case of the sun (Mohler et al. 1950). Since Arcturus is known to be a metal-poor star it was thought that the blanketing in the region of interest might be spuriously low. Scans of Arcturus were obtained at the 60" telescope in order to explore this possibility, with the result that the dip at 8804 Å is fully as strong as in the program stars. Two possibilities remain: (1) there is an error in the calibration of Vega; (2) there exists a gradual depression in the continuum near 8804 Å for the stars that have been studied. That the first explanation

is implausible is shown by the fact that the Oke (1964), the Oke and Schild (1970), and the Hayes (1970) calibrations all yield the same dip in the continuum. It is puzzling, however, that there appears to be no correlation of the size of the discontinuity with spectral type or luminosity class. To explore this further a series of scans covering a large range in spectral type (kindly provided by Dr. Hyron Spinrad from his galaxy spectrum synthesis program) was transformed to the absolute system. An inspection of the scans shows that the discontinuity sets in rather abruptly near F0, with little change in depth as one proceeds to later spectral types.

The second notable feature of the deblanketed scans is the persistence of a flux excess at 5264 Å in the dwarfs amounting to approximately .05 mag. Errors in the placement of the continuum on the tracings at this wavelength cannot be the cause since, if anything, the continuum was drawn too low. To reduce the blanketing corrections by .05 mag would necessitate lowering the continuum to a point where it would obviously pass through the upper portions of the absorption lines. Plate calibrations were carefully checked at this point in order to eliminate photometric errors. In order to investigate the possibility that the blanketing correction at neighboring wavelengths might be too low due to a depression of the true continuum by the wings of strong lines on the superposition of many weak lines, synthetic spectra were very

kindly computed by Dr. R. A. Bell for K0 and K3 dwarf models in the regions covered by the 5000, 5264 and 5350 Å passbands. Although the line list in Dr. Bell's program is extensive, no trace of a depression in the continuum was evident. Possible molecular absorption was also investigated, but with negative results. Pending a future clarification of the mystery, the intensities at 5264 and 8804 Å were ignored in the fitting of calculated model fluxes to the observed points.

V. MODEL ATMOSPHERES

a) Description of the models

The model atmospheres used in this work were generated by means of the program Atlas written by R. Kurucz of the Smithsonian Astrophysical and Harvard College Observatories (Kurucz 1969 a, b). The opacities include H^-, H, H_2^+, He^-, Mg, Si, Fe, and electron and Rayleigh scattering. Since H^- is the most important opacity source and the bulk of the electrons are supplied by the metals in all the stars under study, it was essential to include the correct abundances of the important electron donors Mg, Si, Fe (along with Na and Ca in the coolest stars) in the "solar abundance" models. The adopted solar abundances for these elements are given in Table 7; it should be noted that Fe is now recognized as an important supplier of electrons due to the recent revision in its abundance (Gartz et al. 1969).

The usual assumptions of plane-parallel stratification and local thermodynamic equilibrium were employed in all the models. Convection within the framework of the mixing length theory was also included, with the ratio of mixing length to scale height equal to 1. Convection carries only a very small percentage of the flux in the case of the giants and becomes important only in the coolest dwarf 61 Cyg B. The usual choice of 5000 Å for the standard optical depth was not adhered to since the emitted flux in this wavelength

TABLE 7

SOLAR ABUNDANCES*

ELEMENT	ABUNDANCE	SOURCE
He	11.0	1
Fe	7.6	2
Si	7.5	4
Mg	7.5	5
Ca	6.2	5
Na	6.2	3

*Abundances are given as log (el./H)+12

Sources:

1. Peimbert and Costero 1969
2. Gartz et al. 1969
3. Lambert and Warner 1968a
4. Lambert and Warner 1968b
5. Lambert and Warner 1968c

region is rather small in the cooler stars; instead it was decided to calculate the standard opacities at 8000 Å. One convenient result of this choice is that $T(\tau = 1)$ is almost exactly equal to T_{eff} in all the models. The Rosseland mean optical depths were also calculated by the program for purposes of comparison with other model atmospheres.

The models were iterated to one percent flux and flux derivative constancy, except in the case of the deeper layers where convection becomes important. Flux constancy is much too severe a criterion in this case, since fluctuations of only a few degrees can produce large changes in the convective energy transport. Therefore the calculations were terminated when two successive iterations produced essentially the same temperature structure in the layers responsible for the continuous emission. 61 Cyg B presented special difficulties since all attempts at convergence resulted in large oscillations in the temperature. The best flux constancy both in and above the convective zone was achieved by forcing the temperature gradient below $\tau = 1$ to be adiabatic, with the result that the deviation of the flux and flux derivative from constancy is about 4% in the radiative region, a figure which became progressively worse upon subsequent iterations. The first iteration was therefore chosen to represent the star.

Atmospheric parameters believed to be representative of

normal stars were chosen for all the initial models; i.e., solar abundances and logarithmic gravities of 4.4 - 4.6 for the dwarfs and 2.7 - 1.9 for the giants (G9III - K5III). It turns out that the emergent flux is quite insensitive to the gravity and the chemical composition, a result which is due to the fact that H^- remains the dominant opacity source over the entire range of gravities and temperatures used for the models. For purposes of illustration models for a typical dwarf and giant are reproduced in Figures 6 and 7.

b) The Balmer Lines

The hottest stars in the program possess H_α line wings of measurable strength and therefore provide another means of obtaining the temperature. The main source of broadening is collisions with other hydrogen atoms (i.e., resonance broadening) (Traving and Cayrel 1960); in this case there is essentially no dependence on the surface gravity, but there is some dependence on the metal abundance, as can be seen from the following simple argument. The depth at some point in the line wing is given by

$$D \propto \frac{k_\nu}{\kappa}$$

where k_ν and κ denote the absorption in the line and in the continuum, respectively. Assuming the line broadening to be of the resonance type and the continuous absorption to be due to H^-, we have

TEFF 5000. LOG G 4.400 NORMAL ITERATION 1

FRACTIONAL ABUNDANCES HYDROGEN 0.900 HELIUM 0.100

AL-5.70 C-3.50 CA-5.80 CO-7.30 CR-6.60 FE-4.40 K-7.10 MG-4.50 MN-6.90 N-4.10 NA-5.80 NE-3.40 NI-6.10 O-3.20 SI-4.50 TI-7.20

	TAU 8000.	TEMP	PRESSURE	ELECTRON NUMBER	DENSITY	ABSORPTION COEFFICIENT	HEIGHT (KM)	GRADIENTS ADIAB	GRADIENTS RADIAT	ION FRACTIONS H 1	ION FRACTIONS HE 1	ION FRACTIONS HE 2	PER CENT FLUX ERROR	PER CENT FLUX DERIV
1	0.0	4034.1	0.944E 03	0.108E 12	0.375E-08	0.682E-02	0.665E 03	0.40E 00	0.60E-03	1.000	1.000	0.000	0.319	0.500
2	0.100E-02	4043.6	0.189E 04	0.216E 12	0.749E-08	0.133E-01	0.420E 03	0.40E 00	-0.37E-01	1.000	1.000	0.000	0.320	0.431
3	0.133E-02	4021.6	0.305E 04	0.299E 12	0.122E-07	0.187E-01	0.396E 03	0.40E 00	-0.15E-02	1.000	1.000	0.000	0.320	0.650
4	0.178E-02	4041.5	0.354E 04	0.343E 12	0.141E-07	0.210E-01	0.379E 03	0.40E 00	0.13E-01	1.000	1.000	0.000	0.320	0.541
5	0.237E-02	4039.9	0.413E 04	0.382E 12	0.164E-07	0.234E-01	0.362E 03	0.40E 00	-0.14E-03	1.000	1.000	0.000	0.320	0.406
6	0.316E-02	4041.3	0.491E 04	0.432E 12	0.195E-07	0.263E-01	0.344E 03	0.40E 00	0.32E-02	1.000	1.000	0.000	0.321	0.488
7	0.422E-02	4044.6	0.584E 04	0.492E 12	0.232E-07	0.297E-01	0.326E 03	0.40E 00	0.49E-02	1.000	1.000	0.000	0.321	0.504
8	0.562E-02	4048.3	0.696E 04	0.558E 12	0.276E-07	0.335E-01	0.309E 03	0.40E 00	0.55E-02	1.000	1.000	0.000	0.322	0.486
9	0.750E-02	4052.4	0.828E 04	0.634E 12	0.328E-07	0.378E-01	0.291E 03	0.40E 00	0.74E-02	1.000	1.000	0.000	0.323	0.480
10	0.100E-01	4058.7	0.984E 04	0.718E 12	0.389E-07	0.425E-01	0.274E 03	0.40E 00	0.97E-02	1.000	1.000	0.000	0.324	0.485
11	0.133E-01	4066.0	0.117E 05	0.817E 12	0.462E-07	0.479E-01	0.256E 03	0.40E 00	0.12E-01	1.000	1.000	0.000	0.326	0.481
12	0.178E-01	4075.8	0.139E 05	0.930E 12	0.547E-07	0.539E-01	0.239E 03	0.40E 00	0.16E-01	1.000	1.000	0.000	0.328	0.482
13	0.237E-01	4087.9	0.165E 05	0.106E 13	0.647E-07	0.609E-01	0.222E 03	0.40E 00	0.20E-01	1.000	1.000	0.000	0.331	0.477
14	0.316E-01	4103.5	0.195E 05	0.122E 13	0.764E-07	0.689E-01	0.204E 03	0.40E 00	0.25E-01	1.000	1.000	0.000	0.334	0.472
15	0.422E-01	4122.8	0.231E 05	0.142E 13	0.901E-07	0.782E-01	0.187E 03	0.40E 00	0.31E-01	1.000	1.000	0.000	0.339	0.465
16	0.562E-01	4147.0	0.274E 05	0.165E 13	0.106E-06	0.890E-01	0.170E 03	0.40E 00	0.39E-01	1.000	1.000	0.000	0.346	0.460
17	0.750E-01	4177.2	0.323E 05	0.194E 13	0.124E-06	0.102E 00	0.153E 03	0.40E 00	0.49E-01	1.000	1.000	0.000	0.355	0.456
18	0.100E 00	4214.7	0.381E 05	0.230E 13	0.145E-06	0.117E 00	0.136E 03	0.40E 00	0.61E-01	1.000	1.000	0.000	0.366	0.451
19	0.133E 00	4260.9	0.447E 05	0.276E 13	0.168E-06	0.135E 00	0.119E 03	0.40E 00	0.76E-01	1.000	1.000	0.000	0.381	0.440
20	0.178E 00	4317.6	0.524E 05	0.336E 13	0.195E-06	0.157E 00	0.102E 03	0.40E 00	0.93E-01	1.000	1.000	0.000	0.401	0.429
21	0.237E 00	4386.8	0.611E 05	0.415E 13	0.224E-06	0.183E 00	0.850E 02	0.40E 00	0.11E 00	1.000	1.000	0.000	0.426	0.423
22	0.316E 00	4471.0	0.711E 05	0.519E 13	0.255E-06	0.215E 00	0.684E 02	0.40E 00	0.14E 00	1.000	1.000	0.000	0.459	0.404
23	0.422E 00	4572.8	0.825E 05	0.657E 13	0.290E-06	0.251E 00	0.517E 02	0.40E 00	0.17E 00	1.000	1.000	0.000	0.501	0.353
24	0.562E 00	4695.0	0.955E 05	0.837E 13	0.326E-06	0.293E 00	0.349E 02	0.40E 00	0.20E 00	1.000	1.000	0.000	0.555	0.327
25	0.750E 00	4841.3	0.110E 06	0.107E 14	0.366E-06	0.340E 00	0.178E 02	0.40E 00	0.23E 00	1.000	1.000	0.000	0.632	0.309
26	0.100E 01	5014.9	0.128E 06	0.138E 14	0.408E-06	0.388E 00	0.0	0.40E 00	0.26E 00	1.000	1.000	0.000	0.736	0.268
27	0.133E 01	5218.7	0.148E 06	0.178E 14	0.455E-06	0.442E 00	-0.186E 02	0.40E 00	0.29E 00	1.000	1.000	0.000	0.872	0.290
28	0.178E 01	5457.2	0.172E 06	0.233E 14	0.504E-06	0.504E 00	-0.383E 02	0.40E 00	0.32E 00	1.000	1.000	0.000	1.094	0.437
29	0.237E 01	5734.9	0.198E 06	0.329E 14	0.555E-06	0.617E 00	-0.585E 02	0.40E 00	0.38E 00	1.000	1.000	0.000	1.448	0.524
30	0.316E 01	6075.7	0.226E 06	0.550E 14	0.596E-06	0.884E 00	-0.773E 02	0.39E 00	0.51E 00	1.000	1.000	0.000	-0.276	-4.629
31	0.422E 01	6451.0	0.251E 06	0.868E 14	0.623E-06	0.123E 01	-0.940E 02	0.38E 00	0.55E 00	1.000	1.000	0.000	-9.986	1.358
32	0.562E 01	6770.7	0.273E 06	0.183E 15	0.646E-06	0.227E 01	-0.108E 03	0.38E 00	0.63E 00	0.999	1.000	0.000	6.060	-4.906
33	0.750E 01	7006.5	0.289E 06	0.271E 15	0.662E-06	0.316E 01	-0.118E 03	0.37E 00	0.53E 00	0.999	1.000	0.000	-19.113	7.759
34	0.100E 02	7212.7	0.307E 06	0.382E 15	0.682E-06	0.422E 01	-0.128E 03	0.36E 00	0.52E 00	0.999	1.000	0.000	41.280	53.102
35	0.133E 02	7427.9	0.324E 06	0.512E 15	0.699E-06	0.544E 01	-0.139E 03	0.34E 00	0.52E 00	0.998	1.000	0.000	283.331	92.923
36	0.178E 02	7633.1	0.342E 06	0.709E 15	0.717E-06	0.726E 01	-0.149E 03	0.33E 00	0.49E 00	0.998	1.000	0.000	755.125	23.131
37	0.237E 02	7814.9	0.360E 06	0.927E 15	0.736E-06	0.925E 01	-0.158E 03	0.32E 00	0.42E 00	0.997	1.000	0.000	522.112	-85.374

Fig. 6.--Model atmosphere (normal gravity) for K2 dwarf.

TEFF 5000. LOG G 2.700 NORMAL ITERATION 1

FRACTIONAL ABUNDANCES HYDROGEN 0.900 HELIUM 0.100

BL-5.70 C-3.50 CA-5.90 CO-7.30 CR-6.60 FE-4.40 K-7.10 MG-4.50 MN-6.90 N-4.10 NA-5.80 NE-3.40 NI-6.10 O-3.20 SI-4.50 TI-7.20

	TAU 8000.	TEMP	PRESSURE	ELECTRON NUMBER	DENSITY	ABSORPTION COEFFICIENT	HEIGHT (KM)	GRADIENTS ADIAB	GRADIENTS RADIAT	ION FRACTIONS H 1	ION FRACTIONS HE 1	ION FRACTIONS HE 2	PER CENT FLUX ERROR	PER CENT FLUX DERIV
1	0.0	4044.5	0.108E 03	0.181E 11	0.429E-09	0.122E-02	0.330E 05	0.40E 00	0.75E-03	1.000	1.000	0.000	-0.475	-0.810
2	0.100E-02	4056.0	0.216E 03	0.361E 11	0.855E-09	0.232E-02	0.209E 05	0.40E 00	-0.43E-01	1.000	1.000	0.000	-0.475	-0.489
3	0.133E-02	4070.5	0.348E 03	0.539E 11	0.139E-08	0.340E-02	0.147E 05	0.40E 00	-0.47E-02	1.000	1.000	0.000	-0.475	-1.299
4	0.178E-02	4050.0	0.401E 03	0.615E 11	0.159E-08	0.390E-02	0.189E 05	0.40E 00	0.18E-01	1.000	1.000	0.000	-0.476	-0.835
5	0.237E-02	4054.1	0.463E 03	0.699E 11	0.183E-08	0.430E-02	0.181E 05	0.40E 00	0.38E-02	1.000	1.000	0.000	-0.477	-0.904
6	0.316E-02	4055.1	0.545E 03	0.805E 11	0.216E-08	0.502E-02	0.173E 05	0.40E 00	0.27E-02	1.000	1.000	0.000	-0.478	-0.834
7	0.422E-02	4057.8	0.643E 03	0.924E 11	0.254E-08	0.574E-02	0.164E 05	0.40E 00	0.50E-02	1.000	1.000	0.000	-0.480	-0.828
8	0.562E-02	4061.8	0.756E 03	0.106E 12	0.299E-08	0.656E-02	0.156E 05	0.40E 00	0.66E-02	1.000	1.000	0.000	-0.482	-0.821
9	0.750E-02	4056.5	0.890E 03	0.122E 12	0.351E-08	0.747E-02	0.148E 05	0.40E 00	0.83E-02	1.000	1.000	0.000	-0.487	-0.816
10	0.100E-01	4072.3	0.105E 04	0.140E 12	0.413E-08	0.850E-02	0.139E 05	0.40E 00	0.11E-01	1.000	1.000	0.000	-0.495	-0.806
11	0.133E-01	4080.5	0.123E 04	0.161E 12	0.484E-08	0.966E-02	0.131E 05	0.40E 00	0.13E-01	1.000	1.000	0.000	-0.510	-0.794
12	0.178E-01	4090.4	0.145E 04	0.185E 12	0.568E-08	0.110E-01	0.123E 05	0.40E 00	0.17E-01	1.000	1.000	0.000	-0.491	-0.781
13	0.237E-01	4107.5	0.170E 04	0.213E 12	0.666E-08	0.125E-01	0.115E 05	0.40E 00	0.21E-01	1.000	1.000	0.000	-0.478	-0.763
14	0.316E-01	4118.1	0.200E 04	0.246E 12	0.779E-08	0.141E-01	0.106E 05	0.40E 00	0.26E-01	1.000	1.000	0.000	-0.487	-0.742
15	0.422E-01	4137.3	0.236E 04	0.284E 12	0.912E-08	0.161E-01	0.982E 04	0.40E 00	0.33E-01	1.000	1.000	0.000	-0.492	-0.721
16	0.562E-01	4161.5	0.276E 04	0.331E 12	0.107E-07	0.183E-01	0.899E 04	0.40E 00	0.40E-01	1.000	1.000	0.000	-0.501	-0.693
17	0.750E-01	4191.4	0.325E 04	0.389E 12	0.124E-07	0.209E-01	0.815E 04	0.40E 00	0.50E-01	1.000	1.000	0.000	-0.501	-0.667
18	0.100E 00	4228.5	0.381E 04	0.455E 12	0.145E-07	0.236E-01	0.731E 04	0.40E 00	0.61E-01	1.000	1.000	0.000	-0.529	-0.635
19	0.133E 00	4274.3	0.447E 04	0.540E 12	0.168E-07	0.269E-01	0.648E 04	0.40E 00	0.74E-01	1.000	1.000	0.000	-0.387	-0.597
20	0.178E 00	4330.4	0.525E 04	0.644E 12	0.195E-07	0.305E-01	0.561E 04	0.40E 00	0.90E-01	1.000	1.000	0.000	-0.764	-0.565
21	0.237E 00	4398.5	0.614E 04	0.776E 12	0.225E-07	0.347E-01	0.474E 04	0.40E 00	0.11E 00	1.000	1.000	0.000	-1.106	-0.568
22	0.316E 00	4483.3	0.724E 04	0.940E 12	0.259E-07	0.393E-01	0.385E 04	0.40E 00	0.13E 00	1.000	1.000	0.000	-0.697	-0.564
23	0.422E 00	4584.3	0.850E 04	0.115E 13	0.298E-07	0.442E-01	0.296E 04	0.40E 00	0.15E 00	1.000	1.000	0.000	-0.596	-0.512
24	0.562E 00	4705.8	0.100E 05	0.140E 13	0.341E-07	0.494E-01	0.200E 04	0.40E 00	0.17E 00	1.000	1.000	0.000	-0.569	-0.429
25	0.750E 00	4851.1	0.119E 05	0.174E 13	0.391E-07	0.554E-01	0.102E 04	0.40E 00	0.20E 00	1.000	1.000	0.000	-0.673	-0.304
26	0.100E 01	5023.9	0.139E 05	0.219E 13	0.445E-07	0.619E-01	0.0	0.40E 00	0.22E 00	1.000	1.000	0.000	-0.812	-0.104
27	0.133E 01	5226.1	0.165E 05	0.290E 13	0.505E-07	0.724E-01	-0.105E 04	0.40E 00	0.26E 00	1.000	1.000	0.000	-0.812	0.083
28	0.178E 01	5472.5	0.193E 05	0.423E 13	0.562E-07	0.946E-01	-0.307E 04	0.40E 00	0.34E 00	1.000	1.000	0.000	-0.804	-0.293
29	0.237E 01	5754.6	0.224E 05	0.751E 13	0.630E-07	0.143E 00	-0.725E 04	0.39E 00	0.47E 00	1.000	1.000	0.000	-1.707	-0.803
30	0.316E 01	6073.6	0.240E 05	0.124E 14	0.683E-07	0.210E 00	-0.366E 04	0.38E 00	0.63E 00	1.000	1.000	0.000	-1.399	0.777
31	0.422E 01	6429.5	0.250E 05	0.202E 14	0.643E-07	0.441E 00	-0.426E 04	0.36E 00	0.12E 01	0.999	1.000	0.000	-0.392	4.848
32	0.562E 01	6806.3	0.252E 05	0.672E 14	0.425E-07	0.902E 00	-0.461E 04	0.32E 00	0.19E 01	0.998	1.000	0.000	1.006	11.633
33	0.750E 01	7178.2	0.247E 05	0.122E 15	0.260E-07	0.160E 01	-0.496E 04	0.29E 00	0.19E 01	0.995	1.000	0.000	44.436	16.246
34	0.100E 02	7526.1	0.239E 05	0.176E 15	0.161E-07	0.232E 01	-0.507E 04	0.25E 00	0.13E 01	0.993	1.000	0.000	82.659	27.054
35	0.133E 02	7914.2	0.230E 05	0.230E 15	0.597E-08	0.354E 01	-0.528E 04	0.23E 00	0.11E 01	0.991	1.000	0.000	201.319	65.346
36	0.178E 02	7981.3	0.229E 05	0.231E 15	0.595E-08	0.411E 01	-0.549E 04	0.22E 00	0.10E 01	0.989	1.000	0.000	581.755	133.851
37	0.237E 02	8057.6	0.230E 05	0.362E 15	0.584E-08	0.531E 01	-0.570E 04	0.20E 00	0.94E 00	0.985	1.000	0.000	1571.597	199.723

Fig. 7.--Model atmosphere (normal gravity) for K0 giant.

$$k_\nu \propto N_H^2$$

$$\kappa \propto N_e \, N_H$$

Therefore,

$$D \propto \frac{N_H}{N_e}$$

Since the electron donors are almost totally ionized in the stars that are hot enough to possess measurable H_α wings

$$D \propto N_H/N_M$$

In other words, there is a dependence on the metal to hydrogen ratio.

The program used to compute the Balmer line profiles was written by Deane Peterson and is designed to be used in conjunction with the Atlas model atmospheres. The program performs calculations using both the Griem (1964) and the Edmonds, Schluter, and Wells (1967) Stark broadening theories; however, since the dominant broadening mechanism in the program stars is resonance broadening there is very little difference between the results obtained using the two theories.

c) The Line Strengths

The abundance program that was used in the present work is called **Width4** and is also designed to be used in conjunction with **Atlas**. In effect it calculates the depths at various points in a line, which it then integrates to give the equivalent width. The abundance of the element is varied

until agreement is achieved with the equivalent width obtained from measurements. If strong lines are used it is necessary to choose the proper values of the velocity and damping parameters. The exact way in which the program was used will be described in subsequent chapters.

VI. THE ABUNDANCE ANALYSIS

a) Temperatures

A proper analysis of a stellar atmosphere requires a good knowledge of its temperature structure. As noted in the previous chapter, the chief temperature criterion used in this work is the set of deblanketed continua obtained by means of a photoelectric scanner in conjunction with tracings of high dispersion spectra. The temperatures obtained by fitting these continua to the calculated emergent fluxes from model atmospheres are not true effective temperatures since the effects of line blocking on the atmospheric structure were not taken into account in the models. Rather, the derived temperatures are characteristic of the continuum forming regions of the star and are not a measure of the total emitted flux. Ignoring the line absorption in the models results in too high a value for the boundary temperature and therefore wrong parameters for the region of formation of strong neutral lines. The effect of this on the derived abundances will be discussed in subsequent sections.

A second temperature criterion for the hotter stars is the strength of the wings of H_α. Figure 8 shows the measured and predicted profiles for the hottest star in the program, ξ Boo A; the agreement between the scanner and H_α temperature is quite good. The SMR dwarfs ρ^1Cnc, 14 Her, and 54 Psc all possess H_α wings that are too shallow for the

Fig. 8.--H_α profile in ξ Boo A from three plates. The error bars indicate the maximum and minimum measured values for each point. The profile from the adopted model (T_{eff} = 5600 K) has been drawn in.

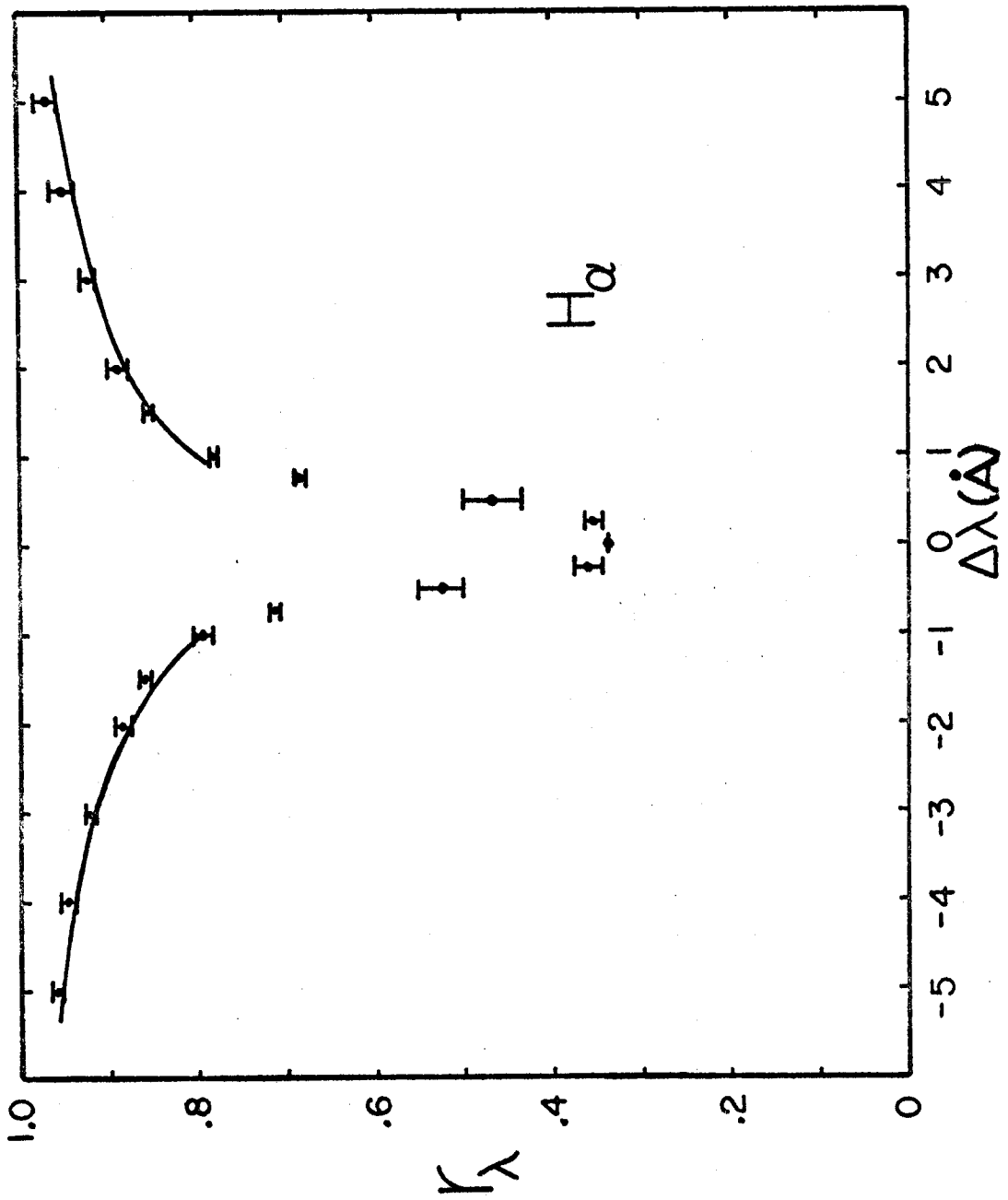
1.0
.8
.6
.4
.2
0
r_λ
-5
-4
-3
-2
-1
0
1
2
3
4
5
$\Delta\lambda(\AA)$
H_α

scanner temperature, a discrepancy that is partly explained by the dependence of H_α wing absorption on metal abundance. An unbelievably high abundance ($\sim$ .7 dex w. r. t. the sun) is required to completely remove the discrepancy in the case of ρ^1Cnc and 54 Psc, a figure which is not supported by the subsequent abundance analysis. Errors in drawing in the continuum may be partially responsible. It is interesting to note that H_α is considerably weaker in the SMR star HR 1614 than it is in HR 8832, a Yerkes standard of the same temperature, although the wings are rather weak in both stars due to their late spectral type.

Although reliable temperatures could be obtained for only a few stars by means of the H_α wing profiles, complete H_α profiles were drawn for all the stars from tracings of the spectra, with averaging done in a straightforward manner if more than one plate was available. Two rather interesting features soon became apparent: (1) stars with strong H and K reversals have a greater residual intensity in the case of H_α; (2) the core of H_α is quite asymmetrical in giants cooler than the Hyades, with the centroid displaced to the red. A very slight asymmetry is also detectible in the Hyades giants as well as in the cooler dwarfs. In connection with (1) it is interesting to note that stars with strong H and K reversals also appear to possess a measurable He line at λ10830 (Vaughan and Zirin 1968), adding further motivation to spec-

ulations on the presence of strong chromospheric activity in these stars. The H_α asymmetry in (2) is due to the presence of a strong CoI line at λ6563.41; a graphic separation of the profile of H_α in the spectrum of Arcturus (Griffin 1969) and the profile of Co λ5483.35 (approximately the same e. p. and strength as λ6563.41 according to Moore [1959]) results in a completely symmetrical core.

The excitation temperature varies from element to element and is not a good parameter on which to base the choice of a model for a star. Therefore the scanner temperature remains as the main temperature criterion, except in the case of 70 Oph A where no scans were obtained due to the proximity of the secondary component. For this star the temperature was chosen from a consideration of the H_α wings, the excitation temperature, and the R-I color.

A comparison of the temperatures obtained in this work with those derived by other workers generally shows good agreement. For example, the temperatures of μ Leo and the Hyades giants derived by Strom et al. (1971) differ by 100 K or less from the results presented here. In most cases, however, comparisons are not possible since workers often list excitation and ionization temperatures relative to some standard star.

b) gf values

Originally it was decided to use absolute gf values available in the literature, such as those published by Corliss and Bozman (1962) and Corliss and Warner (1964). In fact, several curves of growth for various elements were constructed using these gf values and lines measured for the program stars. However, the scatter in the curves was often extremely large and, particularly in the case of Fe I, a rather pronounced wavelength dependence was occasionally apparent. Another difficulty was that many weak lines in the red region of the spectrum had no published gf values, which meant that some of the most useful lines for an abundance determination could not be used. Therefore, it was decided to employ solar gf values in which the effect of the atmosphere had been subtracted out by means of a model solar atmosphere. An immediate consequence of this choice is, of course, that all the derived stellar abundances are thereby expressed relative to the solar values.

A number of circumstances make the sun a favorable choice as a comparison star for an analysis of late-type spectra. First of all, lines lying on the linear or the flat part of the stellar curve of growth will generally lie well back on the linear part of the solar curve, thus minimizing the uncertainties in the exact shape of the solar curve of growth.

Secondly, the main source of continuous absorption is expected to remain H^- throughout spectral type K, thus avoiding complications that might arise if stars with widely different opacity sources were compared. In addition, the sun is the only star for which it is possible to obtain a direct determination of the T-τ relationship, thereby increasing the reliability of the derived solar gf values.

When the sun is used as a reference star it is generally recommended that the solar spectrum be recorded with the same equipment and at the same dispersion as the stellar spectrum under study. In the case of relatively cool stars, however, the corresponding solar absorption lines are often so weak that only the highest dispersions are capable of yielding accurate measurements. Therefore, the second revision of Rowland's atlas (Moore et al. 1966) was used as the source of solar equivalent widths, with corrections made on the basis of direct measurements in the Utrecht Atlas (Minnaert et al. 1940) if the published values were obviously in error.

The equivalent width of a weak line can be separated into components that depend on the atmospheric structure on the one hand and the gf value of the transition on the other; i.e.,

(1) $\log (W/\lambda)_{weak} = \log \Gamma + \log gf + \log (N_{el}/N_H)$

which is the representation used by Cayrel and Jugaku (1963).

The solar gf value for a weak line is then easily obtained by subtracting the unsaturated line strength Γ and the abundance from the measured equivalent width. Γ, of course, is calculated by means of a model for the solar atmosphere. In the case of strong lines the situation is a bit more complicated, and the lines must be de-saturated with the aid of a suitable curve of growth before the above formula can be used. Various theoretical and empirical solar curves of growth are available in the literature; the major difference between them is in the position of the turnoff of the damping portion of the curve. As was pointed out above, however, most of the lines in the program are quite weak in the sun, so the choice of the proper curve is not too critical. It was decided to use the Cowley (1964) empirical curve of growth since its shape at the shoulder closely resembles the curve derived directly from the Atlas models. Calculations also showed that the difference between the neutral and the ion curve of growth is quite small in the sun, justifying the use of one curve for all the lines. The vertical coordinate, however, had to be changed depending on the atomic weight of the element in question; for this purpose a turbulent velocity of 1.8 km/sec was assumed.

It was also necessary to adopt a model for the sun in order to calculate the Γ's. Many solar T-τ relationships have appeared in the literature; most are in reasonable

agreement in the region of formation of weak lines and the continuum, but large differences appear in the temperature structure near the surface where the strong lines are formed. It is for this reason that it was decided to treat the effect of saturation in the strong lines with the empirical Cowley curve; it is therefore necessary to consider only the deeper layers where the weak lines are formed. The T-τ adopted here is the one used by Cayrel and Jugaku (1963), Krishna Swamy (1966), and Bell (1970). For $\tau_{5000} > 2$ it lies quite close to the T-τ used by Holweger (1967) in his empirical solar model and deviates only slightly from the Bilderberg model (Gingerich and de Jager, 1968). One small complication is the fact that the equivalent widths in Moore et al. (1966) are determined for the center of the solar disk while the program calculates line strengths averaged over the entire disk. Rather than undertake a modification of the program it was decided to change the T-τ slightly in the following way. Cayrel and Jugaku (1963) have presented tables of unsaturated line strengths (i.e., Γ's) for the center of the solar disk and for a grid of model dwarf atmospheres. By interpolation in the grid it was found that an atmosphere with $T_{eff} = 5930$ K yielded the same line strength integrated over the disk as the model at $T_{eff} = 5780$ K yielded at the center of the disk; the equality holds for ions as well as neutrals. Therefore, the solar T-τ used in the present

program was scaled upward by 2.5% in T. It had originally been planned to use the solar Γ's published by Cayrel and Jugaku (1963), but comparison with the results from Atlas and Width4 showed discrepancies amounting to as much as .2 dex for a few elements. These differences were of a systematic nature and were found to hold for all the models in the grid. The derived solar gf values depend, of course, on the assumed abundances of the elements in the sun; i.e., what is really obtained is log gf + log $(N_{el}/N_H)_\odot$. This provides a means for checking the gf values with the values available in the literature. A plot of the published log gf against the log gf + log$(N_{el}/N_H)_\odot$ used in this work should yield a value of the abundance equal to the abundance obtained by using the published log gf values, provided that the model atmosphere used is similar to the one employed here. Such plots were constructed for several elements, with the result that there was generally good consistency between the sets of gf values. Of particular importance are the values for Fe I and Fe II, and the plots for these two ions are illustrated in Figures 9 - 11. In the case of Fe II there are no published gf values for the yellow-red region of the spectrum, so comparison was made with the "astrophysical" gf values derived by Warner (1968) from Deneb and Sirius. The agreement is reasonably good, thereby increasing confidence in the results obtained in this work. The solar gf values are

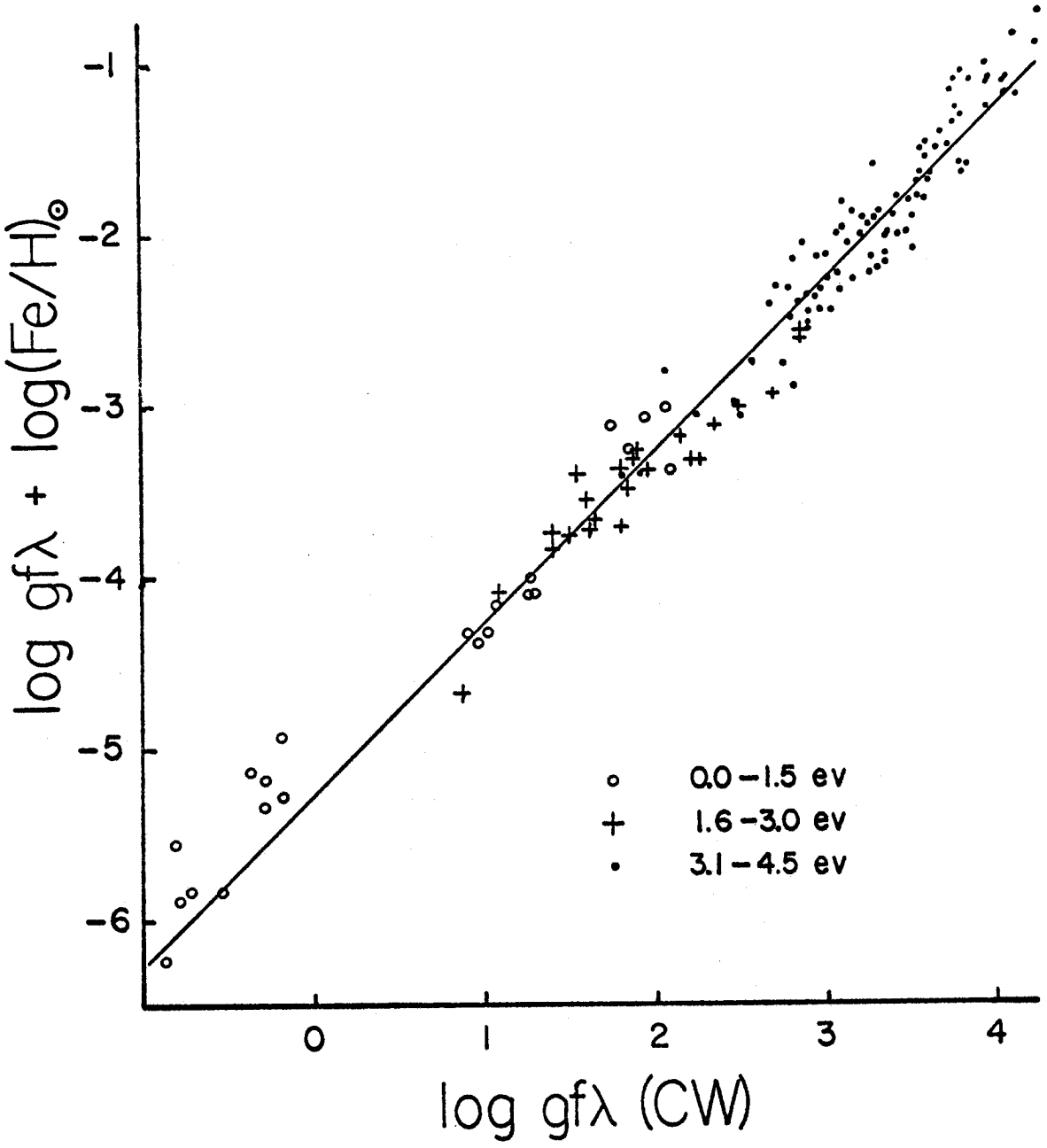

Fig. 9.--Comparison of the astrophysical Fe I gf values derived in this work with the experimental values of Corliss and Warner (1964). The straight line implies log $(Fe/H)_\odot$ = -5.3, which compares well with the value of -5.4 obtained by Aller et al. (1964) using Corliss and Warner's gf values.

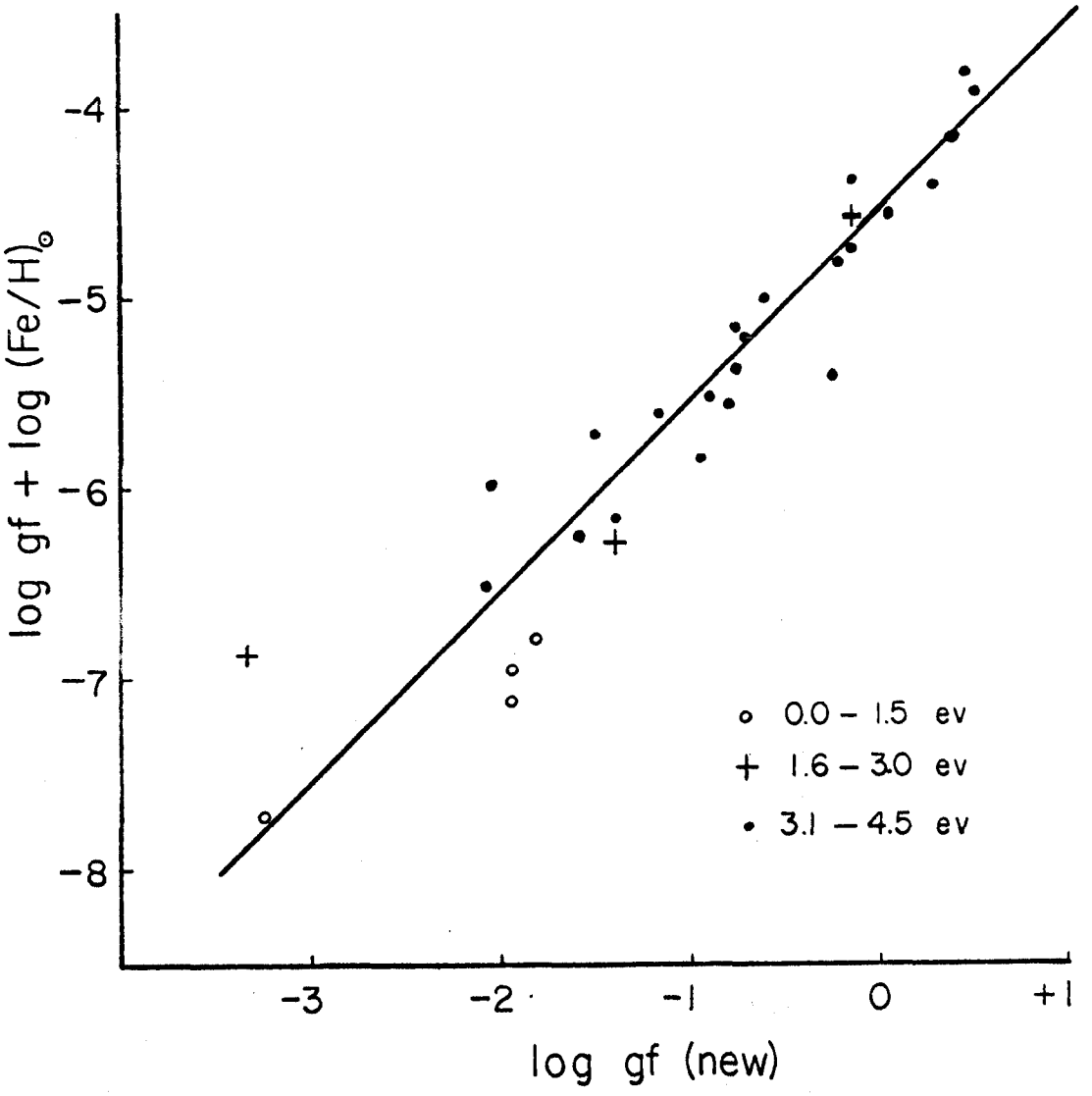

Fig. 10.--Comparison of the astrophysical Fe I gf values derived in this work with the new experimental gf values in Gartz and Kock (1969), Bridges and Wiese (1970), Richter and Wulff (1970), and Wolnick et al. (1970). The straight line yields log (Fe/H)$_\odot$ = -4.5, in good agreement with the new revised solar Fe abundance (Gartz et al. 1969).

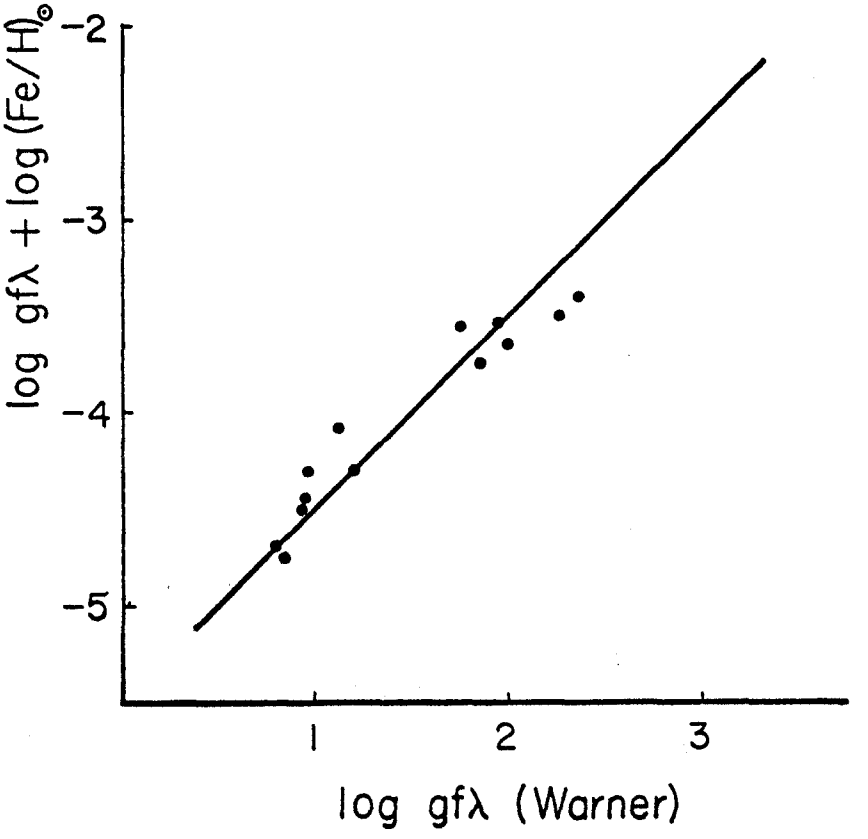

Fig. 11.--Comparison of the astrophysical Fe II gf values derived in this work with the astrophysical gf values of Warner (1968). The straight line yields log $(Fe/H)_{\odot}$ = -5.5, the same value as obtained by Warner (1968) in his analysis using Fe II lines.

not tablulated here but will be supplied to anyone who wishes to use them.

c) Dwarf Abundances from Cayrel and Jugaku Models

As mentioned in the previous section, Cayrel and Jugaku (1963) have calculated unsaturated line strengths for the center of the solar disk and for a series of dwarf models with log g = 4.5, thereby providing a quick method by which to obtain stellar abundances relative to the sun. The models all incorporate a scaled solar T-τ relation, as well as the usual assumptions of L.T.E. and plane-parallel stratification. The discrepancies noted in the previous section in the values of Γ are of a systematic nature and will cancel out in a differential analysis. The abundance analysis is very simple and involves the plotting of a curve of growth with the following abscissa:

$$\log Y = \log X_{\odot} - \log \Gamma_{\odot} + \log \Gamma_{\star} \qquad (2)$$

where $\log X_{\odot}$ is the abscissa read off from a solar curve of growth which has been normalized such that the ordinate and abscissa are equal on the linear part of the curve. From equation (1) it is seen that log Y is equivalent to

$$\log Y = \log \Gamma_{\star} + \log gf + \log (N_{el}/N_H)_{\odot}$$

Therefore, the abundance relative to the sun is given by the

intercept of the linear part of the empirical curve with the log Y axis. The accuracy of the result depends, of course, on how well the model from which the Γ_*'s were derived represents the star being analyzed. A check is provided by an analysis of the corresponding ionized lines, and the model is varied until consistent abundances are obtained for ions and neutrals. Another check is provided by the fit of lines of varying excitation potential, but this is of lower accuracy in practice.

Using the above method, a preliminary abundance analysis was performed for the dwarfs in the program, and the results are shown in Table 8. The effective temperature is nominal and does not characterize the total flux from the model. The velocity parameter was obtained by a comparison of the Fe curves of growth with the theoretical curves of Hunger (1956) for pure absorption in the Milne-Eddington model. These curves resemble the Cowley (1964) curve and the curves generated by Atlas - Width4 quite closely in the "shoulder". Two curves of growth for ρ^1 Cnc (Fe I and Fe II) are reproduced in Figures 12 and 13 for purposes of illustration. In most cases the accuracy of the fit to the theoretical curve is on the order of .1 dex.

Thus far the results have been quite self-consistent, but no use has yet been made of the scanner energy distributions. When the fluxes from the Cayrel and Jugaku models

TABLE 8

DWARF ABUNDANCES FROM CAYREL AND JUGAKU MODELS*

	ξ Boo A	70 Oph A	ρ^1 Cnc	14 Her	σ Dra	54 Psc
θ_{eff}	.90	.925	.95	.95	.95	.95
V(km/sec)	2.6	2.8	2.2	2.2	2.3	2.2
Na	-.05	.34	.55	.66	.05	.27
Ca	.10	.27	.33	.44		.20
YII†	.12	.00	-.06	.16		
Sc†	-.01	.00	.27	.27		-.15
Sc II	-.14	.00	.09	.27		-.15
V	-.02	.23	.35	.44		.18
Cr	-.01	.14	.27	.29		.04
CrII	-.05	.13	.41	.49		.04
Ti	-.05	.12	.28	.35		.20
TiII	-.08	.08	.35	.44		.04
Mn	-.23	.10	.38	.64		.14
Mg†	.03	.24	.36	.44		.06
Fe	-.04	.13	.31	.38	-.03	.04
FeII	-.01	.04	.30	.37	-.03	.04
Si	-.09	.10	.32	.30		.04

* Abundances are given as log $(el/H)_*$ - log $(el/H)_\odot$

† Abundances for these elements are of low weight

Table 8 (continued)

DWARF ABUNDANCES FROM CAYREL AND JUGAKU MODELS*

	ε Eri	HR 6806	HR 8832	HR 1614	61 Cyg B
θ_{eff}	.95	.975	1.00	1.00	1.15
V(km/sec)	2.6	2.6	2.5	2.4	2.4
Na	.24	.14	.40	.76	-.13
Ca	.26	.13	.28	.43	-.03
YII†	-.63	-.41		.82	
Sc†		-.20		.53	
ScII	-.15	-.19	-.17	.07	
V	.27	.11	.22	.57	
Cr	.12	-.13	.11	.35	-.30
CrII	.12	-.06	-.03	.49	
Ti	.20	.02	.17	.42	-.17
TiII	-.01	-.05	.18	.44	-.09
Mn	.12	-.27	.14	.37	
Mg†	.30	.21	.17	.42	-.38
Fe	.07	-.06	.05	.26	-.30
FeII	-.03	.00	.06	.24	
Si	-.09	-.13	-.12	.15	-.30

*Abundances are given as log $(el/H)_*$ - log $(el/H)_\odot$

† Abundances for these elements are of low weight

Fig. 12.--ρ^1 Cnc: Fe I curve of growth (yellow - red region). The Γ's (unsaturated line strengths) for the star are from the Cayrel and Jugaku (1963) T_{eff} = 5300 K model and the log $X_\odot$'s are from the Cowley (1964) curve.

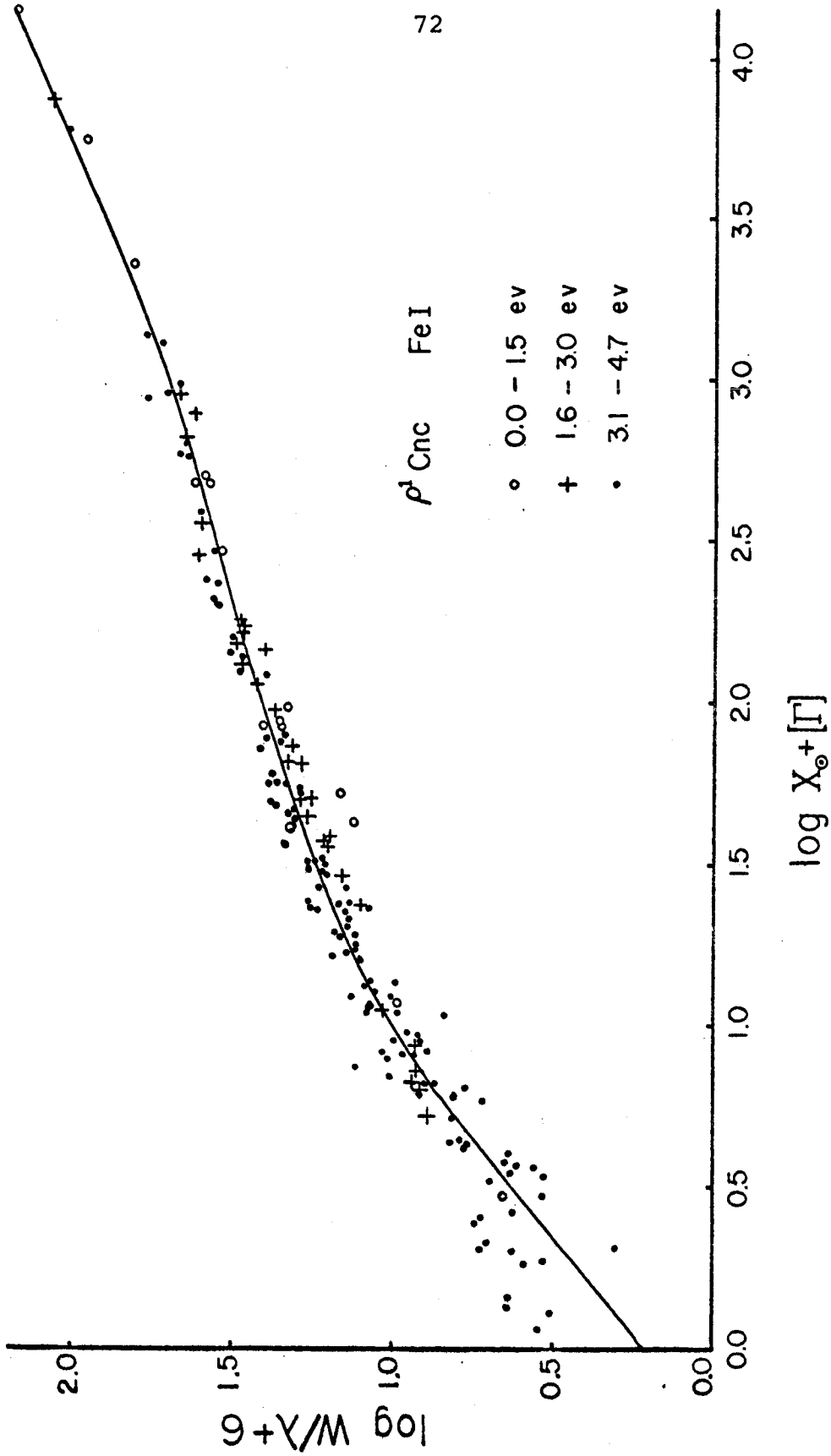
ρ¹ Cnc Fe I
∘ 0.0 – 1.5 ev
+ 1.6 – 3.0 ev
• 3.1 – 4.7 ev
log W/λ+6
log χ₀+[Γ]
0.0
0.5
1.0
1.5
2.0
2.5
3.0
3.5
4.0

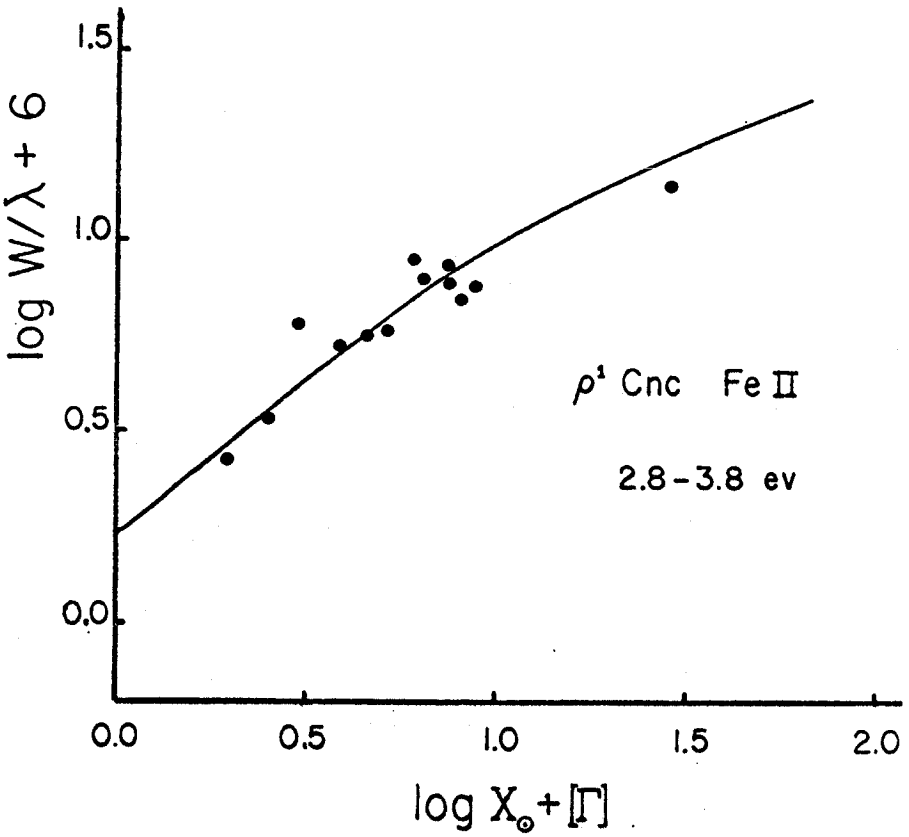

Fig. 13.--ρ^1 Cnc: Fe I curve of growth (yellow - red region). The Γ's for the star are from the Cayrel and Jugaku (1963) T_{eff} = 5300 K model and the log $X_\odot$'s are from the Cowley (1964) curve.

are compared with the measured fluxes, however, a rather large discrepancy is seen to arise; namely, the predicted fluxes are characteristic of a considerably higher temperature than is indicated by the scans, and the situation becomes worse with later spectral type. Figures 14 and 15 provide an illustration of this phenomenon in the case of ξ Boo A and HR 1614. A solution would be to use correspondingly cooler models for the stars, but this results in divergent abundances for ions and neutrals, as may be seen in Figures 16 and 17, which illustrate curves of growth of Fe I and Fe II in the case of HR 8832. One of the curves has been constructed for $\theta_{eff} = 1.00$ while the other is for $\theta_{eff} = 1.125$, which is the temperature of the model that fits the scanner energy distribution. Several points are worth noting: (1) the scatter in the points becomes larger as one progresses toward later spectral types (compare with Figure 12); (2) the main difference in the two Fe I curves lies in the lower value of the velocity parameter (V = 1.9 km/sec) derived from the cooler model, while the abundance, depending mostly on weak lines of high excitation, remains essentially the same; (3) the scatter is somewhat diminished in the $\theta_{eff} = 1.00$ Fe I curve, but the difference is rather slight, considering the large temperature difference; (4) the fit of the ion and neutral curves is obviously much better with the hotter model. In connection with (2) it

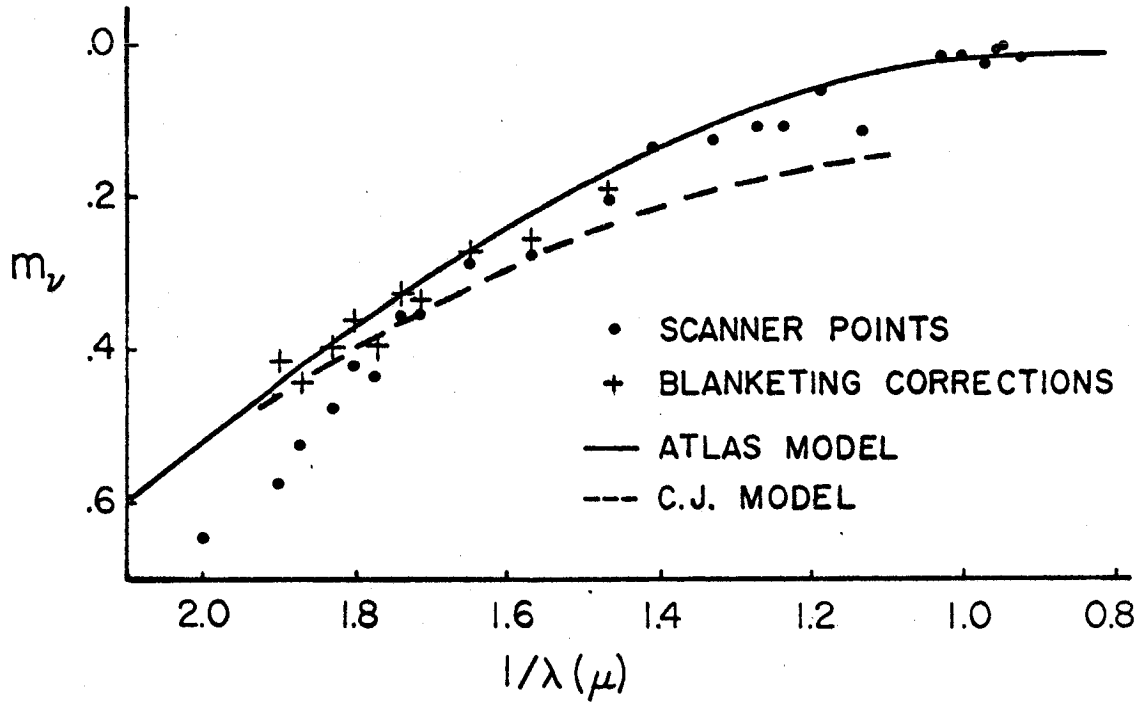

Fig. 14.--Deblanketed scan of ξ Boo A. The Cayrel and Jugaku model that forces equality of the ion and neutral abundances has been drawn in (T_{eff}(C.J.) = 5600 K); it is apparent that a lower model temperature is needed to obtain agreement with the scan. Note also the persistent dip at 8804 Å ($1/\lambda$ = 1.135).

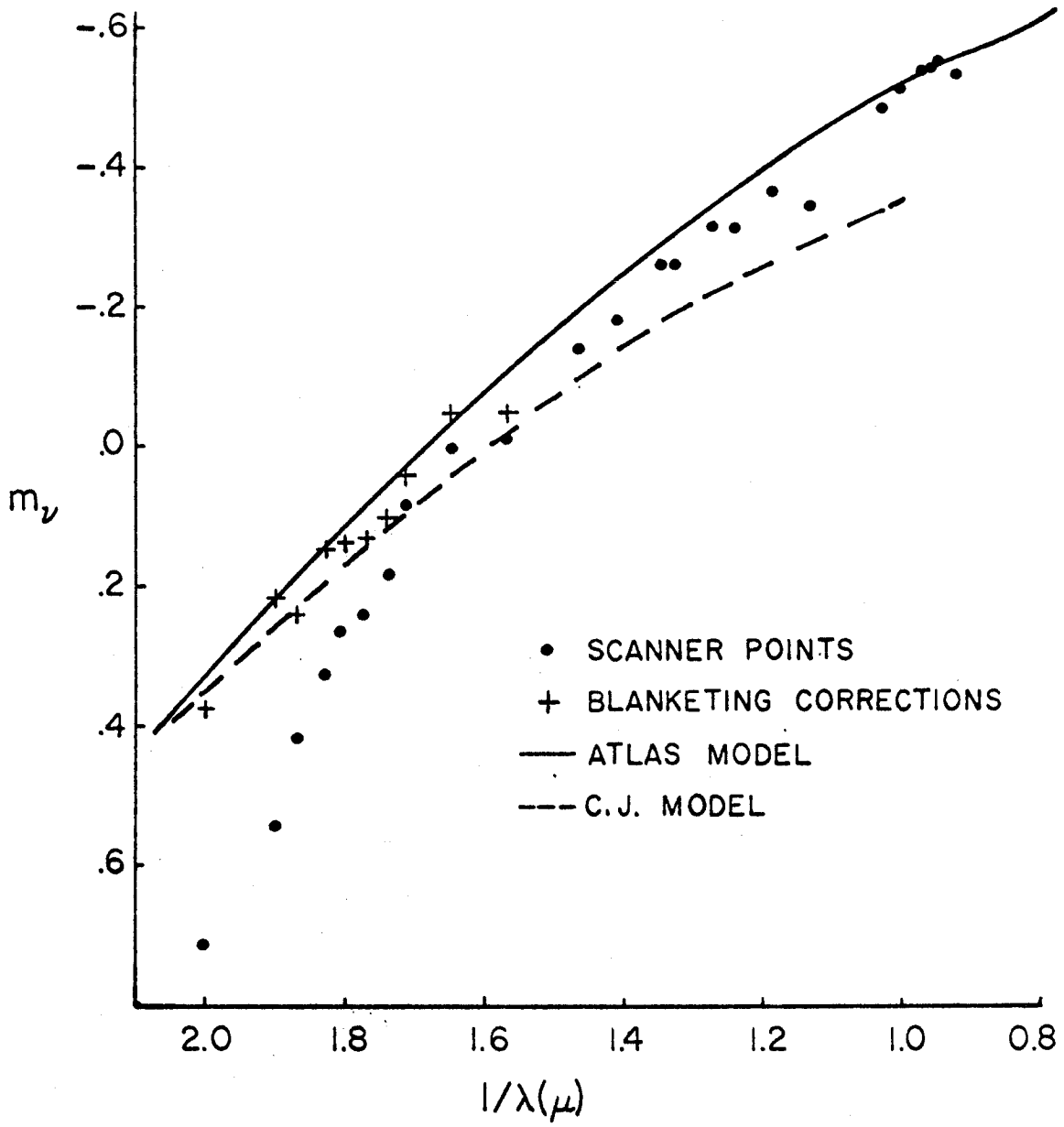

Fig. 15.--Deblanketed scan of HR 1614. It is apparent that the Cayrel and Jugaku model (T_{eff}(C.J.) = 5040 K), which forces equality of ion and neutral abundances, is too hot.

Fig. 16.--HR 8832: curve of growth (yellow - red region). The Cayrel and Jugaku model (T_{eff}(C.J.) = 5040 K) has been chosen to force equal abundances from Fe I and Fe II. The symbols are the same as in Fig. 12.

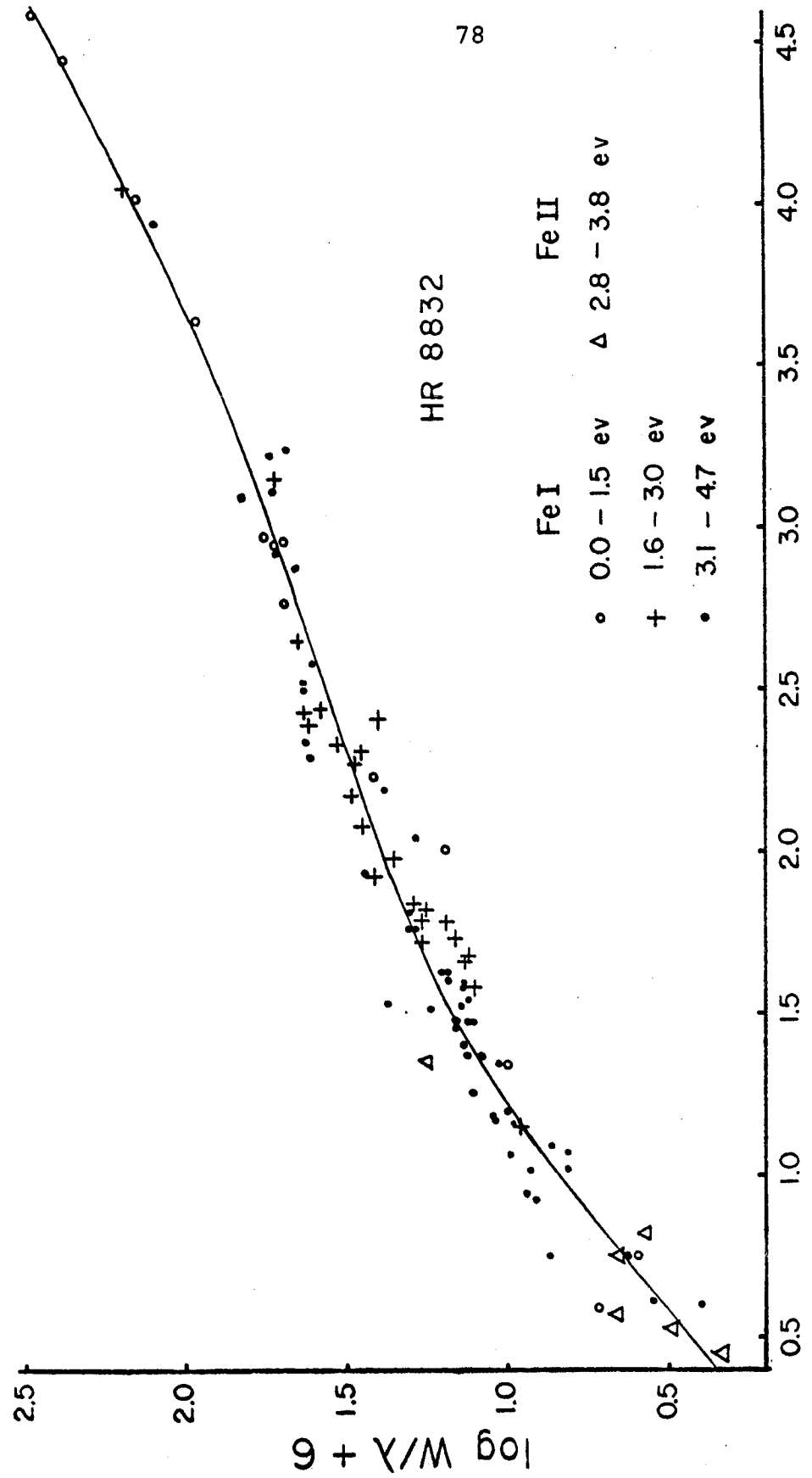
HR 8832
Fe I
Fe II
○ 0.0 – 1.5 ev
△ 2.8 – 3.8 ev
+ 1.6 – 3.0 ev
• 3.1 – 4.7 ev
log W/λ + δ
log $X_\odot$ + [Γ]
2.5
2.0
1.5
1.0
0.5
0.5
1.0
1.5
2.0
2.5
3.0
3.5
4.0
4.5

Fig. 17.--HR 8832: curve of growth (yellow - red region). The Cayrel and Jugaku model (T_{eff}(C.J.) = 4480 K) has been chosen to provide agreement with the scanner energy distribution. Note the large discrepancy between the Fe I and Fe II points. The symbols are the same as in Fig. 12.

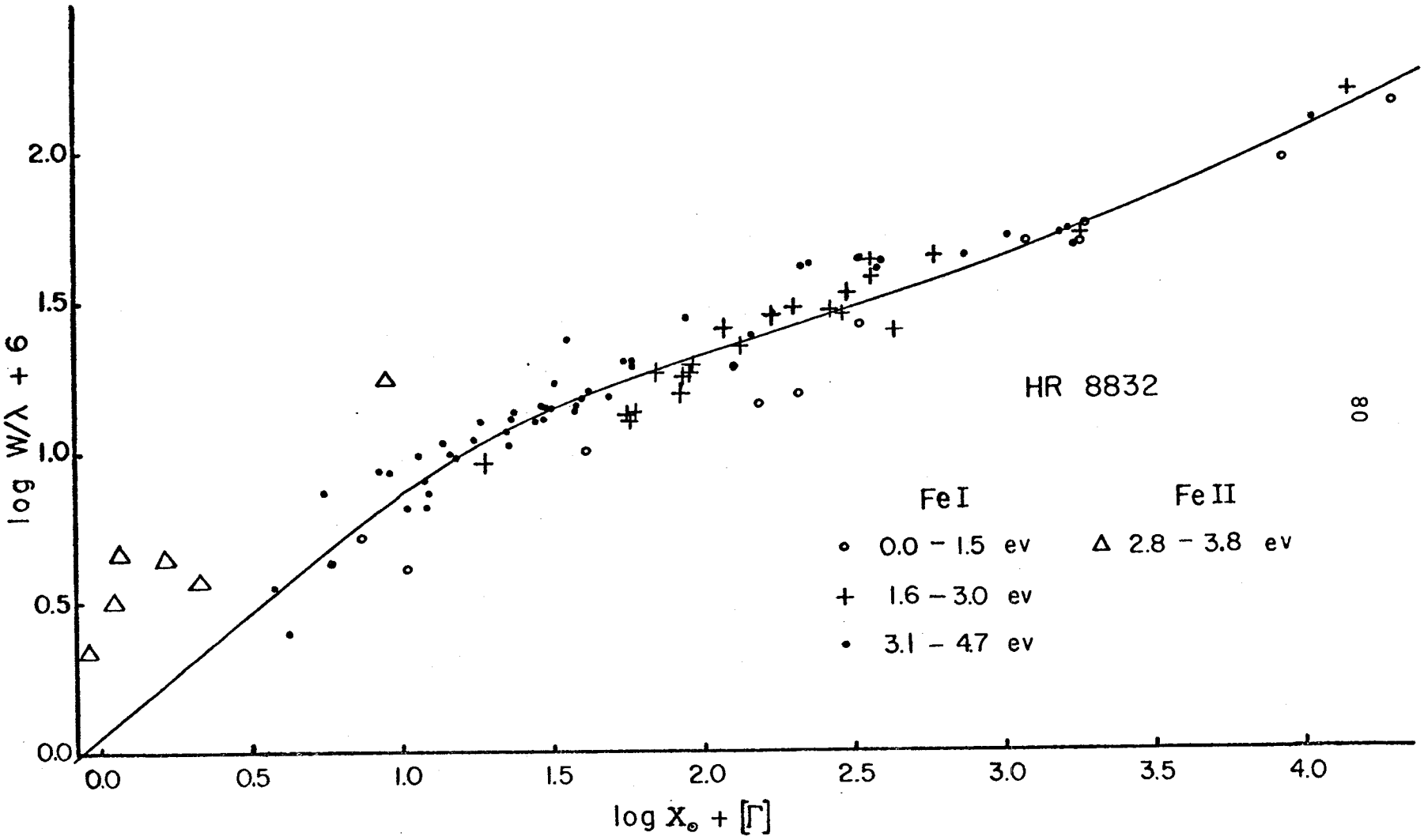
HR 8832
Fe I
Fe II
0.0 – 1.5 ev
1.6 – 3.0 ev
3.1 – 4.7 ev
2.8 – 3.8 ev
log W/λ + 6
log X₀ + [Γ]
0.0
0.5
1.0
1.5
2.0
2.5
3.0
3.5
4.0

should be mentioned that the abundances of elements that are easily ionized, e.g., Na and Ca, will depend strongly on the temperature of the assumed model in the range of spectral types being considered.

In spite of the as yet unexplained anomalies discussed above, the relative abundance of the metals derived for stars with similar temperatures should be fairly reliable. Thus, an inspection of Table 8 reveals that the stars found by Taylor (1970) to be strongly SMR (ρ^1 Cnc, 14 Her, and HR 1614) are indeed overabundant by $\sim$ .3 dex compared with the other dwarfs in the program. 54 Psc, listed as SMR on the basis of its strong CH and CN absorption, appears to be overabundant only in Na, while 70 Oph A, stated by Taylor (1969) as having Hyades abundances, appears to possess a marginally high abundance of Ca as well as Na. The temperature chosen for ε Eri is undoubtedly too high relative to the other stars with θ_{eff} = .95 since a comparison of the respective scans reveals its energy distribution to be considerably redder. A lower temperature would, of course, result in lower abundances, especially for Na.

d) Rough Analysis of the Giants

A preliminary rough analysis was also performed for the giants in the program (except ν UMa) and the results are shown in Table 9. The procedure involved the determination of θ_{ex} from the Fe I curve of growth and the assumption that

$\theta_I = \theta_{ex}$; the electron pressure was derived from a consideration of the Fe I - Fe II equilibrium. The solar gf values described previously, as well as the Hunger (1956) theoretical curve of growth with pure absorption in the M.E. model, were employed in the analysis. The exact details are available in any text on stellar atmospheres, e.g., Aller's Astrophysics (1963), and will not be repeated here. The abundances and the electron pressure are expressed relative to a mean for the three Hyades giants in the program.

The abundances in Table 9 are necessarily very rough, but a few trends are worth noting. First of all, only the two hottest SMR giants, HR 8924 and α Ser, have abundances that are substantially above the Hyades, but in no case does the Fe abundance exceed .2 dex. Na is the only element that is systematically overabundant by a large factor in all the SMR giants, which, in a sense, is not surprising since the strength of the Na-D lines is one of the main criteria in the selection of these stars. A second feature is the sharp drop in the relative abundances and the electron pressure after 18 Lib A; even θ UMi, which has been described as very strong lined, has abundances substantially below the Hyades. Part of the difference might well be due to incorrect values of θ_{ex}, but this is certainly not the whole story.

TABLE 9

ROUGH ANALYSIS* OF GIANTS RELATIVE TO THE HYADES

	HR 8924	11 Cep	α Ser	ν Aur	μ Leo	α Ari
θ_{ex}	1.13	1.20	1.20	1.20	1.23	1.23
P_e	.4	-.1	.0	-.3	-.5	-.7
Na	.6	.0	.4	-.1	.2	-.4
Ba II	.1	-.1	-.1	-.2	-.5	-.1
Ca	.5	.1	.2	-.1	-.1	-.2
Y II	-.5	.3	.3	.2	-.3	-.4
Sc	.3	.5	.6	.1	.3	-.3
Sc II	.3	.0	.3	.1	-.3	-.7
V	.8	.2	.5	.1	.2	-.2
Cr	.4	-.1	.2	-.1	.1	-.5
Cr II		.2	.6	.0	.0	-.4
Ti	.7	.1	.2	-.1	.1	-.2
Ti II	.5	-.2	.2	-.1	-.2	-.4
Zr	.6	.1	.3	.0	.1	-.3
Mn	.9	.0	.7	.0	.2	-.2
Mg	.4	-.1	.3	-.2	.0	-.3
Fe	.2	.0	.2	-.2	-.3	-.5
Si	.2	.0	.2	.0	-.1	-.3

*Abundances and P_e expressed logarithmically relative to the Hyades giants

Table 9 (continued)

ROUGH ANALYSIS* OF GIANTS RELATIVE TO THE HYADES

	HD 112127	18 Lib A	16 Aur	θ CMa	θ UMi
θ_{ex}	1.25	1.25	1.35	1.37	1.50
P_e	-.5	-.5	-1.4	-1.3	-2.4
Na	.1	.4	-.5	-.4	.1
Ba II	-.5	-.4	-1.2	-.8	-1.0
Ca	-.1	.0	-.4	-.4	-.2
Y II	-.7	-.1	-1.3	-.3	-.9
Sc	.4	.1	-.4	-.2	-.4
Sc II	-.4	-.2	-.9	-.8	-1.1
V	.3	.1	-.4	.0	-.2
Cr	-.1	.0	-.8	-.4	-.4
Cr II	.4	-.2	-.6	-.3	-.5
Ti	.1	.0	-.4	-.1	-.3
Ti II		-.3	-.7	-.4	-.7
Zr	.1	-.1	-1.0	-.5	-.6
Mn	.3	.0	-1.0	-.6	-.5
Mg	.2	.0	-.6	-.4	-.7
Fe	-.2	-.3	-1.0	-.8	-.9
Si	-.1	-.2	-.8	-.8	-.7

*Abundances and P_e expressed logarithmically relative to the Hyades giants

e) Fine Analysis

Unexpected anomalies have appeared in the results of the preliminary analysis of both the giants and the dwarfs - in the sense of increasing discrepancies with later spectral types. The next logical step in the attempt to clarify the situation is a fine analysis employing the results of the photoelectric measurements as well as the model atmospheres generated by Atlas.

Since the unblanketed models almost certainly give a wrong representation for the region of strong and medium-strong line formation, it was decided to use these lines to interpolate smoothly to the weak-line region of the curve of growth (with the aid of the FeI curve) and to calculate the abundance using a given point on the weak-line region of this mean curve. This procedure allows the use of many weak lines that have no published gf values; possible attendant errors are discussed in part j).

The abscissae of the curves of growth used in the preliminary analysis were

$$\log (gf\lambda)_S - \theta_{ex} \chi$$

in the case of the giants, where the subscript S refers to the fact that the gf values have been derived from the solar atmosphere, and log Y, which is equivalent to

$$\log Y = \log \Gamma_* + \log gf_S + \log (N_{el}/N_H)_\odot$$

in the case of the dwarfs. Therefore, it was possible to determine for each empirical curve of growth the gf_S value corresponding to a given log W/λ on the theoretical Hunger (1956) curve drawn in as the best fit. The derived gf_S's then represented the best value for a line (real or hypothetical) with the same log W/λ, and the abundance could then be derived using only this one representative line. Log gf_S values were derived for all the curves of growth for log W/λ = -5.5, and the turbulent velocities were determined from the vertical shift required to fit the empirical Fe I and the Hunger curves. The value of log W/λ = -5.5 was chosen because, with lines this weak, the derived abundance is quite insensitive to the precise value of the turbulence, and most stars had a least one curve (Fe I) that was reasonably well determined in this region.

In the case of the giants the determination of the gf_S's required the establishment of a mean excitation potential χ for each element; this posed no difficulties since the spread in χ was very small for all the elements except Fe I. Two curves were, in fact, constructed for Fe I - one for χ near 1 ev and another for values near 4 ev (these were used to determine θ_{ex} in the rough analysis); the great majority of Fe I lines in all the stars lie around 4 ev, so that this curve is the more reliable. Vertical shifts were also taken into account in drawing in the best fit for light elements

such as Na and Mg; i.e., an Fe I curve with the proper vertical correction was drawn through the points. In some of the hotter giants, including the three members of the Hyades, coincidence between the low and high e.p. Fe I curves could be achieved only by a downward vertical shift of the low e.p. curve by $\sim$ .04 dex. The effect is similar to the one found by Helfer and Wallerstein (1964) in the Hyades giants, although not quite as pronounced. Figure 18 illustrates the situation in the case of θ^1 Tau. In the stars requiring the vertical shift (11 Cep, ν Aur, and α Ari, in addition to the Hyades) it was found that a similar displacement improved the fit in the case of other elements with low e.p. lines, e.g., V and Ti. The effect on the resulting abundances is a decrease on the order of .1 dex.

The resulting abundances, based on models with assumed normal gravities and solar compositions, are listed in Tables 10 and 11. A glance at Table 10 (the dwarfs) reveals several features: (1) the abundances of the ions and neutrals do not agree, the discrepancy increasing with later spectral type; (2) the abundances of the neutrals are lower and those of the ions are higher than derived from the Cayrel and Jugaku models; (3) the SMR stars ρ^1 Cnc, 14 Her and HR 1614 have noticeably higher abundances than the other dwarfs.

The reason for the discrepancy in (2) is the fact that hotter models were used in the Cayrel and Jugaku method in

Fig. 18.--θ^1 Tau: curve of growth for low e.p. Fe I lines. A vertical shift of 0.06 dex is necessary to obtain agreement with the 4 ev Fe I curve.

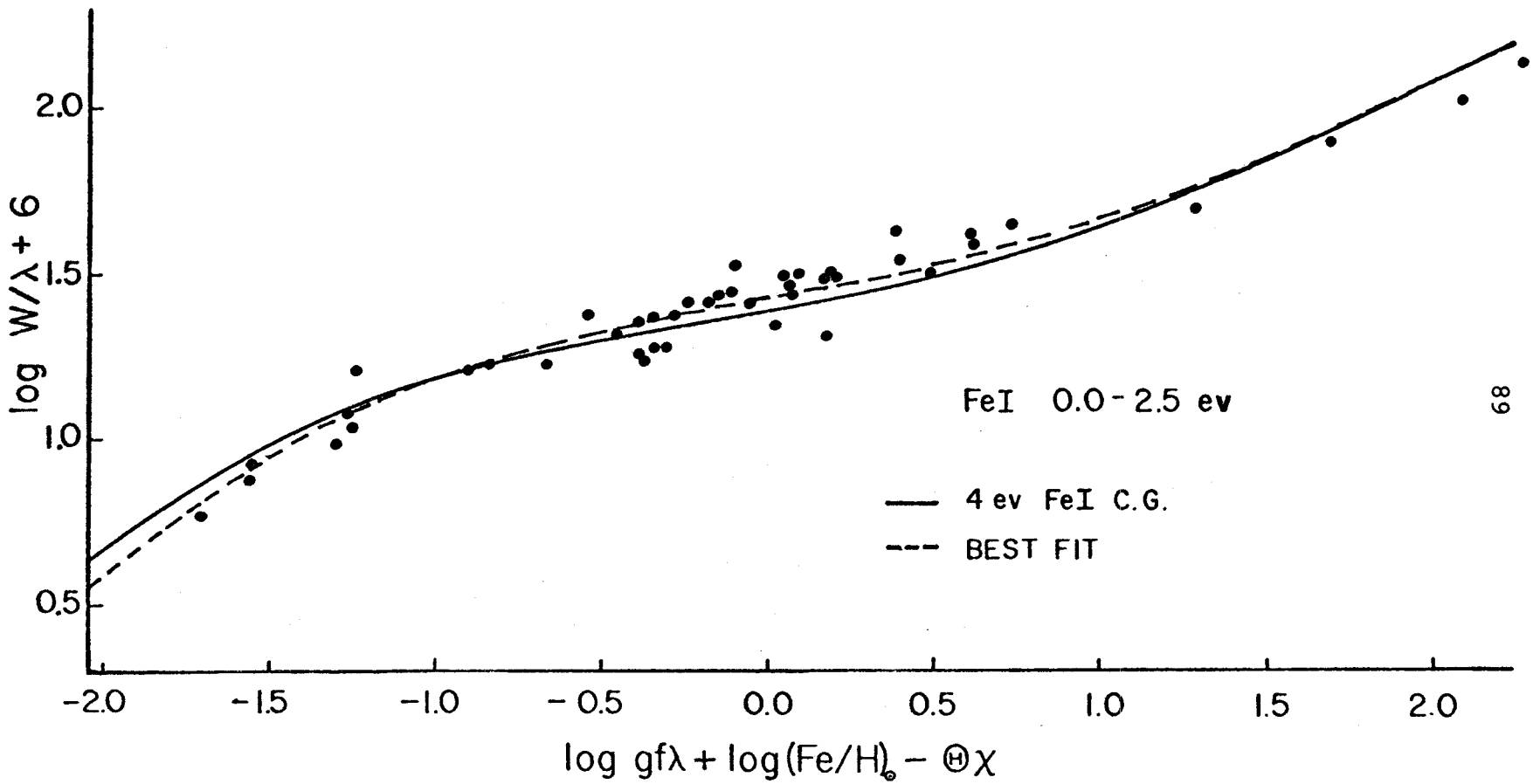
log W/λ + 6
2.0
1.5
1.0
0.5
-2.0
-1.5
-1.0
-0.5
0.0
0.5
1.0
1.5
2.0
log gfλ + log(Fe/H)⊙ − ΘχI
FeI 0.0 - 2.5 ev
4 ev FeI C.G.
BEST FIT

TABLE 10

DWARF MODEL ATMOSPHERE ABUNDANCES* FROM YELLOW-RED SPECTRA

	ξ Boo A	70 Oph A	ρ^1 Cnc	14 Her	σ Dra	54 Psc
T_{eff}	5600	5500	5400	5400	4300	5300
log g	4.4	4.4	4.4	4.4	4.4	4.4
v_ξ	2.3	2.5	1.9	1.9	2.0	1.9
Na	-.23	.17	.46	.54	-.12	.13
Ba II	.22	.02	.15	.21	.23†	.26
Ca	-.08	.10	.24	.33		.03
Sc	-.22†	.00†	.21	.29		-.04
Sc II	.08	.22	.32	.48		.09†
V	-.28	.07	.30	.37		.02
Cr	-.17	.01	.16	.15		-.13
Cr II	.14†	.24†	.35	.34		.21†
Ti	-.19	-.04	.20	.25		-.02
Ti II	-.04	.04	.34	.34		.11
Mn	-.38	-.04	.20	.42		-.13
Mg	-.15†	.11†	.23†	.30†		-.09†
Fe (1)	-.30	-.14	.09	.16	-.32	-.21
Fe (4)	-.24	-.11	.11	.18	-.22	-.15
Fe§	-.26	-.12	.11	.18	-.25	-.17
Fe II	.22	.19	.41	.40	.21	.29
Si	-.10	.10	.36	.29		.09

*Abundances are expressed logarithmically relative to the sun.

†Abundance has low weight.

§Fe is the mean of the abundance from the high and low e.p. lines, with Fe(1) given 1/3 weight.

Table 10 (continued)

DWARF MODEL ATMOSPHERE ABUNDANCES* FROM YELLOW-RED SPECTRA

	ε Eri	HR 6806	HR 8832	HR 1614	61 Cyg B
T_{eff}	5150	5000	4800	4900	3700
log g	4.4	4.4	4.4	4.4	4.6
v_{ξ}	2.3	2.3	2.2	2.1	2.2
Na	-.02	-.15	.09	.53	-.70
Ba II	.31	-.03	.04	.26	-.08
Ca	.01	-.15	-.06	.19	-.65
Sc	-.15†	-.27†	.03†	.06†	-.30
ScII	.12	.10	.22†	.37	
V	-.04	-.23	-.15	.34	-.43
Cr	-.14	-.43	-.13	.06	-.53
CrII	.37	.15		.25†	
Ti	-.15	-.27	-.20	.05	-.61
Ti II	.09	.02	.58†	.50	
Mn	-.20	-.66	-.22	-.06	-.21†
Mg	.08†	.03†	.07†	.29†	.03†
Fe (1)	-.29	-.41	-.40	-.08	-.65
Fe (4)	-.14	-.25	-.12	.07	.06†
Fe§	-.19	-.30	-.21	.02	-.65
Fe II	.33	.45	.67	.67	2.53†
Si	.01	.02	.18	.35	.84†

*Abundances are expressed logarithmically relative to the sun.
†Abundance has low weight.
§Fe is the mean of the abundance from the high and low e.p. lines, with Fe (1) given 1/3 weight.

TABLE 11

GIANT MODEL ATMOSPHERE ABUNDANCES*

	θ^1Tau	γ Tau	ε Tau	HR 8924	11 Cep	α Ser	ν Aur	μ Leo
T_{eff}	5150	5050	5050	4900	4800	4750	4750	4650
log g	2.7	2.7	2.7	2.6	2.5	2.5	2.5	2.4
v_ξ	1.4	1.4	1.6	1.5	1.5	1.8	1.4	1.8
Na	.17	.33	.28	.66	.20	.57	.10†	.43
Ba II	.57†	.52†	.48†	.13†	.39†	.63†	.35†	.24†
Ca	.10	.11	.23	.46	.10	.29	-.07	.15
Y II	.09†	-.18†	-.07†		.16†	.14	.24†	-.18†
Sc	.18	.14	.29	.25	.62†	.71†	.12†	.54†
Sc II	.18	.28	.29	.12	.21	.37	.44	.23
V	.24	.28	.29	.78	.41	.72	.16	.55
Cr	.16	.15	.21	.30	.04	.35	.00	.27
Cr II	.12	.29	.42		.41	.73	.32	.53
Ti	.20	.05	.08	.47	.16	.31	-.02	.25
Ti II	.22	.29	.37†	.23†	.09†	.35†	.23†	.30†
Zr	.18†	.06†	-.04	.26	.11†	.28	-.10	.18~
Mn	.24†	.14†	.29†	.92†	.25†	.89†	.10†	.54†
Mg	.13	.10	.19	.35†	.00†	.49†	-.05†	.16†
Fe (1)	.11	.00	.04	.00	-.03	.20	-.17	-.01
Fe (4)	.22	.08	.09	.10	.09	.24	-.07	-.01
Fe§	.18	.05	.07	.07	.05	.23	-.10	-.01
Fe II	.16	.14	.19	.03	.10	.20	.13	.14
Si	.15	.17	.22	.19	.12	.34	.23	.20

*Abundances are expressed logarithmically relative to the sun.
†Abundance has low weight.
§Fe is the mean of the abundances from the high and low e.p. lines, with Fe(1) given 1/3 weight.

Table 11 (continued)

GIANT MODEL ATMOSPHERE ABUNDANCES*

	α Ari	HD112127	18 Lib A	16 Aur	ν UMa	θ CMa	θ UMi
T_{eff}	4650	4600	4550	4250	4200	3900	3750
log g	2.4	2.3	2.3	2.1	2.1	1.9	1.7
v_ξ	1.6	2.4	2.0	1.6	1.9	1.7	1.9
Na	-.10	.25	.72	-.19	.04	-.41	.39
Ba II	.59†	.30†	.41†	.16†	1.12†	.41†	.81†
Ca	.06	-.01	.21	-.19	-.13	-.46	-.08
Y II	-.06		.06	-.50†		.33†	.44†
Sc	-.07†	.51†	.34†	-.13†		-.83†	-.19†
Sc II	.05	-.05	.21	.18	.38	.24	.58
V	.17	.54	.37	.01	.12	.04	.41
Cr	-.29	-.01	.20	-.51	-.37	-.35	.04
Cr II	.37	.79†	.32†	.51	.57	.95†	1.35†
Ti	-.01	.14	.09	-.19	-.21	-.28	-.01†
Ti II	.41†	-.23†	.26	.42†	1.18†	.64†	1.18†
Zr	-.19	.04	-.08	-.83†	-.32	-.86	-.48
Mn	.10†	.48†	.32†	-.50†	-.03†	-.06†	.56†
Mg	-.15†	.19†	.23†	-.03†	-.17†	.17†	.31†
Fe (1)	-.25	-.13	-.01	-.41	-.16	-.35	.26
Fe (4)	-.19	-.07	-.02	-.39	-.20	-.09	.17
Fe§	-.21	-.09	-.02	-.39	-.19	-.22	.20
Fe II	.13	.04†	.17	.32	.48	.82	1.42
Si	.19	.14	.21	.02	.31	.48	.73

*Abundances are expressed logarithmically relative to the sun.
†Abundance has low weight.
§Fe is the mean of the abundances from the high and low e.p. lines, with Fe(1) given 1/3 weight.

order to force equality of the ions and neutrals, while in the present method the temperatures were derived independently. It should be noted that the "effective temperatures" used in the two methods are both nominal (i.e., are not directly related to the total emitted flux although the T_{eff} in the Cayrel and Jugaku models comes closer to being so), and while the Atlas T_{eff} is a characteristic temperature of the continuum forming regions, such is not the case with the Cayrel and Jugaku models. In fact the energy distributions from the two sets of models will be equal if the Cayrel and Jugaku T_{eff} is decreased by 7%. Thus, even though the same T_{eff} is obtained for ξ Boo A by the two methods, the Cayrel and Jugaku model is hotter by $\sim$ 300° in the weak line and continuum forming regions. With this in mind, it is seen that consistent results are obtained by the two methods.

Looking now at the giant abundances (Table 11) we find the same discrepancies between the ions and neutrals as in the dwarfs, although the situation is not too bad for stars of earlier type than 16 Aur (K3 III). In fact the neutral and ion abundances agree nicely in θ^1 Tau, while for HR 8924 a slight underabundance is even derived for the ions. The latter result indicates that HR 8924 may belong to luminosity class III - IV, a conclusion which appears reasonable also on the basis of the absolute magnitude data (see Chapter II). A comparison with the rough analysis (Table 9) shows good

agreement for the hotter stars, but for the cool stars the rough analysis predicts much lower ion abundances; the abundances of neutral elements that are mostly ionized even at low temperatures (e.g., Na and Ca) are in fair agreement for all the stars, however. The differences are, of course, due to the fact that in the rough analysis the Fe I and Fe II abundances were forced to be equal, thereby providing a relationship that allows the derivation of the electron pressure; as noted previously the derived P_e is extremely low for stars cooler than 18 Lib A, which implies that the spectroscopic gravity will also be very small.

As a next step, the gravity in the Atlas models was varied in order to force equality between the ions and neutrals; Tables 12 and 13 show the results.

The procedure involved an estimate of the gravity change required for each new model, the calculation of the appropriate model, and the derivation of a new set of abundances (which showed much better agreement between the neutrals and ions). Instead of now generating another complete set of models to remove any small discrepancies, the following method was employed. In all the models the weak line strengths vary as $(a \cdot g)^{\alpha}$, where a is the abundance of the electron donors and $\alpha \simeq 0.5$ for the ions and $\alpha \simeq 0$ for lines of neutral elements that are mostly ionized. A grid of values of α was calculated for various temperatures and gravities for several

TABLE 12

DWARF ABUNDANCES* WITH FORCED EQUALITY OF IONS AND NEUTRALS (YELLOW-RED SPECTRA)

	ξ Boo A	70 Oph A	ρ^1 Cnc	14 Her	σ Dra	54 Psc
T_{eff}	5600	5500	5400	5400	5300	5300
log g	3.8	3.9	3.6	3.8	3.7	3.8
log a:	-.3	.0	.2	.2	-.3	-.2
Na	-.23	.17	.46	.54	-.12	.13
Ba II	-.14	-.19	-.11	.03	-.21	-.14
Ca	-.08	.10	.24	.33		.03
Sc	-.22†	.00†	.21	.29		-.04
Sc II	-.31	-.01	.06	.30		-.27
V	-.28	.07	.30	.37		.02
Cr	-.17	.01	.16	.15		-.13
Cr II	-.25†	.02†	.07	.16		-.16†
Ti	-.19	-.04	.20	.25		-.02
Ti II	-.43	-.18	.06	.16		-.26
Mn	-.40	-.06	.17	.40		-.17
Mg	-.17†	.09†	.20†	.28†		-.13†
Fe (1)	-.37	-.18	.04	.13	-.41	-.28
Fe (4)	-.30	-.14	.06	.15	-.29	-.21
Fe§	-.32	-.15	.06	.15	-.33	-.23
Fe II	-.23	-.05	.11	.20	-.31	-.14
Si	-.27	.00	.22	.20		-.10

: a ≡ mean of Fe, Mg, Si abundances.
*Abundances are expressed logarithmically relative to the sun.
†Abundance has low weight.
§Fe is the mean of the abundance from the high and low e.p. lines, with Fe(1) given 1/3 weight.

Table 12 (continued)

DWARF ABUNDANCES* WITH FORCED EQUALITY OF IONS AND NEUTRALS (YELLOW-RED SPECTRA)

	ε Eri	HR 6806	HR 8832	HR 1614	61 Cyg B††
T_{eff}	5150	5000	4800	4900	3850
log g	3.6	3.3	2.7	3.2	1.2
log a:	-.2	-.3	-.3	.0	-1.3
Na	-.02	-.15	.09	.53	-.64
Ba II	-.13	-.63	-.58	-.03	-1.86
Ca	.01	-.16	-.06	.19	-.78
Sc	-.15†	-.27†	.03†	.06†	-.53
Sc II	-.32	-.51	-.70†	-.16	
V	-.04	-.23	-.18	.34	-1.32
Cr	-.14	-.43	-.16	.06	-1.14
Cr II	-.07	-.47		-.28†	
Ti	-.15	-.27	-.24	.05	-1.16
Ti II	-.35	-.60	-.34†	-.03	
Mn	-.28	-.80	-.46	-.18	-1.58†
Mg	.00†	-.11†	-.17†	.17†	-1.28†
Fe (1)	-.43	-.64	-.77	-.27	-2.16
Fe (4)	-.25	-.44	-.45	-.10	-1.44†
Fe§	-.28	-.50	-.51	-.03	-1.92
Fe II	-.20	-.30	-.49	.01	-.71†
Si	-.25	-.36	-.40	.01	-.97†

: a ≡ mean of Fe, Mg, Si abundances.

*Abundances are expressed logarithmically relative to the sun.

†Abundance has low weight.

§Fe is the mean of the abundance from the high and low e.p. lines, with Fe(1) given 1/3 weight.

††log g has been determined from blue plate data.

TABLE 13

GIANT ABUNDANCES* WITH FORCED EQUALITY OF IONS AND NEUTRALS

	θ^1Tau	γ Tau	ε Tau	HR 8924	11 Cep	α Ser	ν Aur	μ Leo
T_{eff}	5150	5050	5050	4900	4800	4750	4750	4650
log g	2.5	2.3	2.2	2.7	2.3	2.0	1.9	1.9
log a:	.2	.1	.1	.2	.0	.3	-.1	.1
Na	.17	.33	.28	.66	.20	.57	.10	.43
Ba II	.57†	.39†	.31†	.24†	.30†	.55†	.09†	.08†
Ca	.10	.11	.23	.46	.10	.29	-.07	.15
Y II	.09†	-.31†	-.24†		.07†	.06†	-.06†	-.34†
Sc	.18	.14	.29	.25	.62†	.71†	.12†	.54†
Sc II	.18	.15	.12	.25	.12	.29	.15	.07
V	.24	.28	.29	.78	.41	.72	.16	.55
Cr	.16	.15	.21	.30	.04	.35	.00	.27
Cr II	.12	.16	.24		.32	.65	.04	.36
Ti	.20	.05	.08	.47	.16	.31	-.02	.25
Ti II	.22	.16	.19†	.37†	.00†	.27†	-.05†	.13†
Zr	.18†	.06†	-.04	.26	.11†	.28	-.10	.18†
Mn	.24†	.13†	.27†	.93†	.23†	.88†	.08†	.51†
Mg	.13	.08	.17	.36†	-.02†	.48†	-.07†	.13†
Fe (1)	.11	-.02	.00	.04	-.07	.19	-.22	-.06
Fe (4)	.22	.06	.06	.13	.07	.23	-.12	-.06
Fe§	.18	.03	.04	.10	.02	.22	-.15	-.06
Fe II	.16	-.01	.00	.15	.00	.12	-.15	-.03
Si	.15	.11	.13	.26	.07	.29	.07	.09

: a $\equiv$ mean of Fe, Mg, Si abundances.
*Abundances are expressed logarithmically relative to the sun.
†Abundance has low weight.
§Fe is the mean of the abundance from the high and low e.p. lines, with Fe(1) given 1/3 weight.

Table 13 (continued)

GIANT ABUNDANCES* WITH FORCED EQUALITY OF IONS AND NEUTRALS

	α Ari	HD112127	18 Lib A	16 Aur	ν UMa	θ CMa	θ UMi
T_{eff}	4650	4600	4550	4250	4200	4000	3850
log g	1.6	2.0	1.9	.7	.7	.3	-.5
log a:	-.3	.0	.1	-.5	-.4	-.5	-.4
Na	-.10	.25	.72	-.19	.04	-.27	.57
Ba II	.15†	.18†	.28†	-.63†	.38†	-.40†	-.18†
Ca	.06	-.01	.21	-.19	-.13	-.29	.11
Y II	-.51		-.07	-1.31†		-.57†	-.65†
Sc	-.08†	.51†	.34†	-.13†		-.69†	-.06†
Sc II	-.34	-.17	.09	-.62	-.38	-.68	-.60
V	.15	.54	.37	.01	.12	.06	.32
Cr	-.31	-.01	.20	-.51	-.37	-.33	-.02
Cr II	-.10	.67†	.19†	-.34	-.23	-.23†	.04†
Ti	-.03	.14	.09	-.19	-.21	-.18	.08
Ti II	-.06†	-.35†	.13	-.43†	.38†	-.33†	-.13†
Zr	-.21	.04	-.08	-.83†	-.32	-.71	-.33
Mn	-.01†	.46†	.29†	-.74†	-.26†	-.47†	-.02†
Mg	-.26†	.17†	.20†	-.27†	-.40†	-.27†	-.31†
Fe (1)	-.42	-.17	-.06	-.86	-.54	-.92	-.57
Fe (4)	-.34	-.10	-.06	-.72	-.53	-.69	-.55
Fe§	-.37	-.12	-.06	-.77	-.53	-.77	-.55
Fe II	-.42	-.10†	.01	-.78	-.56	-.81	-.49
Si	-.25	.06	.13	-.56	-.23	-.47	-.30

: a ≡ mean of Fe, Mg, Si abundances.
*Abundances are expressed logarithmically relative to the sun.
†Abundance has low weight.
§Fe is the mean of the abundances from the high and low e.p. lines, with Fe(1) given 1/3 weight.

ions and neutrals and this was used to derive the final value of a•g (a is completely equivalent to g in the effect on the abundances).

An attempt was made to determine the accuracy of the derived spectroscopic gravities. In the most favorable cases (the hottest stars) the accuracy of the relative shifts in the neutral and ion curves of growth is expected to be about .10 dex (averaged over the Fe, Ti, and Cr neutral-ion pairs), while for the coolest stars the value is around .20 dex. Errors of this size will result in uncertainties in log (a•g) of .2 and .4 dex, respectively. In addition, errors in the assumed temperatures will also produce errors in the derived gravities. For example, the use of Hayes' calibration of Vega would increase the scanner temperatures by slightly less than 2%, which would result in somewhat lower ion abundances; the effect is a systematic increase of .2 to .3 dex in the derived values of the spectroscopic gravity. The total error in the derived gravities is thus expected to be between .4 and .7 dex for the hottest and coolest stars, respectively.

Taking the above errors to be in the most favorable sense (i.e., in the direction of too small derived gravities) it is seen that for the giants the gravity begins to be unacceptably low at T = 4250 K, while in the case of the dwarfs the values are all too low, particularly for T < 5150 K. HR 8832, for example, has a spectroscopic gravity characteristic

of a giant.

It was thought that some error might have been introduced into the foregoing analysis by the scarcity and relative weakness of ionized lines in the yellow-red spectral region, particularly in the case of the dwarfs. An analagous analysis was therefore carried out for most of the dwarfs based on line measurements on tracings of blue plates. Equivalent widths of neutral and ionized Fe, Ti, and Cr were measured in the wavelength region longward of 4500 Å on IIa-O plates; line blending is serious even in this region of blanketing minimum and the continuum is rather poorly defined for the cooler dwarfs. Nonetheless, many ionized lines could be measured even in 61 Cyg B, although the region longward of 4700 Å had to be eliminated due to the extremely strong MgH absorption. Table 14 shows the results, which show fairly good agreement with the numbers obtained by means of the previous analysis. The largest difference is in the value of the gravity for HR 8832, but for the stars as a group there is no systematic trend toward higher gravities.

There does, however, appear to be a slight difference in the abundances, in that somewhat lower values are derived for Ti and Cr from the blue spectra. In the case of Fe, however, there is good agreement, and since the Fe curve of growth is the best determined it seems probable that there is no large difference in the photometry of the blue and yellow-red regions.

TABLE 14

DWARF ABUNDANCES* WITH FORCED EQUALITY OF IONS AND NEUTRALS
(BLUE SPECTRA)

	T_{eff}	log g	Fe	Fe II	Ti	Ti II	Cr	Cr II
ξ Boo A	5600	3.9	-.36	-.42	-.48	-.45	-.30	-.28
70 Oph A	5500	3.9	-.11	-.17	-.10	-.08	-.10	.08
ρ^1 Cnc	5400	3.5	.16	.04	.08	.12	.15	.26
14 Her	5400	3.4	.26	.19	.20	.21	.24	.42
HR 8606	5000	3.3	-.50	-.56	-.55	-.58	-.45	-.26
HR 8832	4800	3.4	-.44	-.37	-.47	-.56	-.42	-.29
HR 1614	4900	3.1	-.05	-.18	.07	.24	.24	.32
61 Cyg B	3850	1.2	-1.56	-1.28	-1.48	-1.89	-1.07	-1.17

*Abundances are expressed logarithmically relative to the sun. The overall metal abundance, log a, is the same as in Table 13.

Inspection of the tables reveals that the effect of a change in the gravity on the abundances derived from neutral lines of mostly ionized elements is extremely small. Fe, Si and Mg, the main electron donors, all have high ionization potentials, however, so that their abundances are more or less gravity dependent. For the three coolest stars (61 Cyg B, θ CMa, and θ UMi) the gravity change is so large that a difference in the emergent flux distribution of the corresponding models becomes evident, necessitating a slight increase in the value of T_{eff} in order to maintain agreement with the scans.

f) Stellar Masses

It is of some interest to determine what masses are implied by the derived gravities. The surface gravity, expressed relative to the solar value, is given by

$$(3) \quad \log (g/g_{\odot}) = \log (M/M_{\odot}) + 4 \log (T_e/T_{e_{\odot}}) + .4(M_b - M_{b_{\odot}})$$

where T_e denotes the true effective temperature, as opposed to the nominal T_{eff}. The differences between the two temperatures are expected to be fairly small, so that T_{eff} could be used in equation (3) with little attendant error. It was decided, however, to calculate true effective temperatures for at least some of the program stars, using the general procedure employed by Oke and Conti (1966).

The method involves a measurement of the total flux blocked by the absorption lines, whereupon T_e is given by

$$T_e = T_{eff} \, (F/F_c)^{\frac{1}{4}}$$

where F is the total flux from the star and F_c is the flux from the line-free model that best fits the continuum between the lines. The flux ratios were obtained by superimposing the scanner points directly on the emergent flux distribution curve of the appropriate model, the fit being achieved by means of the de-blanketed points. The scanner wavelengths cover the region λλ4000-10800, where the data of Taylor (1970) and ST were used for λ<5000 Å. In order to obtain information on the absorption further in the infrared the equivalent widths of features in the λλ11400-25130 region of Arcturus measured by Montgomery et al. (1969) were summed and converted to η's (blocking fractions) covering 500 Å intervals. Although the CO bands are quite strong, the fraction of total flux removed remains rather small, particularly since the energy curves of K stars are fairly low in the region of maximum line strength (2.4μ). Since there is no scanner data for λ<4000 Å the blanketing in this region was set equal to that obtained for the 30 Å passband centered on λ4227 of Ca I.

Effective temperatures were calculated for four stars (ρ^1 Cnc, HR 8832, μ Leo, and θ UMi), and since the corrections to the nominal T_{eff} were small in each case (≃ 3%) the

values of T_e for the remaining stars were simply obtained by interpolation. The results (Table 15) are in excellent agreement with those of Oke and Conti (1966) when proper account is taken of the different absolute calibrations of Vega that were used. The internal error in log T_e is expected to be about 0.006 dex (75 K at T =5000 K); systematic errors may well be somewhat larger, but this will not alter any of the conclusions reached here. Figure 19 shows the energy curve for μ Leo, with the scanner points and the absorption from CO included. It is apparent that the bulk of the radiation is in the near infrared, which reduces the effect of the strong absorption in the blue and visual regions.

The absolute magnitudes of the dwarfs were calculated by means of the parallaxes published in the General Catalogue of Trigonometric Stellar Parallaxes (Jenkins 1952), with accuracies better than 0.1 mag in most cases. The trigonometric parallaxes of the giants are much too uncertain for all but a few of the nearest stars, i.e., α Ari and α Ser; however, H and K line magnitudes for several giants were kindly provided by Dr. Olin Wilson, and in a few cases the reversal widths were measured by the writer. Bolometric corrections were obtained from Johnson (1966).

The masses, calculated by equation (3), are given in Table 15 along with the relevant data. Effective temperatures based on Johnson's (1966) values of T_e vs. R-I are

Fig. 19.--Line blanketing in μ Leo relative to the adopted Atlas model. The blanketing in the far infrared is from the data of Montgomery et al. (1969) for Arcturus. Note the rather small effect of the heavy blanketing in the blue on the total emergent flux.

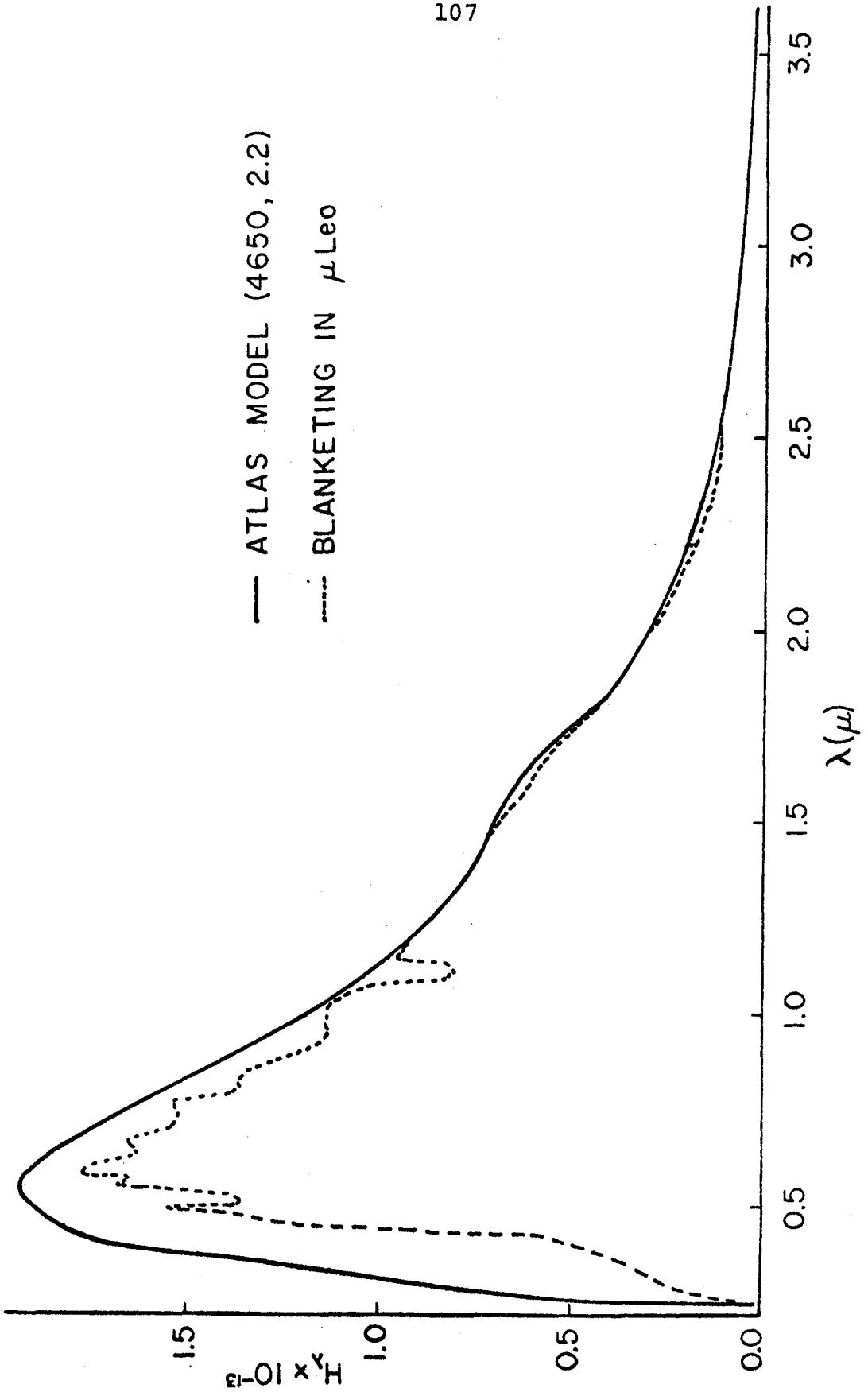
ATLAS MODEL (4650, 2.2)
BLANKETING IN μ Leo
$H_\lambda \times 10^{-13}$
1.5
1.0
0.5
0.0
0.5
1.0
1.5
2.0
2.5
3.0
3.5
λ(μ)

TABLE 15

SPECTROSCOPIC MASSES AND EFFECTIVE TEMPERATURES

STAR	T_e	T_e(J)	M_v	B.C.	log g	$M/M_\odot$
ξ Boo A	5450		5.35	-.05	3.8	.2
70 Oph A	5310	5440	5.39	-.12	3.9	.3
ρ^1 Cnc	5180	5340	5.29	-.12	3.6	.2
14 Her	5180	5340	5.64	-.12	3.6	.1
σ Dra	5120	5290	5.94	-.12	3.7	.1
54 Psc	5120	5390	5.84	-.12	3.8	.2
ε Eri	5000	5000	6.14	-.22	3.6	.1
HR 6806	4850	4920	6.30	-.26	3.3	.05
HR 8832	4650	4760	6.48	-.33	3.1	.03
HR 1614	4750	4920	6.30	-.26	3.2	.04
61 Cyg B	3650	3900	8.35	-.90	1.2	.0004
θ^1 Tau	5000		.80	-.20	2.5	1.0
γ Tau	4900		.80	-.20	2.3	.8
ε Tau	4900	4810	.54	-.24	2.2	.7
HR 8924	4700		3.2†	-.26	2.7	.2
11 Cep	4650	4680	1.3*	-.32	2.3	.6
α Ser	4560	4580	1.1§	-.36	2.0	.4
ν Aur	4610	4580	.2**	-.36	1.9	.7
μ Leo	4440	4460	.4†	-.42	1.9	.7
α Ari	4500	4300	.2**	-.42	1.6	.4
HD 112127	4400	4460	.4††	-.44	2.0	1.0
18 Lib A	4370	4370	1.5§§	-.47	1.9	.3
16 Aur	4130	4090	-.3**	-.72	.7	.2
ν UMa	4080	4100	-.7†	-.70	.7	.2
θ CMa	3780	3960	.3§	-.86	.3	.05
θ UMi	3660	3820	-1.0§	-1.04	-.5	.04

† Wilson (1971)

* K-line magnitude measured by the writer

§ Mean of K-line and trig. parallax

§§ Bidelman (1958)

†† Blaauw (1963)

** Trig. parallax

included for purposes of comparison with the temperatures derived in this work.

It is apparent that the low spectroscopic gravities have resulted in unacceptably low masses. In fact, two of the visual binaries, ξ Boo A and 70 Oph A, have well determined orbits and, therefore, reliable masses of 0.83 and $0.89 M_{\odot}$ respectively (Harris et al. 1963); comparison with Table 15 reveals that the spectroscopic masses are lower by factors between 3 and 4. A judicious stretching of the possible errors can explain away the discrepancies in this case, but the situation gets completely out of hand for slightly cooler stars.

g) Molecular Bands

Information on surface gravities can be obtained from luminosity sensitive molecular bands; for example, CN and C_2 are both known to correlate positively with luminosity while, on the other hand, MgH exhibits a negative correlation. The difficulty in working with CN is that it is necessary to use the lines in the infrared CN red system in order to avoid the heavy blanketing which is present throughout the spectral region occupied by the CN violet system. The SMR stars all possess enhanced CN absorption, but their spectroscopic gravities are no lower than those of the comparison stars, leading to the conclusion that nitrogen may well share in the metal enrichment in these stars. The work of Greene (1969) on α Ser also supports this interpretation.

An article on C_2 Swan band strengths in ρ^1 Cnc, 14 Her, and 70 Oph A by Greenstein and Oinas (1968) is reproduced in the Appendix. The results show that the enhanced C_2 absorption in ρ^1 Cnc and 14 Her can be explained on the basis of dwarf model atmospheres with equal carbon and oxygen abundances, while the C/O ratio in 70 Oph A is only slightly higher than in the sun. Subsequently, an attempt was made to measure C_2 lines in the K2 dwarf HR 6806, but the band proved to be much too weak, in keeping with the interpretation, based on Schadee's (1968) models, that the star has a gravity characteristic of a dwarf and normal metal abundances.

The spectroscopic gravity of HR 8832 (log g = 3.0) is low enough to approach a giant of the same spectral class. It was therefore decided to compare the strength of the MgH (0,0) band near 5180 Å with that of the giant star 11 Cep, which has the same effective temperature and a spectroscopic gravity of log g = 2.3. Several lines in Schadee's (1964) list were measured in the region between 5050 and 5200 Å. Line blending and uncertainties in the placement of the continuum are severe in this region, but these effects should cancel out to some extent in a differential comparison of the two stars. Rotational line strengths S_K were calculated from formulae in Schadee (1964) and the usual graphs of log W_K/S_K vs. K(K+1) were constructed. Although the scatter was fairly large, particularly for HR 8832, the band intensity log W_o/S_o

turned out to be 2.0 ± 0.3 and 1.0 ± 0.2 respectively for HR 8832 and 11 Cep; i.e., the ratio of the number of MgH molecules "above the photosphere" in the two stars is ten to one. In order to compare this result with the model predictions the following simple one-layer approximation was used. The number of molecules N above the atmosphere is given approximately by

$$N(MgH) = \frac{\tau P_{MgH}}{\kappa M_H \bar{\mu} P_g} \tag{3}$$

Introducing the dissociation constant K(T), where

$$K(T) = \frac{P_{Mg} P_H}{P_{MgH}}$$

and assuming that $\bar{\mu} = 1.27$ and $N_{Mg}/N_H = 3.2 \times 10^{-5}$ the following expression is obtained:

$$N(MgH) = 1.2 \times 10^{19} \frac{\tau P_g (1-x)}{\kappa K(T)} \tag{4}$$

where x is the degree of ionization of Mg. Values of P_g, κ, and T were obtained from the (4800, 4.4) and (4800, 2.6) models at (Rosseland) optical depths of 0.06, 0.12, and 0.22; three points were chosen in order to determine what effect the exact choice of the "representative point" would have on the derived values. The dissociation constants K(T) were obtained from Tsuji (1964). The values of N(MgH) turned out

to be 5.5×10^{15}, 7.5×10^{15}, and 8.3×10^{15} for the dwarf atmosphere, and 9.5×10^{14}, 1.1×10^{15}, 1.1×10^{15} for the giant. Assuming that the mean depth of formation of MgH could be different in the two stars, the maximum and minimum ratios of the number of molecules above the photosphere turn out to be 8.7 and 5.0 respectively. When compared with the empirical ratio of 10 it is seen that a gravity difference larger than 1.8 dex is required to explain the relative strengths of MgH. It appears, therefore, that the spectroscopic gravities in the cool dwarfs are much too low.

h) The H-R Diagram

An H-R diagram for the program stars, constructed from the data in Table 15, is presented in Figure 20. It was decided to employ T_e as the abscissa instead of the usual B-V since the latter is sensitive to metal abundances. Also included in the diagrams are loci of the old galactic clusters M67 (Sandage 1955) and NGC 188 (Sandage 1962), in addition to a plot of cool stars in the solar neighborhood with $\pi > 0''.050$ and R-I colors in the literature; a list of nearby field stars with accurate parallaxes was obtained from Arp (1958). The B-V colors in the published cluster diagrams (corrected for reddening) were transformed to R-I via Johnson's (1966) calibration and thence to the T_e of Table 15 by means of the R-I vs. log T_e relation for the program stars

Fig. 20.--H-R diagram for the program stars and nearby field stars with accurate parallaxes. Note the tendency of the SMR giants to lie near the old open cluster loci. Note also the positions of the SMR dwarfs on the upper bound of the main sequence.

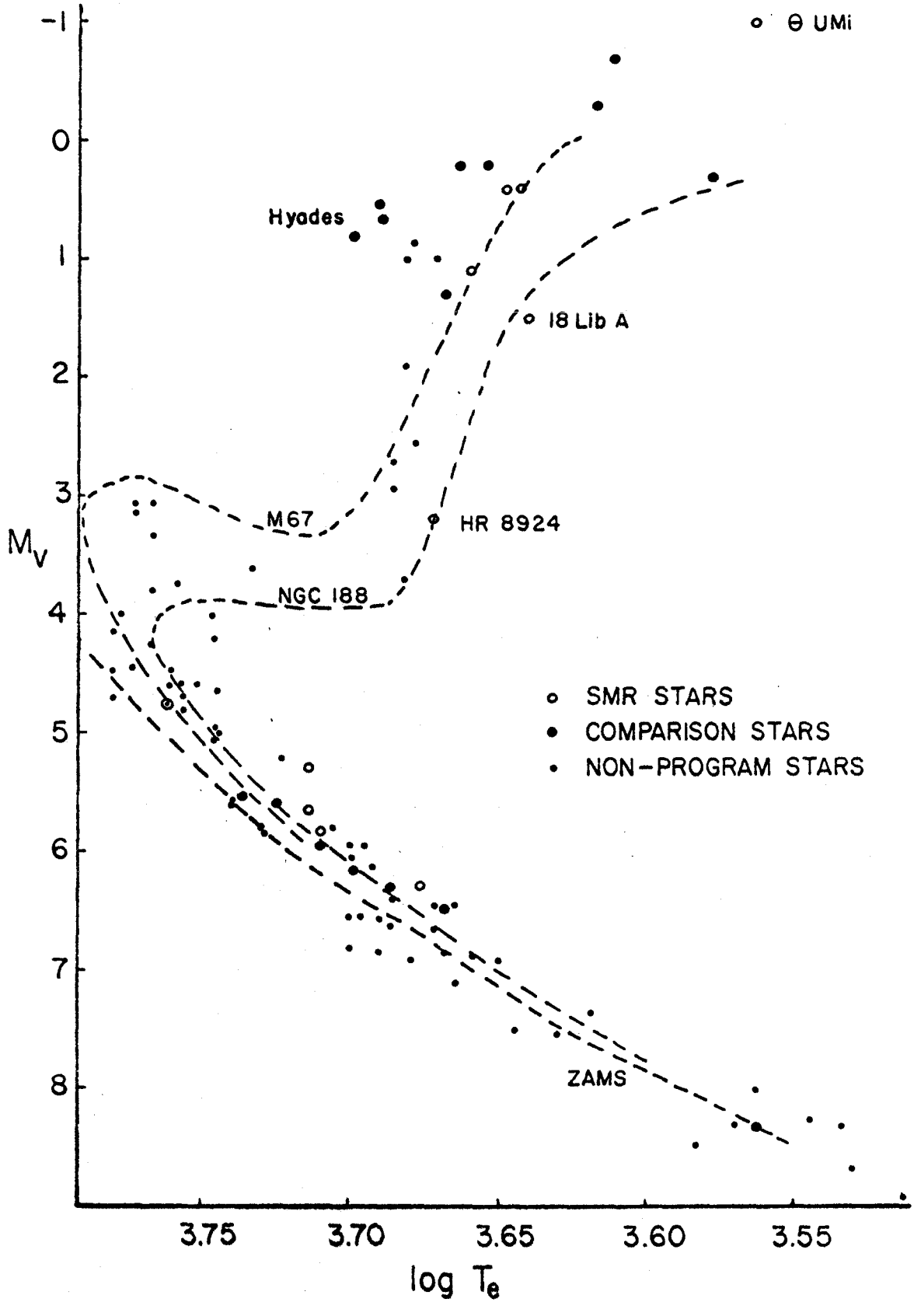
θ UMi
Hyades
18 Lib A
M67
HR 8924
NGC 188
SMR STARS
COMPARISON STARS
NON-PROGRAM STARS
ZAMS
M_V
log T_e
-1
0
1
2
3
4
5
6
7
8
3.75
3.70
3.65
3.60
3.55

(Figure 21). The zero age main sequence of Johnson and Iriarte (1958) is also included in the diagram. The positions of HD 112127 and θ UMi are rather uncertain, the absolute magnitude of the former being estimated from Blaauw's (1963) calibration and the close spectral similarity to μ Leo, while in the case of the latter the K line and the trigonometric parallax give highly discordant absolute magnitudes (-1.4 and 1.5 respectively). The width of H_α (greater than that of any other star in the program) and the presence of fairly strong H and K reversals, however, argue against placing θ UMi among the group of extremely old and underluminous stars. Greater weight was therefore given to the K line magnitude than to the rather small and uncertain trigonometric parallax (0".019).

An inspection of Figure 20 reveals various interesting features. First of all, a comparison of the positions of the Hyades giants with Iben's (1964) evolutionary tracks (transformed to the M_v, log T_e plane) yields a mass on the order of 2.5 $M_\odot$. However, the SMR giants, with the possible exception of θ UMi, lie near the loci of the old open clusters M67 and NGC 188, and can therefore be presumed to possess masses in the neighborhood of 1 $M_\odot$ (Demarque 1968), particularly since the ST scans indicate close composition similarities between the cluster and field SMR giants. It is interesting to note that Demarque (1968) is able to obtain a

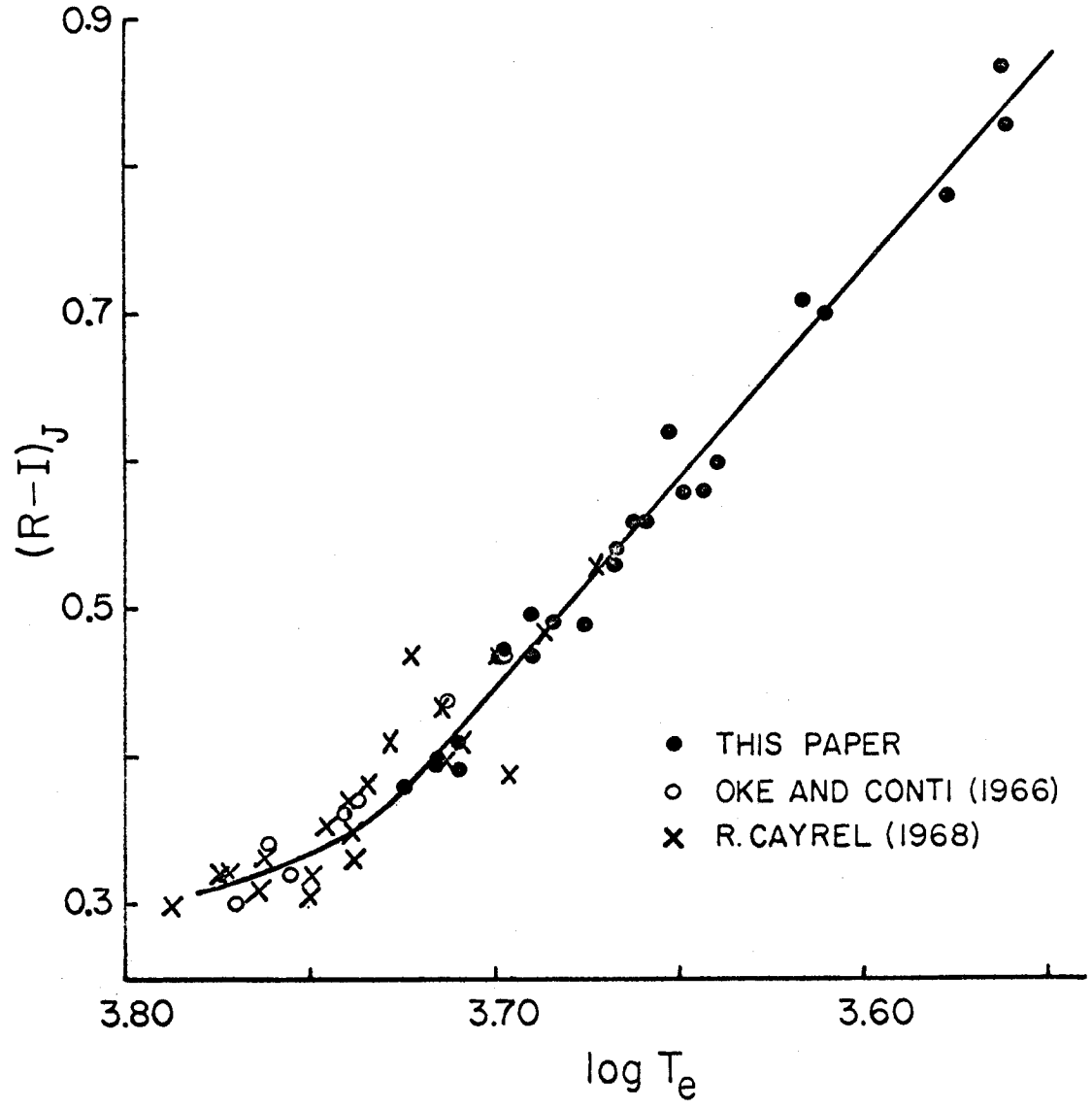

Fig. 21.--Log T_e vs. $(R-I)_J$ calibration. The Oke and Conti points have been changed slightly to comply with the recent revision in the absolute calibration of Vega. There is no systematic difference between the calibration for dwarfs and giants in the sample considered here.

detailed fit between his models and the H-R diagram of NGC 188 only by assuming a metal abundance that is twice solar. The fact that the SMR giants appear to be old and underluminous was also noted by ST. As in the case of the hotter dwarfs, the errors in the early K giant spectroscopic masses are large enough not to rule out agreement with the expected masses; but, just as with the dwarfs, the differences become huge with later spectral types.

Another feature in Figure 20 is the fact that the SMR dwarfs lie near the upper bound of the stars defining the main sequence. The large spread in absolute magnitudes for stars with the same temperature has been noted by Taylor (1970), who ascribes the effect to possible variations in helium abundance. It is well known that the position of a star above or below the main sequence is dependent on the chemical composition (cf. Demarque 1967, Cayrel 1968), in the sense that a metal-rich or helium-poor star will be brighter than a metal-poor or helium-rich one with the same effective temperature, provided that other factors such as convection do not change. Figure 22 represents an H-R diagram, on a larger scale, of the program dwarfs and those dwarfs found by Taylor to be SMR that have more than one parallax determination in the literature. Included are also the main sequences calculated by Demarque (1967) for various compositions, as well as the locus of NGC 188. The latter is included only as an aid in visualizing the

Fig. 22.--Positions of SMR and normal dwarfs on the main sequence. Demarque's (1967) theoretical main sequence loci are labeled by their values of X and Z (fractional abundances of hydrogen and the metals). The zero age and present day locations of the sun are also included. Note the strong tendency of the SMR dwarfs to lie high on the main sequence. The highest lying comparison star, HR 8832, has line indices comparable to the Hyades dwarfs in Taylor's (1970) diagrams.

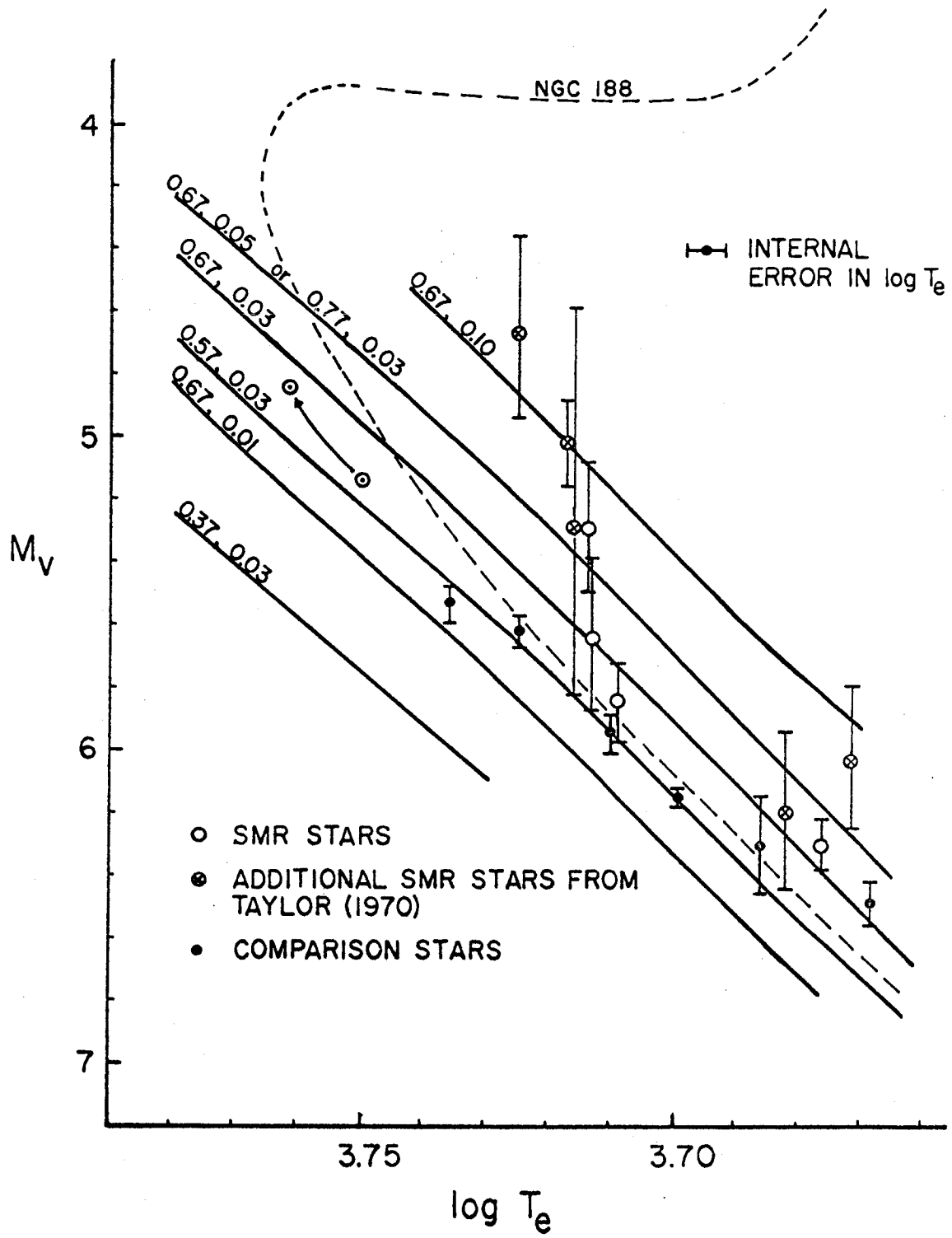
NGC 188
0.67, 0.05 or 0.77, 0.03
0.67, 0.03
0.57, 0.03
0.67, 0.01
0.37, 0.03
0.67, 0.10
INTERNAL ERROR IN log T_e
SMR STARS
ADDITIONAL SMR STARS FROM TAYLOR (1970)
COMPARISON STARS
M_V
4
5
6
7
3.75
3.70
log T_e

relationship with Figure 20 - its position on the vertical scale is dependent, of course, on the assumed chemical composition. The transformation from Taylor's temperature index [6620] to log T_e was effected by the transformation [6620] → (R-I) → log T_e. A glance at Figure 22 reveals that the SMR dwarfs all lie quite high on the main sequence, although the error bars are rather large in some cases. For example, 54 Psc lies lower than ρ^1 Cnc, a result which is consistent with the abundances derived here. HR 8832 also lies rather high, in keeping with its position near the Hyades in Taylor's line strength diagrams, although the abundances derived in the present work are a bit lower; the presence of the large gravity defect in this star, however, renders the results of the analysis rather suspect.

Taylor (1970) has constructed an H-R diagram for those dwarfs in his program having accurate parallaxes, but claims to find no correlation between metal abundance and height above the main sequence. However, of the ten stars listed by him as lying more than three probable errors above the fiducial Hyades main sequence three are SMR, two (HR 8832 and HD 160346) have above average line blocking in several passbands, two (ξ Boo A and σ Dra) are in the present program and are found to lie substantially below the metal-rich stars and two (12 Oph and HR 5568) have [6620] indices (used as the abscissa in Taylor's diagram) that are much too red for the published R-I colors. A rough correlation

between metal enhancement and height above the main sequence appears, therefore, to exist, although a quantitative assessment of the effect is not possible due to the presence of large probable errors in many of the parallaxes.

The data does not rule out the possibility that variations in helium content may be responsible for some of the luminosity dispersion in Figure 22. Even a rather small variation in the helium abundance can have a large effect on the relative luminosities; according to Faulkner's (1967) quasi-homology relations, a reduction of the helium abundance by number from 0.1 (the value used in the models) to 0.0 results in a brightening of 0.8 mag. The effect on the stellar spectrum, however, is practically negligible – calculations with a 5500 K hydrogen-rich model show that changes in ion and neutral weak line strengths amount to only 0.02 and -0.04 dex respectively, with no difference in the emergent continuum.

Evolutionary brightening for K dwarfs is probably negligible due to the large time scales required. Even increasing the helium content by substantial amounts will not have a very large effect on the time that it takes a star to reach the turn-off point on the main sequence (cf. Faulkner 1967). Moreover, a high helium abundance increases the effective gravity in a stellar atmosphere, and would therefore increase the observed gravity defect in the program stars. In addition, if it is assumed that the SMR dwarfs are evolved

helium-rich stars, one would expect the neutral line strengths to increase uniformly – a circumstance that is contradicted by the results obtained here.

i) Discussion of Previous Work

Model atmosphere analyses have been performed by other observers for some of the stars in the program; it is obviously of interest to compare the ion and neutral abundances deduced by them with the results of the present work.

G. Cayrel (1966) has analyzed HR 8832 by means of the Cayrel and Jugaku (1963) models, utilizing spectrograms with dispersions of 13 Å/mm in the yellow-red and 10 Å/mm in the blue. The gravity was assumed to be 4.5 in the log from the outset, while the temperature was obtained from calculations of the profiles of the Na-D and Mg triplet lines and the calibration of Oke and Conti's (1966) $(\theta_e)_c$ vs. R-I, where $(\theta_e)_c$ is the temperature of the model that best fits the flux between the lines. From these considerations a value of θ_{eff} = 1.07 was adopted, although the calculated weak line strengths show that a model with θ_{eff} = 1.05 was actually used in deriving the abundances. It turns out, however, that the θ_{eff} in the Cayrel and Jugaku models is quite different from the $(\theta_e)_c$ of the Swihart and Fischel (1960) models that were used by Oke and Conti. In fact, a direct comparison shows that the latter are very similar to the Atlas models and, in fact, that $(\theta_e)_c = \theta_{eff}$ (Atlas). The use of $(\theta_e)_c$ in the

Cayrel and Jugaku models therefore results in a temperature that is too high by about 325 K in the continuum and weak line forming regions; in fact, a temperature of θ_{eff} (Cayrel) = 1.125 is needed to match the observed flux in the continuum.

Even with the adopted temperature, however, the abundance derived from Fe II is greater than that for Fe I by 0.28 dex. The abundance from Ti II is greater than that from Ti I by only 0.08 dex; however, the theoretical curve of growth has been drawn through the Ti II points so as to yield a minimum value for the abundance. Indeed, if the curve is passed through the middle of the scatter of points defining the moderately strong line region (there are no weak lines) an overabundance of about 0.25 dex is obtained. The strong lines should actually fall below the neutral-line curve of growth, as will be seen in section j), which increases the discrepancy even further. The discrepancy for Zr I, II is 0.75 dex while that for Sc I, II is 0.02 dex; both values are of low weight, however, since only a few line measurements are available. The abundance of La from only one line of La II is 0.70 dex relative to the sun.

The above discrepancies point to the conclusion that either the temperature of the model is too low or the gravity is too high. However, as was seen above, the temperature is already much too high, leaving as the only alternative a

drastic reduction in the gravity. This is in complete agreement with the results of the present work.

G. Cayrel (1966) has also analyzed a group of K giants relative to the standard ε Vir. It is of some interest that the spectroscopic gravities of the two coolest ones, HD 6833 and φ Aur, turn out to be unexpectedly low: 1.3 and 1.0 dex respectively. The R-I colors of these stars, on Johnson's system, are 0.64 and 0.72, which imply effective temperatures of approximately 4280 and 4020 K respectively. A comparison with Table 15 indicates that HD 6833 is cooler than 18 Lib A by about 100 K, while φ Aur has roughly the same temperature as ν UMa. It will be remembered that it was for stars cooler than 18 Lib A that the gravity defect in the giants became unacceptably large; Mrs. Cayrel's results provide good confirmation of this result.

Strom et al. (1971) have published an analysis of several K giants, including γ Tau, ε Tau, μ Leo, and φ Aur. The models employed by them were generated by Atlas and are therefore similar to the ones used here. The plate material and line measurements that were used were not homogeneous, however, and small systematic errors might therefore be expected.

The derived parameters for the two Hyades giants are in reasonably good agreement with the values obtained here; in particular, the gravities differ by only about 0.2 dex. The microturbulence derived by Strom et al. is much too high in

all the stars, however, since V_t was obtained by matching the calculated curve of growth of the unblanketed model atmosphere with the empirical curve. Since the line free model predicts strong lines that are always too shallow the resultant V_t will be much too large. The parameters for μ Leo are somewhat different from the values derived here, the temperature and the gravity obtained by Strom et al. both being higher by 100 K and 0.7 dex, respectively. It should be noted that the temperature and gravity obtained by Strom et al. were both derived spectroscopically, with no use made of the information on the colors; in fact, Strom et al. state that their temperatures for the SMR stars might be a bit too high. A reduction of the temperature of μ Leo by 100 K necessitates lowering the gravity by almost 0.4 dex in order to preserve equality between the abundances from the ions and neutrals. This results in fairly good agreement (within a factor of two) with the gravity derived here.

The gravity obtained by Strom et al. for φ Aur is 2.0 in the log, much higher than the value from Mrs. Cayrel's analysis. However, only two Fe II lines were used by Strom et al. in deriving the spectroscopic gravity, while Mrs. Cayrel employed 16 lines of Fe II and 21 of Ti II; much greater weight must therefore be given to her result. A reduction of the model temperature used by Strom et al. (T = 4500 K), which is much too high for the published

infrared colors, will also substantially lower the gravity.

An analysis of μ Leo and φ Aur has just been completed by Vaziaga (1971). The effective temperature and the gravity were determined from profiles of strong metal lines (Na I, Mg I, and Fe I), the ionization equilibrium, and mass estimates based on the positions of the stars in the H-R diagram. The use of line profiles for obtaining model parameters is open to some criticism, however, since the uncertainty in the placement of the continuum for stars of type K2 III or later renders the wing profiles of all except possibly the Na D lines highly uncertain. The Mg triplet, particularly, lies in a region of heavy blanketing where the plate sensitivity is changing very rapidly. As for the Fe I lines, only a bare hint at the wing structure is available for the lines in the green region of the spectrum used by Vaziaga. As a result, the fitting of observed to calculated profiles was done essentially on the basis of the line cores, a procedure which presupposes an accurate knowledge of the structure in the extremely tenuous regions of the atmosphere.

The effective temperatures obtained by Vaziaga are presumably "true" effective temperatures since line-blanketed models were constructed for each star. The temperatures and logarithmic gravities for μ Leo and φ Aur are 4500, 2.3 and 4200, 2.0, respectively. The agreement is quite good with the values for μ Leo derived in this work. The R-I, T_e

calibration (Figure 21), however, yields T_e = 4020 for ϕ Aur, substantially lower than Vaziaga's value. A reduction of the temperature by 200 K would lower the gravity to approximately 1.2 dex if equal abundances are to be preserved for ions and neutrals.

In a recent analysis of late type dwarfs, Kandel (1968) finds that the observed wings of the Ca λ4227 and Na D lines are much too shallow for the profiles predicted on the basis of model atmospheres. The hottest star in his program is 61 Cyg B, which requires an effective temperature of 4350 K to fit the Na D profiles. The effective temperature of 61 Cyg B derived in this work is 3650 K, while Johnson's calibration yields 3900 K. The discrepancies become even larger for cooler stars. Although Kandel does not consider low gravity models, it is apparent that a drop in the gravity will have the effect of decreasing the strength of the predicted line wings in the same way as a raising of the temperature. As a way out of the difficulty Kandel postulates the presence of an extra absorber, which would shift the region of formation of the line wings to less dense regions of the atmosphere. This will be discussed further in section j).

Mention should also be made of the work of Krishna Swamy (1966) on ε Eri. Using the T-τ of Cayrel and Jugaku (1963) he adopts a model with T_{eff} = 5050 K and log g = 4.56. The characteristic temperature of the continuum and weak

line forming regions is 5400 K, which is hotter by 250 K than the value used in the present work. In fact, a calculation of the emergent flux from the model shows that it is much too blue by comparison with the scans. The temperature and gravity were derived by Krishna Swamy on the basis of calculated profiles of the wings of strong lines, a procedure that has led to the same sort of discrepancy as found by Kandel, although to a lesser degree in this case.

It is also of some interest to note that Helfer and Wallerstein (1968), in a curve-of-growth analysis of a selection of twenty-seven early K giants, derive spectroscopic masses that are sub-solar in many cases. Only one star, 20 Cyg K3 III, is cool enough (R-I = 0.70) to fall into the category of stars expected to show a large gravity defect; and, in fact, the derived gravity is rather low, with $\Delta \log g = -0.9$ relative to the Hyades.

j) The Gravity Defect

We have seen in the previous section that the results of other observers are not in disaccord with the conclusion that there is a temperature dependent effect which is operating to produce ion lines that are too strong by comparison with the neutral species, the result of which is the derivation of spectroscopic gravities that are unacceptably low. The effect becomes pronounced at approximately the same spectral type (K2-K3) in both the giants and dwarfs, at

temperatures where the abundant electron donors (Fe, Mg and Si) are becoming predominantly neutral. The giants are, of course, much cooler than the dwarfs at this point, so that the gravity itself is playing a role in the gravity defect; indeed, while θ^1 Tau has a reasonable spectroscopic gravity, that of ε Eri, a dwarf with the same effective temperature, is too low by a factor of ten.

Agreement between the neutrals and ions can be achieved for reasonable gravities if the temperatures of the models are systematically increased. In the case of the dwarfs increases of 200, 500, and 1000 K are needed for spectral types K0, K2, and K7, respectively, while for the giants the correction jumps from about 100 K at type K0 to 500 K at K3. It is hard to see, moreover, how the photometric errors could increase drastically for cooler stars. If anything, the neglect of blanketing in the 1μ passbands in the fitting of the scans to the models would be expected to yield temperatures that are too high.

Interstellar reddening is negligible for all the stars, with the possible exception of HD 112127, which is at a distance of about 200 pc. This star lies very close to the north galactic pole, however, so that the reddening can be assumed to be minimal.

As a further check on the scans and in order to investigate the possibility of reddening due to circumstellar grains, the eight-color photometry of Johnson (1966) was

converted to an absolute intensity scale using Johnson's (1965) calibration. This calibration, based on the solar energy curve, has been checked by Becklin (1968), who derived practically the same numbers. The uncertainty in the transformation coefficients beyond 1μ is about 10%, while for shorter wavelengths the accuracy is considerably better. The intensities for ε Eri are plotted in Figure 23, with the scanner points and the energy curve of the adopted Atlas model added for purposes of comparison. The scanner and the Johnson points have been superimposed so as to fit at the V, R, and I bands. The overall agreement is quite good, the slight depression at the K filter (2.2μ) being due possibly to the first overtone band of CO. In particular, there is no indication of the presence of an infrared excess in ε Eri or in any of the other program stars.

The model atmospheres used in this work do not incorporate the effects of the line spectrum on the atmospheric structure. It is well known, however, that the presence of absorption lines results in a drop in the boundary temperature of a star and an increase in the temperature of the slightly deeper layers. A quantitative assessment of the effect in a rigorous fashion has never been carried out, however, and reliance has always been placed on statistical and semi-empirical blanketing schemes. A recent set of calculations by Mihalas and Luebke (1971)

Fig. 23--ε Eri: comparison of Johnson's (1966) points (transformed to the absolute system) with the Atlas model (T_{eff} = 5150 K) that best fits the scanner data. The error bars correspond to 10% errors in the transformation coefficients beyond 1.0 μ (Becklin 1968).

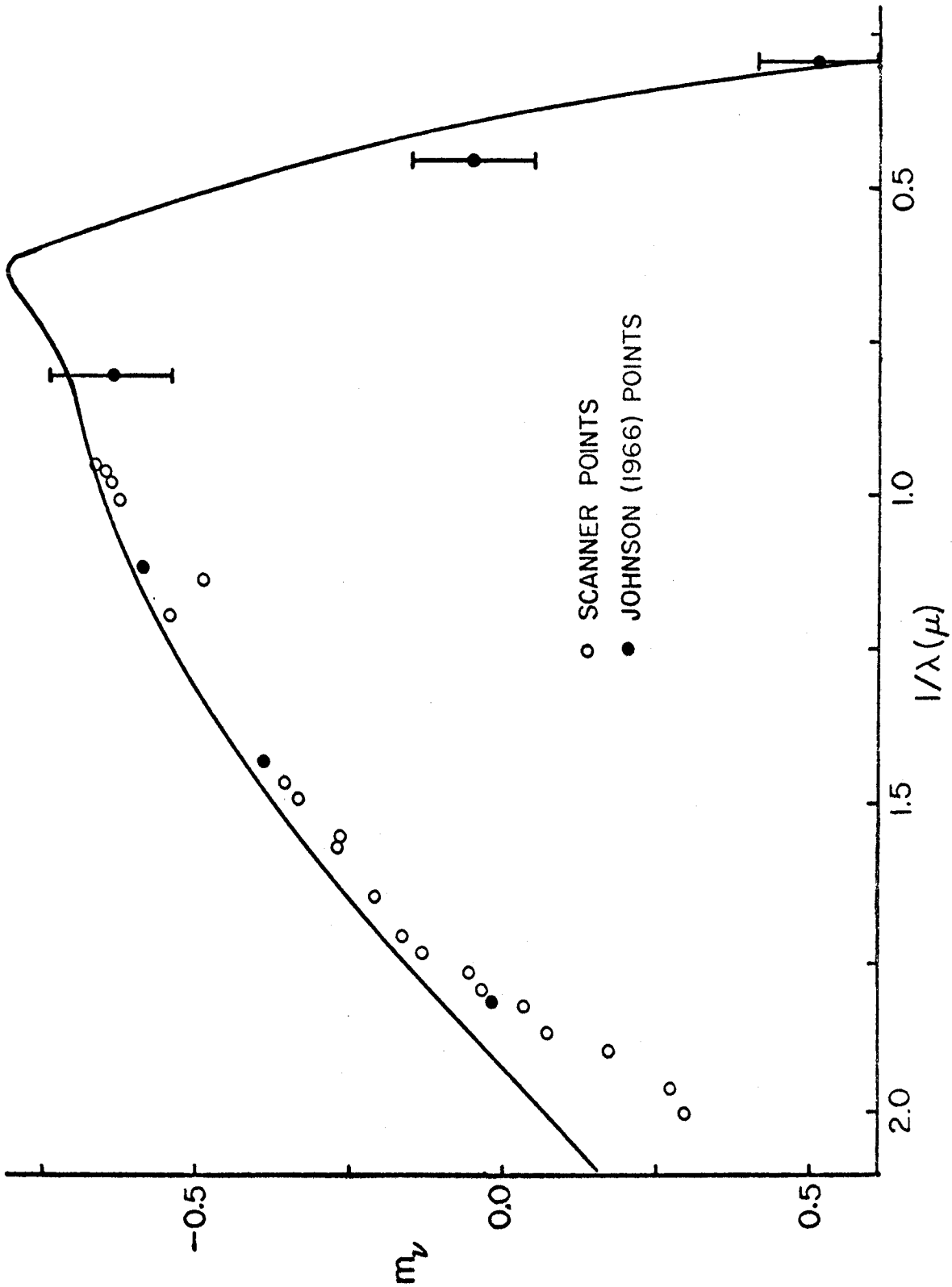
SCANNER POINTS
JOHNSON (1966) POINTS
m_ν
$1/\lambda\,(\mu)$
-0.5
0.0
0.5
1.0
1.5
2.0

demonstrates that the backwarming effect depends essentially on line strength and not very much on the details of line formation; but, by contrast, the temperature drop in the surface layers is a sensitive function of non-LTE effects in the lines.

In order to investigate the effect that changes in the temperature structure would have on the predicted neutral and ion line strengths the following atmospheres were constructed: model a, with a scaled solar T-τ, yielding the same continuum flux as the (4800, 4.4) line-free model; models b, c, and d, similar to a, but with temperature increases beginning at $\tau_R = 0.3$ and extending to increasingly more tenuous layers. The logarithmic gravity was set equal to 4.4 in all cases. The idea was to construct a set of widely differing models, all of which would predict the same continuum slope in the region between 0.5 and 1.0μ. The T-τ of the models are illustrated in Figure 24 and the emergent continua are plotted in Figure 25.

A glance at Figure 25 reveals that the continuum of model a is virtually indistinguishable from the line-free model, while models b, c, and d become increasingly bright shortward of 1.6μ. It should be noted, however, that the slopes shortward of 1.0μ all agree very well, so that the scanner measurements made in this work would be insufficient to separate even the most extreme of the models.

Fig. 24.--Models constructed to yield the same continuum slope shortward of 1.0 μ as the Atlas (4800, 4.4) model: a - scaled solar T-τ; b,c,d - modifications of a. The gravity in all the models is 4.4 in the log.

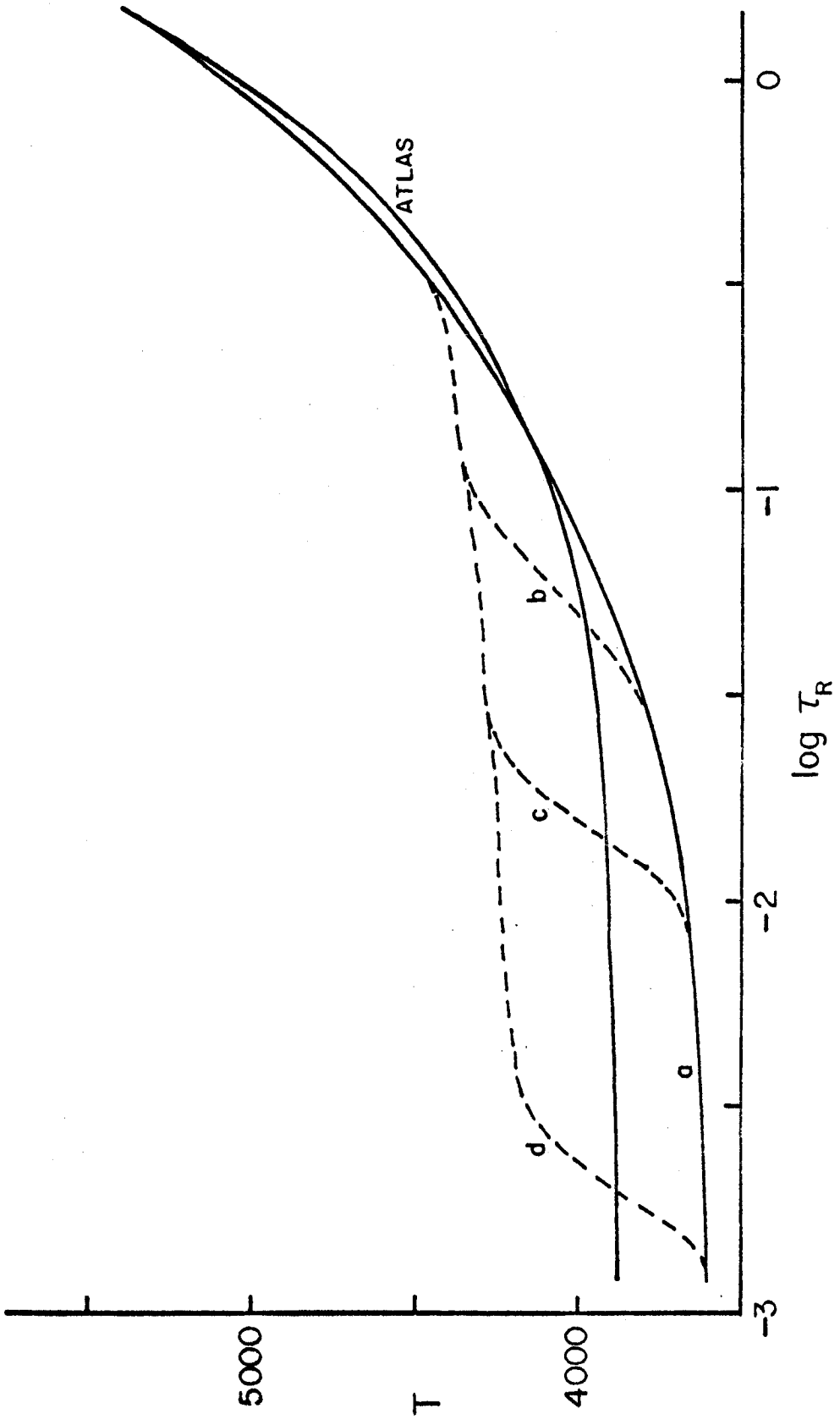
ATLAS
a
b
c
d
5000
4000
T
0
-1
-2
-3
log τ_R

Fig. 25.--Comparison of the emergent fluxes from the models in Fig. 24. The zero point on the vertical scale is arbitrary. Note the identical slopes shortward of 1.0 μ.

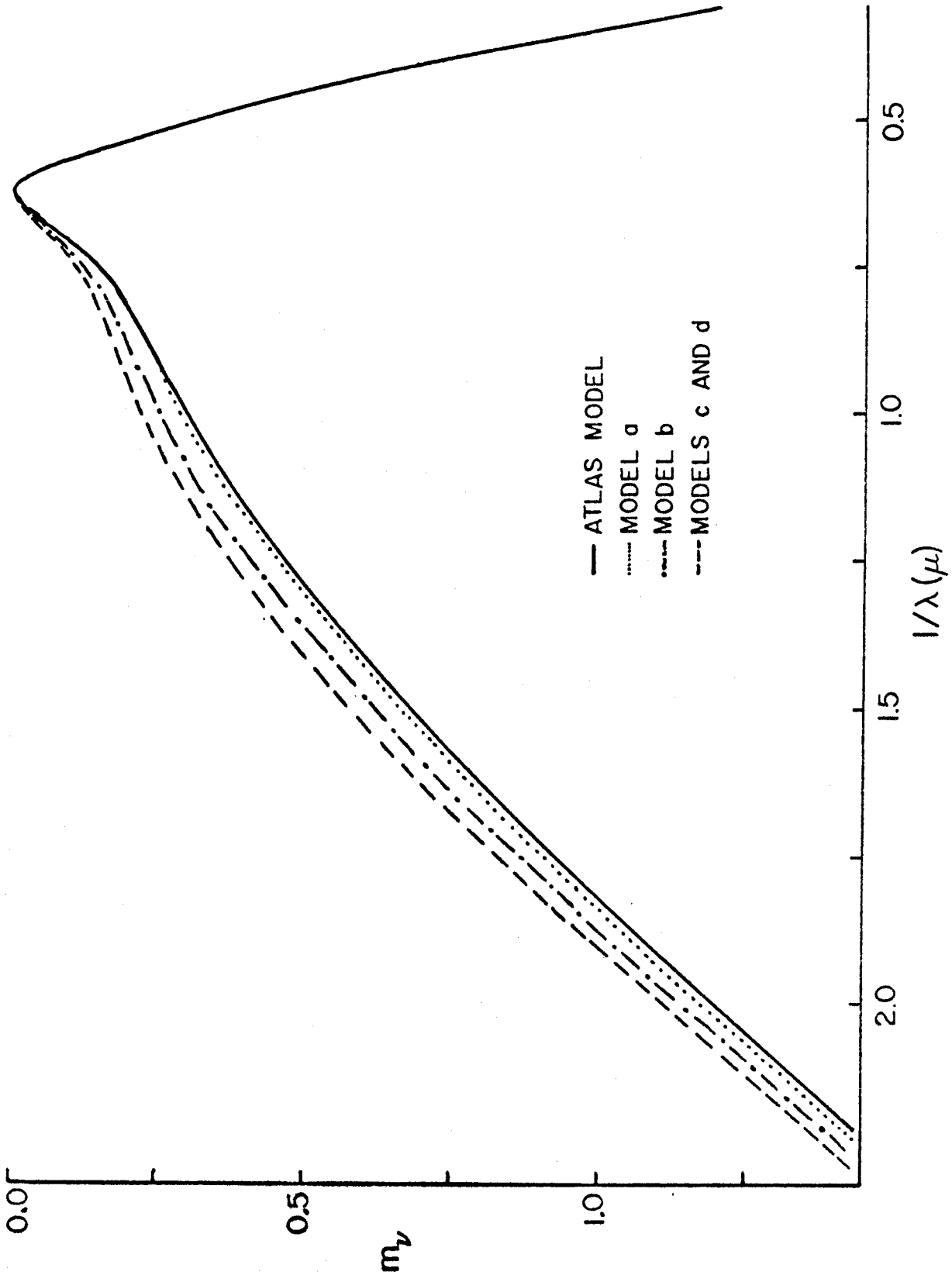
0.0
0.5
1.0
m_ν
2.0
1.5
1.0
0.5
$1/\lambda\,(\mu)$
ATLAS MODEL
MODEL a
MODEL b
MODELS c AND d

The logarithmic weak-line strengths relative to the line-free model are presented in Table 16 for four elements, including the ions and neutrals used in determining the spectroscopic gravities. It is apparent that the differences are quite small, particularly for the ions and high excitation neutrals. The effects of a chromosphere would therefore be expected to be rather small, unless the temperature increase is quite substantial at fairly large optical depths ($\tau \simeq 0.05$). In this case, however, difficulties would arise, such as greatly reduced depths in the cores of strong lines, extremely strong H and K emission, etc. It should be noted, however, that the relative shifts of the ions and neutrals in the most realistic model, a, are in such a direction as to increase the gravity defect, since the line-free model already predicts ion lines that are too weak relative to the neutrals. A change in the right direction by about 0.3 in the log is predicted by model d, but even this is much too small, considering that the gravity defect for HR 8832 is about 1.5 dex. Variations in line strength will, of course, be considerably larger if strong spectral lines formed high in the atmosphere are considered, since the line-free model will obviously predict strong lines that are too shallow by comparison with the blanketed model a. It is for this reason that the strong lines have been treated merely as a means to extrapolate smoothly to the weak line

TABLE 16

LOG Γ'S RELATIVE TO 4800, 4.4
LINE-FREE MODEL

Element	e. p.	a	b	c	d
Fe	1.00	.04	-.01	-.08	-.14
Fe	4.00	-.02	-.04	-.05	-.05
Fe II	3.50	-.02	-.01	.01	.04
Cr	3.00	.05	-.02	-.01	-.17
Cr II	4.00	.03	.02	.01	-.01
Ti	1.50	.13	.04	-.02	-.23
Ti II	1.50	-.01	-.02	-.02	-.03
Na	2.00	.05		-.12	-.20
Na II	2.00	-.01		-.03	

region of the curve of growth and as indicators of the turbulent velocity. The point to remember here is that any lowering of the boundary temperature will act to increase the gravity defect.

Several elements possess only strong lines in the cooler stars, and as discussed in part e) the extrapolation to the weak-line region was performed by assuming that the curve of growth is similar to the Fe I curve of growth with the same excitation potential. In order to check the validity of this procedure, curves of growth for several ion and neutral lines were constructed for all the 4800 K high gravity models; the damping constant was set equal to ten times the classical value in all cases. The resulting curves are fairly similar for all the models, with model a showing the greatest difference in the shape of the neutral and ion curves. Figure 26 illustrates the curves of growth of model a for various excitation lines of Cr and Fe. It is apparent that the difference between the ion and neutral curves is greatest for Fe - which is reasonable since iron is predominantly neutral, thereby accentuating the effects of neutral-ion stratification. A set of curves was also constructed for Na, but when proper allowance was made for the difference in thermal velocities, these were seen to be identical to the Cr curves - which is also reasonable since both Cr and Na are almost fully ionized.

Fig. 26.--Theoretical curves of growth from the scaled solar model (4800, 4.4) at λ = 5600 Å and V_ξ = 2 km/sec. Note the relatively large differences between the ion and neutral curves, particularly in the case of iron.

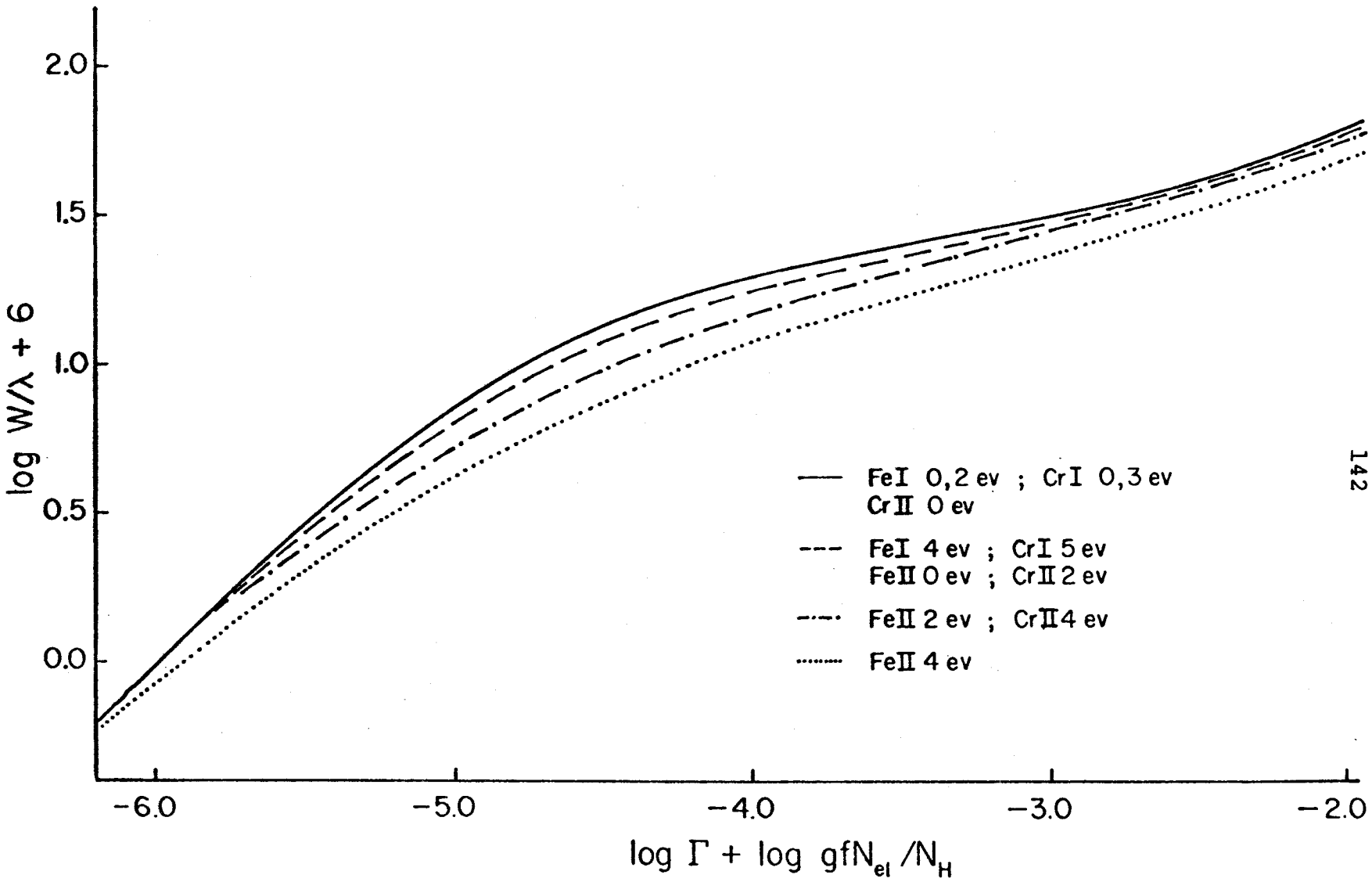
2.0
1.5
1.0
0.5
0.0
log W/λ + 6
-6.0
-5.0
-4.0
-3.0
-2.0
log Γ + log gfN$_{el}$ /N$_H$
FeI 0,2 ev ; CrI 0,3 ev
CrII 0 ev
FeI 4 ev ; CrI 5 ev
FeII 0 ev ; CrII 2 ev
FeII 2 ev ; CrII 4 ev
FeII 4 ev

Let us now determine what abundance errors are to be expected if the neutral Fe curves are used to extrapolate the empirical curves of growth down to log $W/\lambda = -5.5$, which is the representative point at which all the abundances were calculated. Obviously, if the measured equivalent widths are all in the range log $W/\lambda = -5.5$ there will be no errors, provided, of course, that the model chosen for the star is correct. As the lines increase in strength, however, it is apparent from Figure 26 that increasingly large deviations are to be expected. For example, the abundance derived from 4 ev lines of Fe II near log $W/\lambda = -5.0$ will be too low by 0.32 dex, while an underabundance of only 0.10 dex is derived from equally strong lines of Cr II of the same excitation potential. The abundances from low excitation potential lines of mostly ionized elements will, on the other hand, be slightly too high. This discussion is presented in order to indicate the direction of the errors in the abundances of the ions and neutrals due to curve-of-growth effects if only strong lines are available - quantitative results depend on an accurate knowledge of the temperature structure in the tenuous regions of the atmosphere. It is clear, however, that the errors are in the direction of increasing the ion abundances relative to the neutrals, with a resulting increase in the gravity defect.

Another possible explanation of the gravity defect, suggested by Dr. Roger Ulrich (1971) on the basis of his

calculations on convective stellar envelopes, is that the convective motions in the cool stars may lead to rising and falling streams with very different temperatures and that the excess ions might be produced in the hot component. The temperature structure of a two-stream model incorporating a grey atmosphere with T_e = 4250 K, log g = 2.0, and $M = 1.0M_\odot$ was very kindly provided by Dr. Ulrich. The maximum temperature difference between the hot and cold streams increases from 81 K at $\tau_R = 0.1$ to 500 K at $\tau_R = 1.0$, while at $\tau_R = 4.0$ the difference has climbed to 1615 K. In order to calculate the effect that such a difference would have on the abundances, the temperature structure of the (4250, 2.3) Atlas model was altered to produce a hot and a cold model to represent the two streams; the mean difference between the streams was taken to be T(mean) = 2/3 T(max) at each optical depth point. Although the emitted fluxes from the two models are quite different, the averaged energy distribution is almost identical with that of the normal model for wavelengths beyond 5000 Å. Line strengths were calculated for the neutral and ionized species of Fe, Cr, and Ti and the results averaged, with weights depending on the difference in the continuum fluxes. The resulting mean abundances for both ions and neutrals turned out to be virtually identical to those from the normal model.

Thus far no plausible explanation has been found for the gravity defect. One remaining possibility is that the

discrepancy lies in the presence of an unknown absorber which is acting to smoothly depress the continuum in the region shortward of about 1.5μ in such a fashion as to roughly mimic the energy distribution of a cooler star having only H^- opacity. It might be mentioned that the region to the red of 1.5μ, taken by itself, provides very little information on the temperature, as may be seen in Figure 27 in which the continua from the (4900, 4.4) and (5300, 4.4) models are superimposed so as to coincide in the far infrared. The slopes longward of 1.5μ are nearly identical, which means that only absolute flux measurements or a comparison with the relative fluxes at shorter wavelengths could distinguish between the two atmospheres. It is noteworthy that even for the sun there is a possible extra absorber already at 4600 Å, amounting to as much as one half the accepted value (Heintze 1968), although according to Holweger (1970) the continuum depression in this region can be explained by the presence of extremely faint and individually unmeasurable lines. It might be similarly argued that faint lines have formed a pseudo-continuum in the yellow-red "windows" in the program stars and that the blanketing corrections to the scanner points are therefore too small. The fact, however, that the ion-neutral discrepancy sets in at quite different temperatures in the giants and the dwarfs argues rather strongly against this possibility.

Fig. 27.--Comparison of the (5300, 4.4) and (4900, 4.4) model fluxes. The curves have been shifted vertically to coincide in the far infrared. The zero point on the vertical scale is arbitrary.

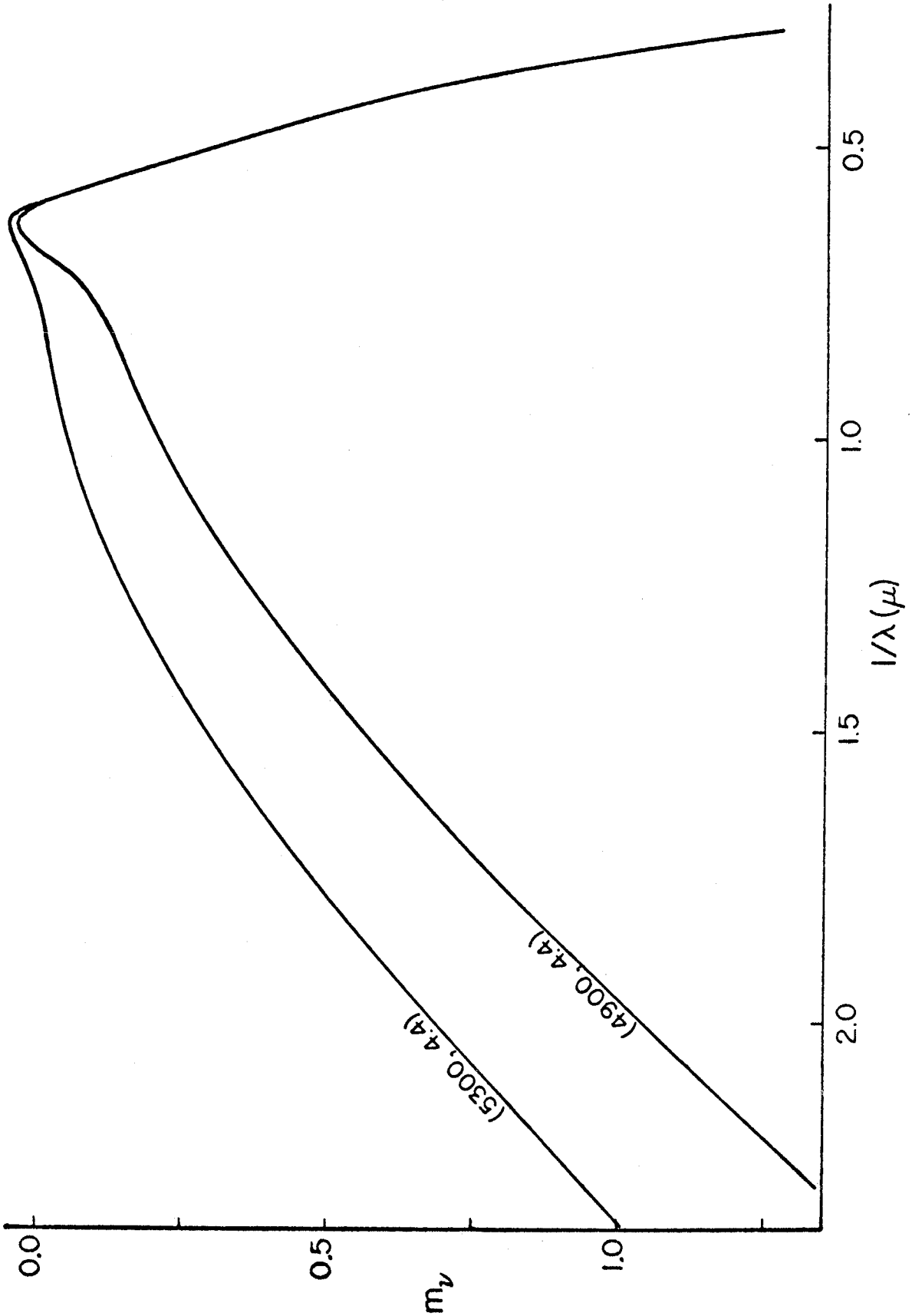
0.0
0.5
1.0
m_ν
2.0
1.5
1.0
0.5
$1/\lambda\,(\mu)$
(5300, 4.4)
(4900, 4.4)

Assuming that an extra absorber is present, it seems reasonable that it should be operating mainly in the cool regions of the atmosphere since the opacities at higher temperatures are presumably fairly well known, at least for wavelengths greater than 5000 Å. Though the effect on the spectral lines depends on a knowledge of the depth dependence of the opacity it is possible that the backwarming effect of the new absorber could begin as far out as the region of formation of the moderately weak neutral lines; the picture could then be similar to model c or d (Figure 24). Somewhat smaller doses of the new absorber would be needed in that case since these models predict diminished ion-neutral discrepancies.

In any case, the new opacity would help explain the following: (1) the ion-neutral discrepancy, which would be due to a falsification of the temperature through the effect on the emergent flux; (2) the results of ST, which indicate that the usual model-atmosphere and curve-of-growth analyses lead to increasingly low metallicities for cool stars; (3) the effect noted by Kandel (1968), that there is a large discrepancy between the predicted and observed strength of the wings of Na D and Ca λ4227 for late K and M type dwarfs. The conclusion (2) of ST is also supported by the abundances derived in this work; i.e., although 16 Aur falls near the mean in the ST line strength diagrams a metal deficiency of 0.5 dex relative to the Hyades is obtained even if a high

gravity is assumed. Even ν UMa, which has stronger lines than 16 Aur but the same temperature, is deficient by about 0.4 dex. The same trend is also present in the dwarfs; i.e., although HR 8832 falls near the Hyades in Taylor's (1970) line strength diagrams its derived abundance, based on the high gravity model, is somewhere between -0.2 and -0.3 dex relative to the Hyades giants. If the low gravity models are used larger abundance differences are, of course, obtained.

The following procedure was used to obtain numerical estimates of the magnitude of the new absorber. The temperature increase necessary to force equality between the neutral and ion abundances in the normal gravity models was calculated for each star in the program; a comparison of the emergent flux from the hotter model with that from the model that agreed with the scans then allowed a determination of the continuum depression that would be necessary in the visual region in order to force the relative fluxes of the two models to agree at 0.5 and 1.0μ. It was then necessary to calculate how much extra absorber would be required to depress the flux in the hot model by this given amount.

The emergent flux is given by the well-known expression:

$$F_\nu = 2 \int_0^\infty S_\nu (\tau) E_2 (\tau) d\tau$$

Setting $S_\nu = B_\nu$ and neglecting constant factors since only relative fluxes are of interest, the formula becomes:

$$F_\nu = \int_0^\infty \{\exp\ [28780/T(\tau_\nu)]\ -1\}^{-1} E_2(\tau_\nu) d\tau_\nu$$

where λ = 5000 Å has been used in the Planck function. Denoting the ratio of the new absorber to the known one by f, the integral becomes:

$$F_\nu = (1+f) \int_0^\infty \{\exp\ [28780/T(\tau_\nu)]-1\}^{-1} E_2\ [(1+f)\tau_\nu] d\tau_\nu$$

where it has been explicitly assumed that the addition of the new absorber will have only a small effect on the overall temperature structure of the star. The ratio of the flux from the depressed-continuum model to that from the original hot model can then be calculated for varying values of f until agreement is obtained with the required flux depression. In order to make the integrals more tractable, the Cayrel and Jugaku (1963) T-τ relation, as written by Krishna Swamy (1966), was employed:

$$T^4 = 3/4\ T_{eff}^4 (1.39 + \tau - 0.815e^{-2.54\tau} - 0.025e^{-30\tau})$$

where $\tau \equiv \tau_R \approx \tau_{5000}$. This T-$\tau$ yields a continuum flux that is virtually identical to that from the Atlas model except in the ultraviolet. It is, of course, necessary to take into account the difference in the parameters T_{eff} (Atlas) and T_{eff} (C. J.) that define the models in order to obtain proper agreement.

The above procedure was carried out for several representative dwarfs and giants, and the results are presented in Table 17. The quantity Δm is the continuum depression required for the hot model, and f is the ratio of the new absorption coefficient to the known one. It is apparent that inordinately large quantities of the new absorber are not required; for example, an increase in the opacity by about 50% or less would resolve the neutral-ion anomaly in all but the coolest dwarf in the program. The original assumption, that the addition of the new absorber would have a rather small effect on the atmospheric structure (T-τ, convection, etc.) appears, therefore, to be valid - particularly since an increasingly small fraction of the total flux is carried in the visual region of the spectrum as one goes to cooler stars. The following relation gives a reasonably good representation of f as a function of g and θ_{eff} (hot) for $f \gtrsim 0.17$ (i.e., for the dwarfs and cool giants):

$$\log (1+f) = 1.0\ \theta_{eff} + 0.05 \log g - 1.0$$

It should be remembered that the above results are rather schematic, since it has been assumed that f is constant with depth in the atmosphere.

The presence of the extra absorber could be checked by comparing the derived abundances of the same element from the infrared and visual regions of the spectrum. This

TABLE 17

MAGNITUDE OF THE NEW ABSORBER

DWARFS

T_{eff}	T_{eff} (hot)	log g	Δm	f*
5400	5600	4.4	0.10	0.17
5000	5500	4.4	0.24	0.42
4800	5400	4.4	0.33	0.51
3700	4700	4.6	0.74	1.50

GIANTS

T_{eff}	T_{eff} (hot)	log g	Δm	f*
5000	5100	2.7	0.06	0.08
4800	4900	2.6	0.06	0.08
4550	4700	2.5	0.08	0.11
4250	4700	2.3	0.31	0.48
3750	4400	1.9	0.54	0.87

*f : $\kappa_{new}/\kappa_{old}$

should be possible for some of the brightest giants such as α Boo or α Tau. In the case of α Boo, however, the scanner effective temperature and the fundamental effective temperature from the measured diameter (Kuiper 1938) agree quite well, which should not be the case if the aforementioned absorber is present. Figure 28 illustrates the energy distribution of α Boo (obtained in order to check the λ8804 effect in Chapter IV) which has been deblanketed by means of the Arcturus Atlas (Griffin 1968); the model that best fits the points has been drawn in and it is clear that the agreement is very good. The model temperature implies an effective temperature on the order of T_e = 4130 K, which compares very well with Kuiper's value of 4090 K. Further evidence that the gravity effect in α Boo is fairly small is provided by the analysis of Griffin and Griffin (1967) who obtain a spectroscopic gravity of log g = 1.7 (and a metal deficiency of a factor of three relative to the sun); they do remark, however, that this value of the gravity is somewhat lower than had been believed previously. Adding yet another conjecture, it might be that the gravity defect is dependent on the metal abundance to some extent, and a drop in the abundance by a factor of three could have the same effect on the unknown absorber as an increase of the temperature by a couple of hundred degrees; this would be sufficient to produce in α Boo the same small gravity defect as observed in HD112127.

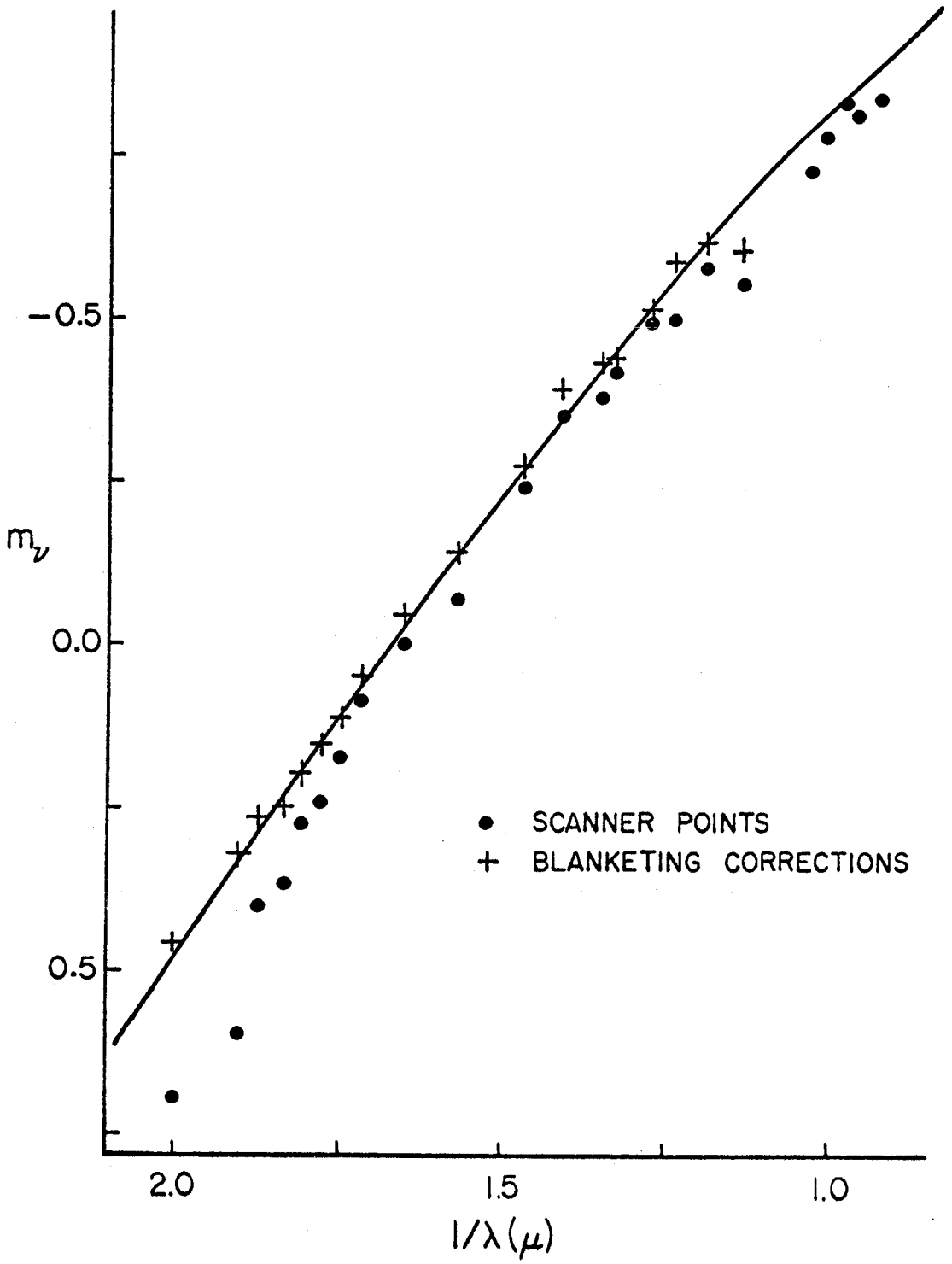

Fig. 28.--Arcturus: deblanketed scan with the energy distribution from the (4250, 2.3) Atlas model drawn in.

k) The Abundances

Although the mystery surrounding the ion-neutral discrepancy has yet to be clarified, the relative abundances of stars of the same temperature should still be fairly reliable. A comparison of the giant abundances with the values obtained by previous observers is presented in Table 18 for Fe, Mg, Ca, and Na. Two sets of abundances, representing the results from the high and low gravity models, are included. A similar compilation for the dwarfs is given in Table 19, although in this case there are fewer analyses available in the literature for comparison. It might be mentioned that the abundances of ST, Taylor (1970), Williams (1971), Peat and Pemberton (1968), Helfer and Sturch (1970), and Hansen and Kjaergaard (1971) are based on photometric spectral indices and might therefore be subject to larger errors than the other analyses; in particular, they require a fairly good knowledge of the gravity since strong damping lines are involved in most of the measurements.

From the tables it is evident that the only element in the SMR stars that is regularly overabundant by a factor of three or more is Na. In the two hottest SMR giants, HR 8924 and α Ser, however, both Mg and Ca substantially exceed the solar abundance, which is not the case in the cooler SMR giants μ Leo and 18 Lib A. In fact, although HR 8924 and α Ser lie no higher than μ Leo and 18 Lib A in the ST line-strength diagrams their metal abundances are substantially

TABLE 18

GIANTS

COMPARISON OF ABUNDANCES WITH PUBLISHED VALUES

Star	Fe	Mg	Ca	Na	Reference
θ^1 Tau	0.18	0.13	0.10	0.17	
	0.18	0.13	0.10	0.17	
	0.14	0.07	-0.01	0.16	HW
	0.2		0.0	0.2	G
	0.23				W
	-0.04	0.02		0.02	HK
		0.00		0.28	PP
		0.35	0.4	0.3	ST
γ Tau	0.05	0.10	0.11	0.33	
	0.03	0.08	0.11	0.33	
	0.11	0.07	0.04	0.28	HW
	0.2		-0.10	0.2	G
	0.26				W
	-0.05	0.03		0.03	HK
	0.0	-0.10	0.00	0.4	SSC
		0.1	0.15	0.3	ST
ε Tau	0.07	0.19	0.23	0.28	
	0.04	0.17	0.23	0.28	
	0.11	0.07	-0.08	0.16	HW
	0.2	-0.1	0.1	0.6	SSC
	0.16				W
	0.02	-0.10		-0.10	HK
		0.1	0.15	0.3	ST
HR 8924	0.07	0.35	0.46	0.66	
	0.10	0.36	0.46	0.66	
	0.43				HK
11 Cep	0.05	0.00	0.10	0.20	
	0.02	-0.02	0.10	0.20	
	0.16				HK

Table 18 (continued)

Star	Fe	Mg	Ca	Na	Reference
α Ser	0.23	0.49	0.29	0.57	
	0.22	0.48	0.29	0.57	
	0.2		0.0	0.4	G
	0.32				W
	0.19			0.39	HK
		0.2	0.1	0.4	ST
ν Aur	-0.10	-0.05	-0.07	0.10	
	-0.15	-0.07	-0.07	0.10	
	-0.07			-0.34	HK
		-0.21	-0.26	-0.32	PP
μ Leo	-0.01	0.16	0.15	0.43	
	-0.06	0.13	0.15	0.43	
	0.1	0.0	0.3	0.7	SSC
	-0.03	0.08	0.48	0.45	V
	0.46			0.00†	W
	0.28			0.79	HK
		-0.05	0.00	0.02	PP
		0.6	0.55	0.65	ST
α Ari	-0.21	-0.15	0.06	-0.10	
	-0.37	-0.26	0.06	-0.10	
	-0.23				W
	-0.19			-0.53	HK
		-0.22		-0.52	PP
HD 112127	-0.09	0.19	-0.01	0.25	
	-0.12	0.17	-0.01	0.25	
	0.29				HS
18 Lib A	-0.02	0.23	0.21	0.72	
	-0.06	0.20	0.21	0.72	
	0.25				HK
16 Aur	-0.39	-0.03	-0.19	-0.19	
	-0.77	-0.27	-0.19	-0.19	
	-0.28				HK

Table 18 (continued)

Star	Fe	Mg	Ca	Na	Reference
ν UMa	-0.19	-0.17	-0.13	0.04	
	-0.53	-0.40	-0.13	0.04	
	-0.13				W
	-0.21				HK
θ CMa	-0.22	0.17	-0.46	-0.41	
	-0.77	-0.27	-0.29	-0.27	
θ UMi	0.20	0.31	-0.08	0.39	
	-0.55	-0.31	0.11	0.57	
	-0.59				HK

References:

G - Griffin (1969)
HK - Hansen and Kjaergaard (1971)
HS - Helfer and Sturch (1970)
HW - Helfer and Wallerstein (1964)
PP - Peat and Pemberton (1968)
SSC - Strom, Strom and Carbon (1971)
ST - Spinrad and Taylor (1969)
W - Williams (1971)

Comments:

1st entry is abundance from high gravity model.

2nd entry is abundance from low gravity model.

The SSC abundances are expressed relative to the sun through the intermediary of ε Vir, which was also analyzed by SSC, using the abundances derived by Cayrel and Cayrel (1963).

†Quoted by Vaziaga (1971)

TABLE 19

DWARFS

COMPARISON OF ABUNDANCES WITH PUBLISHED VALUES

Star	Fe	Mg	Ca	Na	Reference
ξ Boo A	-0.26	-0.15	-0.08	-0.23	
	-0.32	-0.17	-0.08	-0.23	
	-0.4				T
	0.0				H
70 Oph A	-0.12	0.11	0.10	0.17	
	-0.15	0.09	0.10	0.17	
	0.0				D
ρ^1 Cnc	0.11	0.23	0.24	0.46	
	0.06	0.20	0.24	0.46	
	0.4				T
14 Her	0.18	0.30	0.33	0.54	
	0.15	0.28	0.33	0.54	
	0.0				T
σ Dra	-0.25			-0.12	
	-0.33			-0.12	
54 Psc	-0.17	-0.09	0.03	0.13	
	-0.23	-0.13	0.03	0.13	
	0.2				T
ε Eri	-0.19	0.08	0.01	-0.02	
	-0.28	0.00	0.01	-0.02	
			0.0	0.0	KS
	0.0				T

Table 19 (continued)

Star	Fe	Mg	Ca	Na	Reference
HR 6806	-0.30	0.03	-0.16	-0.15	
	-0.50	-0.11	-0.16	-0.15	
HR 8832	-0.21	0.07	-0.06	0.09	
	-0.51	-0.17	-0.06	0.09	
	0.03	0.15	-0.11	0.04	C
HR 1614	0.02	0.29	0.19	0.53	
	-0.15	0.17	0.19	0.53	
	0.4				T
61 Cyg B	-0.65	0.03	-0.65	-0.70	
	-1.92	-1.28	-0.78	-0.64	

References:

C - Cayrel (1966)
D - Dijke (1946)
H - Herbig (1965)
KS - Krishna Swamy (1966)
T - Taylor (1970)

Comments:
1st entry is abundance from high gravity model.
2nd entry is abundance from low gravity model.

greater - a circumstance which the unknown absorber discussed in section j) would neatly resolve. The same general comments are applicable also to the hotter SMR dwarfs ρ^1 Cnc and 14 Her as compared with the cooler HR 1614. It seems safe to say, however, that iron shows only a marginal enhancement in the SMR giants; Vaziaga has reached a similar conclusion in her analysis of μ Leo and ϕ Aur.

A few comments are in order at this point, the first one concerning the claim by Strom et al. that the strengthening of the strong and medium strong lines in μ Leo is due to a much larger than normal lowering of the boundary temperature as a consequence of the enhanced molecular bands as well as a slight increase in the metallicity. That this cannot be the whole explanation is shown by Figure 19, which was constructed for the purpose of calculating the backwarming effect in μ Leo. It is apparent that the red CN bands, although stronger than in the normal giants, are not strong enough to have much of an effect on the atmosphere; and, although the infrared CO blanketing was taken from the spectrum of Arcturus, even a doubling or trebling of the strength of these features will have a negligible effect - in any case, these bands are largely saturated in Arcturus so that they are probably not much stronger in μ Leo.

Additional evidence against a greatly depressed boundary temperature in μ Leo is the fact that the high and low excitation Fe I curves of growth superimpose very well, without

any necessity for a vertical shift. Models with lowered boundary temperatures, however, predict an increasingly large separation of the two curves.

The third piece of evidence against a substantially lowered boundary temperature comes from a suggestion by Wallerstein (1971) that the central depths of strong lines with low transition probabilities (and therefore negligible scattering) should serve as good thermometers for the outer layers of a stellar atmosphere. Wallerstein shows, in fact, that λ6572 of Ca I and λ4571 of Mg I, both of which arise from singlet-triplet transitions, are good candidates for K stars. Since for pure absorption the emission at line center will depend only on the local temperature, the boundary temperature can be obtained from

$$R_c = \frac{B_\nu(T_o)}{B_\nu(T_{eff})} \tag{5}$$

where R_c is the residual intensity at line center. Residual intensities of the λ6572 line were measured in several giants including μ Leo. Corrections due to instrumental effects were made by assuming that the weak comparison lines were representative of the instrumental profile and that the λ6572 line profile could be represented by a Gaussian. The results are given in Table 20, where the values for μ Leo and α Ser are the means from two and three plates, respectively. It is seen that the boundary temperatures of the

TABLE 20

BOUNDARY TEMPERATURES FROM THE λ6572 Ca I LINE

Star	R_c	T_{eff}	T_o	$\Delta T/T_{eff}$
HR 8924	0.25	4900	3750	0.235
11 Cep	0.32	4800	3850	0.20
α Ser	0.38	4750	3900	0.18
ν Aur	0.37	4750	3910	0.175
μ Leo	0.28	4650	3650	0.215
α Ari	0.34	4650	3790	0.185

SMR stars are lower by about 2% than the normal stars, which amounts to a difference of less than 100 K. In particular, the boundary temperature of μ Leo is lower by about 130 K than the mean of the three comparison stars - much smaller than the reduction of 500 K proposed by Strom et al.

It might be argued that the above results have been influenced by somewhat uncertain instrumental profile corrections; the following statistical procedure was therefore adopted as a check. Although the details will depend on the solution of the transfer equation, it would nonetheless be expected that in a graph of line depth vs. line strength the position of the Ca I λ6572 line relative to predominantly scattering lines will be different for stars with greatly differing boundary temperatures. Graphs of (uncorrected) line depth vs. equivalent width for approximately forty "good" lines near 6500 Å were therefore constructed for μ Leo, α Ari, and α Ser. A fairly tight fit was obtained for all three stars (Figure 29) and for all three stars λ6572 fell almost directly on the mean curve, lending further support to the conclusion that there is rather little difference between the surface layers of SMR and normal stars.

The large ultraviolet deficiencies in the SMR stars require explanation, however, in view of the moderately small values of Fe/H. For example, although μ Leo has an iron abundance which is only about 0.2 dex greater than in

Fig. 29.--Line depth vs. equivalent width near 6500 Å. Note that Ca I λ6572 (open circle) falls near the mean line in both μ Leo and α Ari.

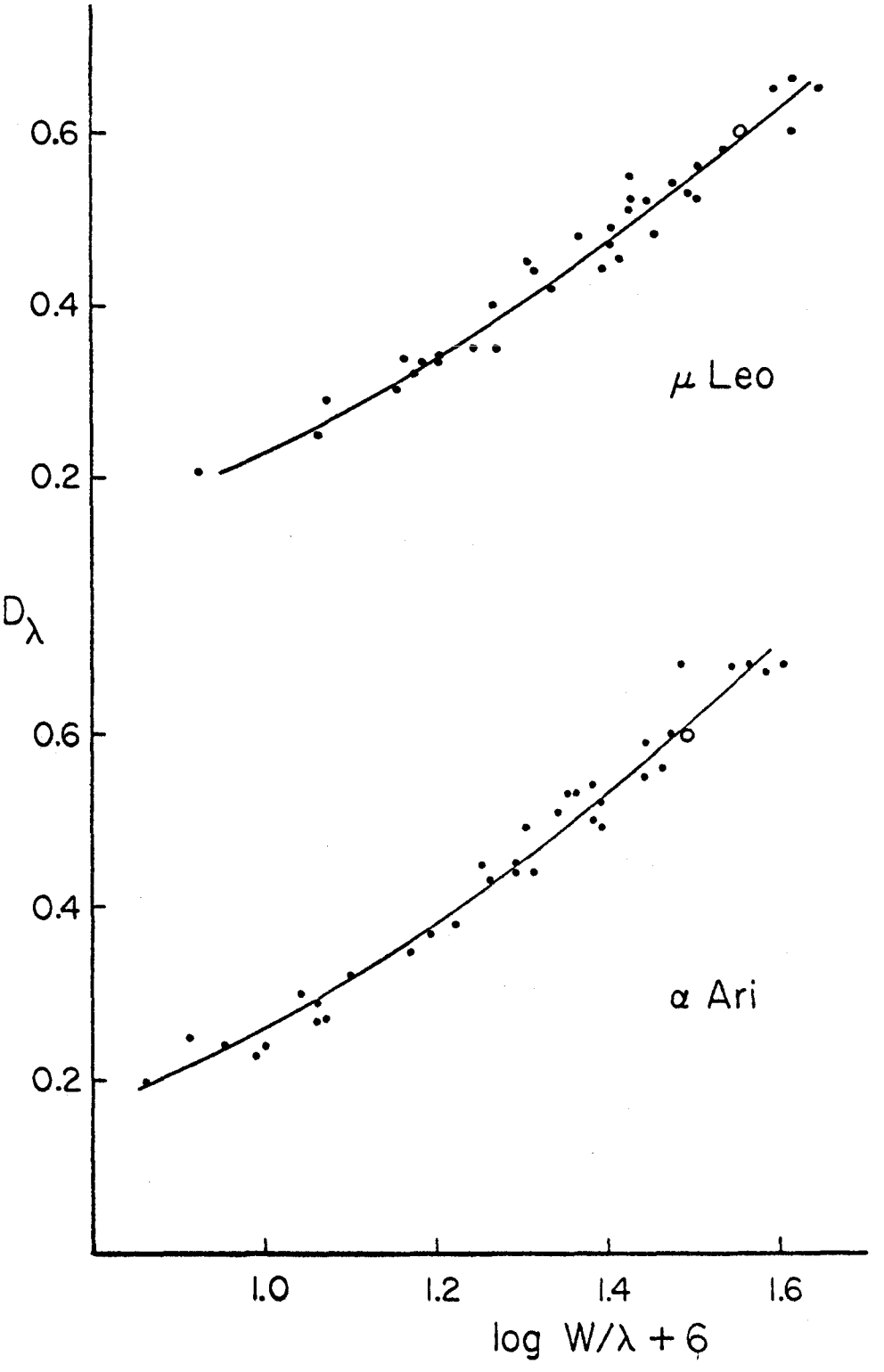
0.6
0.4
0.2
D_λ
μ Leo
0.6
0.4
0.2
α Ari
1.0
1.2
1.4
1.6
log W/λ + 6

α Ari, the difference in U-B indices is 0.27 mag. This is in agreement with ST, who find that Δ(U-B) = 0.26 in μ Leo. Strom et al. (1971) suggest that the large U-B indices might be caused by higher than normal turbulence, but it is apparent from the results of the present work that there is little if any difference in the microturbulence in the SMR and the normal stars. Indeed, the microturbulence even seems to be slightly diminished in the SMR dwarfs. In their calculations of color indices from blanketed models, however, Strom et al. find that even a fairly small increase in the mean metallicity can have a rather large effect on the U-B index. For example, an increase of the metal abundance by a factor of 1.5 in their (5000, 2.0) model produces an increase of 0.17 in U-B.

Another possible cause of the abnormally large U-B indices might be the violet system of CN, which is enhanced in all the SMR stars. Figure 30 shows the continuum in the U and B spectral regions from the (4550, 2.0) model, on which the U and B filter transmission functions (Johnson 1965) have been superimposed. Also included are the approximate locations of the (0,1), (0,0), and (1,0) CN band sequences. It is immediately apparent that the CN absorption will have a much larger effect on the flux coming through the U filter than on the energy through the B filter. The exact variation of U-B with CN strength depends, of course, on the details of the molecular band structure as well as a

Fig. 30.--Effect of the CN violet system on the U and B colors. The emergent flux from the (4550, 2.0) Atlas model has been drawn in, along with the approximate locations of the (0,1), (0,0), and (1,0) band sequences. Note the considerably larger effect of the CN on the U passband.

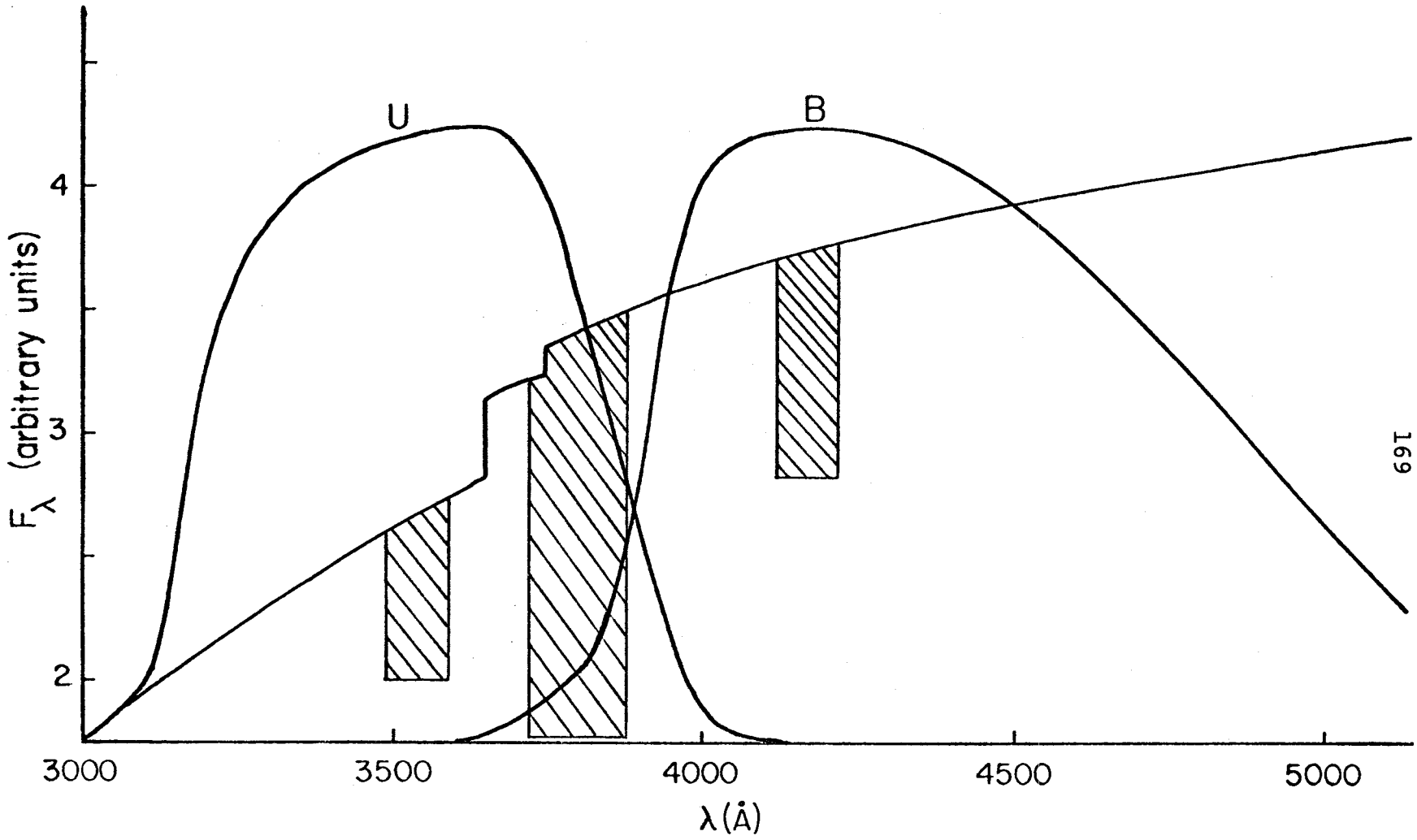
U
B
4
3
2
F_λ (arbitrary units)
3000
3500
4000
4500
5000
λ(Å)
169

knowledge of the true blanketed flux distribution in this spectral region. In fact, the increased importance of line blocking as one progresses toward shorter wavelengths would be expected to make the spectral gradient considerably steeper than in the continuum model, in which case the CN bands would have an even greater influence on U-B, as can be seen from the placement of the CN bands under the filters. As a rough indication of the influence of the CN absorption, calculations were made by assuming that the blocking due to the (0,0) sequence is twice that of the other two sequences and adopting the mean wavelength intervals as shown in Figure 30. Values of U-B were then calculated as a function of the mean depth of the (0,0) band sequence by convolving the model flux with the filter functions. The results are illustrated in Table 21, where Δ(U-B) refers to the difference relative to the U-B of the CN-free model. The values in the table should not, of course, be taken completely literally, but they do indicate the large effect that the violet system of CN can have on the U-B index. In particular, it seems quite reasonable that this, coupled with the effect discussed by Strom *et al.*, could explain the anomalous U-B indices in the SMR stars.

Average values of the metal abundances in the SMR stars relative to comparison stars in the same temperature range are presented in Table 22. 54 Psc is not included in the

TABLE 21

Δ(U-B) AS A FUNCTION OF THE DEPTH OF THE CN (0,0) BAND IN THE (4550,2.0) MODEL

Depth	ΔU	ΔB	Δ(U-B)
0.00	0.00	0.00	0.00
0.20	0.07	0.02	0.05
0.40	0.14	0.03	0.11
0.60	0.21	0.05	0.16
0.80	0.29	0.05	0.23
1.00	0.38	0.08	0.30

TABLE 22

SUMMARY OF AVERAGE SMR ABUNDANCES*

Element	Dwarfs[1]	Giants[2]	θ UMi
Na	0.5	0.5	0.8
Ba	0.2	0.0	0.3
Ca	0.2	0.2	0.4
Y		0.0	0.1
Sc	0.2	0.1	0.4
V	0.3	0.4	0.4
Cr	0.2	0.3	0.4
Ti	0.2	0.3	0.3
Zr		0.2	0.4
Mn	0.3	0.5	0.6
Mg	0.2	0.3	0.1
Fe	0.3	0.1	0.4
Si	0.3	0.1	0.3

*Abundances are relative to the comparison stars.

[1] ρ^1 Cnc, 14 Her, HR 1614.

[2] HR 8924, α Ser, μ Leo, HD 112127, 18 Lib A.

sample of SMR dwarfs since it appears to have a normal chemical composition, possible exceptions being carbon and nitrogen. θ UMi is compared only with θ CMa since the other stars are all considerably hotter, and if the latter is assumed to possess essentially solar abundances (Chapter II) θ UMi emerges as the most extreme SMR star in the program. Since the CN bands are quite strong in all the SMR stars, carbon and nitrogen may well share in the general metal enhancement; in particular, Bell (1970) is able to reproduce the CN band strengths in synthetic spectra of α Ser and μ Leo by doubling the nitrogen abundance.

A glance at Table 22 reveals that the SMR dwarfs are indeed metal rich to a moderate degree, as found by Taylor (1970), but that the level of supermetallicity in the giants is not as high as predicted by ST, the possible exception being θ UMi. Sodium, however, is truly SMR in all the stars. The abundance of iron in the giants is only marginally above normal (0.1 dex), while the abundances of vanadium and manganese might suffer from the effects of complications due to hyperfine structure in the lines. It appears prudent at this point to wait until the gravity discrepancy has been clarified before embarking on a detailed comparison of the abundances derived here with the prediction of various theories on the origin of the chemical elements.

REFERENCES

Alexander, J.B. 1967, M.N., 137, 41.

Aller, L.H. 1963, Atmospheres of the Sun and Stars, 2nd ed. (New York: Ronald Press Co.).

Aller, L.H., O'Mara, J.B., and Little, S. 1964, Proc. Nat. Acad. Sci., 51, 1238.

Arp, H.C. 1958, Hdb. d. Phys. (Berlin: Springer-Verlag), 51, 75.

Becklin, E.E. 1968, unpublished doctoral dissertation, California Institute of Technology.

Bell, R.A. 1970, M.N., 148, 25.

Bidelman, W.P. 1958, Publ. A.S.P., 70, 168.

Blaauw, A. 1963, Stars and Stellar Systems, Vol. 3, ed. K. Aa. Strand (Chicago: University of Chicago Press), p. 383.

Bridges, J.M., and Wiese, W.L. 1970, Ap.J., 161, L71.

Cayrel, G. 1966, Ann. d'Ap., 29, 413.

Cayrel, G., and Cayrel, R. 1963, Ap.J., 137, 431.

Cayrel, R. 1968, Ap.J., 151, 997.

Cayrel, R., and Jugaku, J. 1963, Ann. d'Ap., 26, 495.

Corliss, C.H., and Bozman, W.R. 1962, NBS Monograph 53, Washington, D.C.

Corliss, C.H., and Warner, B. 1964, Ap.J. Suppl., 8, 395.

Cowley, C.R., and Cowley, A.P. 1964, Ap.J., 140, 713.

Davis, S.P., and Phillips, J.G. 1963, The Red System of the CN Molecule (Berkeley and Los Angeles: University of California Press).

Deeming, T.J. 1960, M.N., 121, 52.

Demarque, P. 1967, Ap.J., 150, 945.

_____ 1968, A.J., 73, 669.

Dickow, P., Gyldenkerne, K., Hansen, L., Jacobsen, P.U., Johansen, K.T., Kjaergaard, P., and Olsen, E.H. 1970, Astr. Astrophys. Suppl., 2, No. 1.

Dijke, S.E. van 1946, Ap.J., 104, 27.

Edmonds, F.N. jr., Schluter, H., and Wells, D.C. III 1967, Memoirs of the R.A.S., 71, 271.

Eggen, O.J. 1962, R.O.B., No. 51.

Faulkner, J. 1967, Ap.J., 147, 617.

Gartz, T., and Kock, M. 1969, Astr. Astrophys., 2, 274.

Gartz, T., Holweger, H., Kock, M., and Richter, J. 1969, Astr. Astrophys., 2, 446.

Gingerich, O., and de Jager, C. 1968, Solar Phys., 3, 5.

Gliese, W. 1969, Catalogue of Nearby Stars, Veroffentlichungen des Astronomischen Rechnen-Instituts Heidelberg, Nr. 22.

Greene, T.F. 1969, Ap.J., 157, 737.

Griem, H.R. 1964, Plasma Spectroscopy (New York: McGraw-Hill).

Griffin, R.F. 1961, M.N., 122, 181.

_____ 1964, ibid., 128, 187.

_____ 1968, A Photometric Atlas of the Spectrum of Arcturus, Cambridge Philosophical Society.

_____ 1969a, M.N., 143, 223.

_____ 1969b, ibid., 143, 381.

Griffin, R.F., and Redman, R.O. 1960, M.N., 120, 287.

Griffin, R.F., and Griffin, R. 1967, M.N., 137, 253.

Hansen, L., and Kjaergaard, P. 1971, Astron. Astrophys., 15, 123.

Harris, D.L. 1963, Stars and Stellar Systems, Vol. 3, ed. K. Aa. Strand (Chicago: University of Chicago Press), p. 263.

Harris, D.L., Strand, K. Aa., and Worley, C.E. 1963, Stars and Stellar Systems, Vol. 3, ed. K. Aa. Strand (Chicago: University of Chicago Press), p. 273.

Hayes, D.S. 1970, Ap.J., 159, 165.

Heintze, J.R.W. 1968, B.A.N., 20, 1.

Helfer, H.L., Wallerstein, G., and Greenstein, J.L. 1959, Ap.J., 129, 700.

Helfer, H.L., and Wallerstein, G. 1963, Ap.J. Suppl., 9, 81.

_____ 1968, ibid., 16, 1.

Helfer, H.L., and Sturch, C. 1970, A.J., 75, 971.

Herbig, G.H. 1965, Ap.J., 141, 588.

Hoffleit, D. 1964, Catalogue of Bright Stars (3rd ed.; New Haven: Yale University Observatory).

Holweger, H. 1967, Zs. f. Ap., 65, 365.

_____ 1970, Astron. Astrophys., 4, 11.

Hulst, H.C. van de, and Reesinck, J.J.M. 1947, Ap.J., 106, 121.

Hunger, K. 1956, Zs. f. Ap., 39, 38.

Iben, I. 1964, Ap.J., 140, 1631.

Jenkins, L.F. 1952, General Catalogue of Trigonometric Stellar Parallaxes (New Haven: Yale University Observatory).

Johnson, H.L. 1965, Ap.J., 141, 923.

_____ 1965, Comm. Lunar and Planetary Lab., 3, 73.

_____ 1966, Ann. Rev. Astron. and Ap., 4 (Palo Alto, Calif.; Annual Reviews, Inc.).

Johnson, H.L., and Iriarte, B. 1958, Lowell Obs. Bull., No. 91, 4, 47.

Johnson, H.L., Mitchell, R.I., Iriarte, B., and Wisniewski, W.Z. 1966, Comm. Lunar and Planetary Lab., 4, 99.

Kandel, R. 1968, Proceedings of the Symposium on Low-Luminosity Stars, ed. S.S. Kumar (New York: Gordon and Breach Science Publishers), p. 511.

Keenan, P.C. 1963, Stars and Stellar Systems, Vol. 3, ed. K. Aa. Strand (Chicago: University of Chicago Press), p. 530.

Krishna Swamy, K.S. 1966, Ap.J., 145, 174.

Kuiper, G.P. 1938, Ap.J., 88, 429.

Kurucz, R.L. 1969a, Ap.J., 156, 235.

_____ 1969b, ibid., 138, 213.

_____ 1969c, ibid., 140, 197.

Lutz, T.E. 1971, Pub. A.S.P., 83, 488.

McClure, R.D., and Bergh, S. van den 1968, A.J., 73, 313.

Mihalas, D., and Luebke, W.R. 1971, M.N., 153, 229.

Minnaert, M., Mulders, G.F.W., and Houtgast, J. 1940, Photometric Atlas of the Solar Spectrum 3332 A to 8771 A (Amsterdam: Schnabel).

Mohler, O.C., Pierce, A.K., McMath, R., Goldberg, L. 1950, Photometric Atlas of the Near Infrared Solar Spectrum λ8465 to λ25242, McMath-Hulbert Observatory, University of Michigan Press, Ann Arbor.

Montgomery, E.F., Connes, P., Connes, J., and Edmonds, F.N., Jr. 1969, Ap.J. Suppl., 19, 1.

Moore, C.E. 1959, A Multiplet Table of Astrophysical Interest, Princeton Observatory Contribution No. 20.

Moore, C.E., Minnaert, M., and Houtgast, J. 1966, The Solar Spectrum 2935 A to 8770 A, National Bureau of Standards Monograph 61 (Washington: U.S. Government Printing Office).

Oke, J.B. 1964, Ap.J., 140, 689.

_____ 1965, Ann. Rev. Astron. and Ap., 3 (Palo Alto, Calif.: Annual Reviews, Inc.), p. 23.

Oke, J.B., and Conti, P.S. 1966, Ap.J., 143, 134.

Oke, J.B., and Schild, R.E. 1970, Ap.J., 161, 1015.

Peat, D.W., and Pemberton, A.C. 1968, M.N., 140, 21.

Peimbert, M., and Costero, R. 1969, Bol. Obs. Tonantzintla y Tacuba, No. 31.

Richter, J., and Wulff, P. 1970, Astron. Astrophys., 9, 37.

Sandage, A. 1955, Ap.J., 121, 616.

_____ 1962, ibid., 135, 333.

Schadee, A. 1964, B.A.N., 17, 311.

_____ 1968, Ap.J., 151, 239.

Spinrad, H. 1966, Pub. A.S.P., 78, 367.

_____ 1967, oral communication to IAU Commissions 28 and 45, Prague.

Spinrad, H., and Taylor, B.J. 1969, Ap.J., 157, 1279.

Strom, S.E., Strom, K.M., and Carbon, D.F. 1971, Astr. Astrophys., 12, 177.

Swihart, T.L., and Fischel, D. 1960, Ap.J. Suppl., 5, 291.

Taylor, B.J. 1969, private communication.

_____ 1970, Ap.J. Suppl., 22, 177.

Traving, G., and Cayrel, R. 1960, Zs. f. Ap., 50, 239.

Tsuji, G. 1964, Ann. Tokyo Astron. Obs., 9, 1.

Ulrich, R. 1971, private communication.

Vaughan, A.H., and Zirin, H. 1968, Ap.J., 152, 123.

Vaziaga, M.J. 1971, unpublished doctoral dissertation, University of Paris.

Wallerstein, G. 1971, unpublished.

Warner, B. 1968, M.N., 138, 229.

Williams, P.M. 1971, M.N., 153, 171.

Wilson, O.C. 1959, A.J., 130, 499.

_____ 1962, Ap.J., 136, 793.

_____ 1971, private communication.

Wolnik, S.J., Berthel, R.O., and Waters, G.W. 1970, Ap.J., 162, 1037.

APPENDIX

THE ASTROPHYSICAL JOURNAL, Vol. 153, August 1968

TWO K DWARFS WITH ENHANCED BANDS OF MOLECULAR CARBON*

JESSE L. GREENSTEIN AND VALDAR OINAS
Mount Wilson and Palomar Observatories, Carnegie Institution of Washington
California Institute of Technology
Received June 20, 1968

ABSTRACT

The strong-metallic-line stars ρ^1 Cancri and HD 145675 are found to contain enhanced CN and C_2, and to a lesser extent CH. Comparison with Schadee's models yields C/O ≈ 1. The spectral type of both stars is around K0 V or K1 V, somewhat earlier than the metal lines would indicate. Absolute magnitudes derived from parallax data place both stars on or slightly above the main sequence.

It is well known that stars of spectral type later than about G5 often exhibit considerable diversity in chemical abundances, even for the same spectral and luminosity classes. In addition, there appears to be no one-to-one correspondence between color and spectral types (Wilson 1962). Cayrel has made a detailed study of two early K dwarfs, HD 190404 and HD 219134, of the same spectral type but of different colors, and her results indicate that in these two stars the abundance differences are small, whereas there are important differences in the turbulent velocities and effective temperatures (Cayrel 1966). That study also indicates that sodium may present individual abundance anomalies in dwarfs. Most common are general deficiencies of the metals in high-velocity stars. Metal excess, however, has seldom been demonstrated.

Taylor (1967) and Spinrad and Taylor (1968) have made detailed spectrophotometric scans of many K stars, their results indicating that a sizable fraction of these objects (around 15–20 per cent of the old field population) may be metal-rich. Following their suggestion, Greenstein observed a number of giants and subgiants, which one of us (V. O.) will study in detail. We discuss here the spectra of ρ^1 Cancri and HD 145675 (14 Her), two early K dwarfs which Spinrad and Taylor found to contain enhanced CN, Na I, and Mg I. The dwarfs were studied first in order to determine the full extent of the peculiarities that might exist in supposedly unevolved stars. The spectra were obtained with the 72-inch camera of the 200-inch telescope and have dispersions of 6.8 Å mm^{-1} in the yellow and red and 4.5 Å mm^{-1} in the blue. Microphotometer tracings were made of these spectra as well as of those of two comparison stars of classes K0 V and K2 V (70 Oph A and HD 166620). Whiteoak (1967) has made scans of several K stars, among them HD 145675, HD 166620, and the K0 dwarf HD 185144. As can be seen from Figure 1, HD 145675 and HD 185144 have roughly the same energy distribution in the red, while the relative gradient with respect to HD 166620 places HD 145675 at about K1. On the basis of line-ratio tests (Cr I λ4254.4 to Fe I λ4250.8 and Cr I λ4274.8 to Fe I λ4271.2), the spectral types of HD 145675 and ρ^1 Cancri appear to be around K0. However, the strength of the metal lines would indicate a somewhat later spectral type for both stars.

Since the strength of CN increases monotonically with luminosity, it was important to make sure that ρ^1 Cancri and HD 145675 are really dwarfs. The parallaxes and apparent visual magnitudes of both stars are available in the *Catalogue of Bright Stars* (Hoffleit 1964) and the *General Catalogue of Trigonometric Stellar Parallaxes* (Jenkins 1952). For ρ^1 Cancri, $m_v = 5.94$, $\pi = 0''.074 \pm 0''.007$, and for HD 145675, $m_v = 6.5$, $\pi = 0''.063 \pm 0''.007$; these values yield absolute visual magnitudes of 5.29 ± 0.20 and

* This research was supported by the U.S. Air Force under grant AFOSR-68-1401, monitored by the Air Force Office of Scientific Research of the Office of Aerospace Research.

5.50 ± 0.22, respectively. The parallax of ρ^1 Cancri is based on two independent determinations, while that of HD 145675 comes from only one. The derived absolute magnitudes place both stars near or slightly above the main sequence, since the absolute magnitude of a typical K0 dwarf is around 6.0. Both stars appear to be dwarfs also on the basis of the strength of Sr II λ4077, although this criterion is not quite sensitive enough to separate reliably luminosity classes IV and V in early K stars (Wilson 1962).

The most striking feature in the spectra of ρ^1 Cancri and HD 145675 is the strength of CN, cyanogen, in the band sequences at λλ4216.0 and 3883.4. The intensity of these features greatly exceeds the general metallic-line strengthening mentioned above. In Figure 1, the increased absorption at $1/\lambda = 1.33\ \mu^{-1}$ in HD 145675 corresponds to the (4,1)-band of CN. CH is also somewhat strengthened in both stars, but the strengthening does not greatly surpass the metallic-line intensification. Most surprising is the strength of the C_2 Swan bands, particularly at λλ5165 and 4737 but also at λλ5636, 5586, 5541, and 5129. It is seen in Figure 1 that there is increased absorption in HD

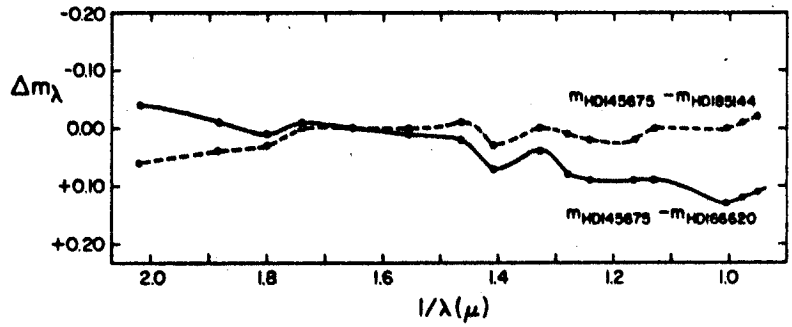

FIG. 1.—Spectrophotometric scans (Whiteoak 1967) of a peculiar early K dwarf HD 145675 as compared with HD 185144 (K0 V) and HD 166620 (K2 V). The dips in the energy distribution are probably due to molecular bands of CN and C_2.

145675 at $1/\lambda = 1.8\ \mu^{-1}$, which corresponds to the (2,3)-band of C_2. Equivalent widths of unblended lines in the (0,0)-band were measured in order to compare the band intensity, (W_0/S_0), with the intensities calculated by Schadee for various compositions, gravities, and effective temperatures (Schadee 1968). Although the scatter in the plot of log (W_K/S_K) versus $K(K+1)$ was fairly large, the logarithm of the band intensity turned out to be approximately 0.6 for ρ^1 Cancri and 1.0 for HD 145675. Based on the assumption that the stars have essentially a solar metal composition, these values indicate that in ρ^1 Cancri the oxygen and carbon abundances are roughly equal, while in HD 145675 there is a slight excess of carbon over oxygen. Essentially, the C/O ratio increases from the solar value (0.6) to slightly above unity; the $C + O \leftrightharpoons CO$ equilibrium frees carbon as the ratio passes through unity. Increasing the metal abundance in the models decreases the observed C_2-band intensity for a given value of the C/O ratio. We cannot say whether C/H increases, lacking information on the strength of the CO lines or [O I], which is not seen.

Lines of neutral carbon were looked for in both stars, but aside from some slight depressions in the continuum there was nothing that could unambiguously be determined to be a line. This was to be expected on account of the high excitation potential of carbon.

Figure 2 (Plate L3) shows selected regions of the spectra of ρ^1 Cancri and 70 Oph A. The strength of the CN bands is obvious; individual C_2 blends are also marked. While the metallic-line spectra are similar, the great strengthening of the wings of Mg I λ5183.6 in ρ^1 Cancri is characteristic of strong-resonance metallic lines.

The intensity of the (0,0)-band of C_2 in 70 Oph A was determined to be $W_0/S_0 = 0.2$, the value being somewhat uncertain because of the errors involved in measuring weak lines. Comparison with Schadee's models yields a C/O ratio slightly greater than that found in the Sun.

We are grateful to Dr. Hyron Spinrad for his early communication of the discovery of strong-line K dwarfs.

REFERENCES

Cayrel, G. 1966, *Ann. d'ap.*, 29, 413.
Hoffleit. D. 1964, *Catalogue of Bright Stars* (3d rev. ed.; New Haven: Yale University Observatory).
Jenkins, L. F. 1952, *General Catalogue of Trigonometric Stellar Parallaxes* (New Haven, Conn.: Yale University Observatory).
Schadee, A. 1968, *Ap. J.*, 151, 239.
Spinrad, H., and Taylor, B. J. 1968 (in preparation).
Taylor, B. J. 1967, *Pub. A.S.P.*, 79, 441.
Whiteoak, J. B. 1967, *Ap. J.*, 150, 521.
Wilson, O. C. 1962, *Ap. J.*, 136, 793.

Copyright 1968. The University of Chicago. Printed in U.S.A.

PLATE L3

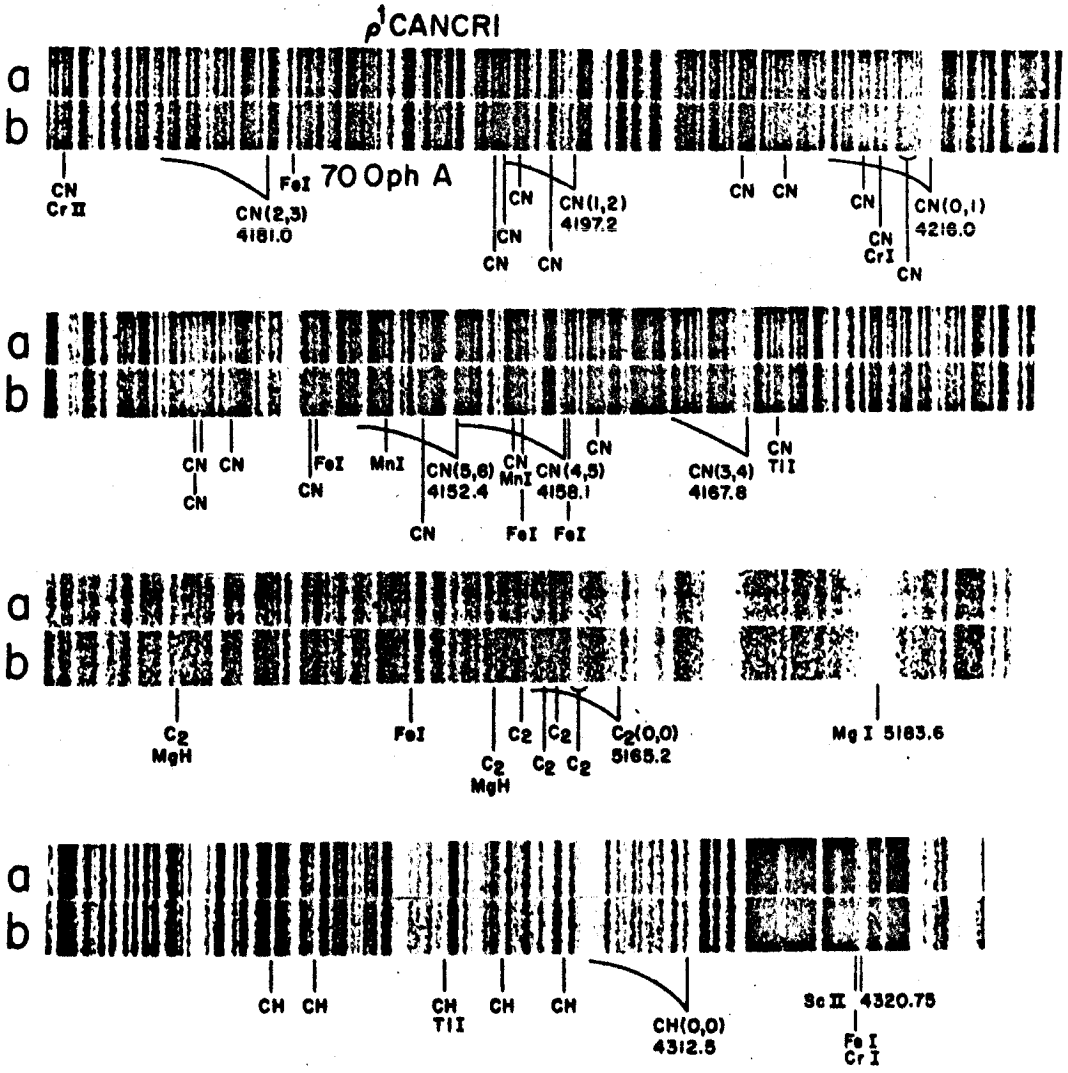

FIG. 2.—Spectra of ρ^1 Cancri compared with 70 Oph A (K0 V). Note the increased strength of CN and C_2 in ρ^1 Cancri. Some metal lines are also strengthened.